Dr. rer. nat. Ute Effner
Dr.-Ing. Mathias Woydt

Slip-rolling and machining of engineering ceramics

Effect of machining related sub-surface modifications on the tribological behaviour under slip-rolling friction of monolithic ceramics and its characterisation by means of ultrasonic microscopy and surface analysis

Research report 259
Berlin, Germany, 2000
English translation from German, 2002

In the frame of the DFG (Deutsche Forschungs-Gesellschaft) special research program 322 697:
"Machining related sub-surface modifications and tribological characteristics
of ceramic materials" of the DFG required under: Wo 521/1 -1 to -6

Impressum

Forschungsbericht 259: **Slip-rolling and machining of engineering ceramics**
2003

Herausgegeben von der Bundesanstalt für
Materialforschung und -prüfung (BAM)
Unter den Eichen 87
12205 Berlin
Telefon: +49 30 8104-0
Telefax: +49 30 8112029
E-mail: info@bam.de
Internet: www.bam.de

Herstellung und Verlag:
Wirtschaftsverlag NW
Verlag für neue Wissenschaft GmbH
27568 Bremerhaven
Telefon: +49 471 94544-0
Telefax: +49 471 945 44-77/-88

Umschlag: Lutz Mittenzwei
Layout: BAM-Referat G.1

ISSN 0938-5533
ISBN 3-89701-976-0

Summary

The present study on the slip rolling friction and wear behaviour of self-mated monolithic ceramics and of ceramic-ceramic-composites under mixed/boundary lubrication has confirmed the expected influence of the following parameters:

a) the material itself,
b) the machining of the functional surface geometry (cylindrical or convex),
c) the interfacial media and
d) the Hertzian pressure.

Unexpected was the finding that the choice of the interfacial media and the machining e.g. the material removal rate determinate the wear coefficient in the range of several orders of magnitude. All materials tested during this program are suited for slip-rolling contacts in unadditivated paraffinic oil even at a contact pressure of 3 GPa, where as for silicone carbide materials the contact pressure should not exceed 1.5 GPa.

An additional surprising finding was that high strength hipped Yttrium-stabilized zirconia exhibited in unadditivated paraffinic oil with a rough polished surface after 20 million of revolution NO detectable wear amount, even measured with an AFM. The surface seemed to be unaffected by the cyclic tribological stress. In contrast, water increased the wear coefficient by 2 to 4 orders of magnitude and enhanced the formation of pitting. In water, silicone nitride exhibited within the ceramics investigated the best wear behaviour.

The initially questions of this research project were answered and a model predicting the machinability was developed within the consortium with the University of Braunschweig. The model and the results enable the industry to select the different ceramics machining parameters giving high removal rates without increasing the wear coefficients and thus helping reduce the machining costs.

The 140 material couples tested over more than 300 million revolutions were incorporated into the numerical tribological data collection Tribocollect, which can be obtained over BAM, lab. VIII.11.

The individual results were published in more than 30 publications.

Future work should be focused on the influence of the machining for higher operating temperatures and on the influence of more common interfacial media on wear coefficient and slip-rolling fatigue resistance.

Contents

Preface

This available report represents the synthesis of the sub-project „Effect of machining related surface modifications on the tribological behaviour under slip-rolling friction of monolithic ceramics and its characterisation by means of ultrasonic microscopy and surface analysis" within the DFG special research program „Machining related surface modifications and tribological characteristics of ceramic materials".

The report is directed to both to the scientifically oriented and industrial readers. For the representation of the results a scientific form was selected, since the determined data can be used for further model development and theoretical treatises.

However also the rather practice-related reader, who would like to include the results purposefully in his construction, finds machining specifications concerning optimal finishing processes and surface roughnesses, resulting in low wear rates of slip-rolling couples. The metallurgical description of the materials tested also permits an optimal selection of comparable material for the desired application.

It was aimed at giving the maximum amount of results and useful information in a small space. For presenting the results, there are classified by the different materials, thus enabling a quick cross check between scientific perceptions and tribological results of the material.

Special value was given to a short summary of the individual results achieved with the tested materials, which emphasizes the most important points at the end of each section and thereby permits a comfortable overview and convenient orientation.

We hope, that this report may contribute to overcome the philosophy „best as possible", if this will not be needed from the design. In all other cases, the implementation of a functional defined surface topography in industry will reduce ceramic costs and more than refund this study.

For making it possible to elaborate this report, the authors thank the German Research Association (DFG) for the fundings and for the cooperations for Mrs. S. Binkowski and Mrs. R. Pahl for metallographic work and the light microscopy pictures, Mrs. S. Benemann for the SEM pictures, Mrs. B. Strauß for the EDX spectra, Mrs. Dr. I. Dörfel for the TEM pictures, Dr. M. Neuber for the ESA spectra, Dr. M. Haubold for the acusto-microscopy pictures, Dr. Th. Schneider for the AFM pictures as well as Mr. J. Schwenzien for the wear volume measurements by means of stylus profilometry and the careful reading of the report. Finally we thank all those colleagues who were not specifically named here, who contributed however through discussion and their interest to this work.

Thank you to Dr. Trivedi (UES Inc.) for the motivation to translate the science report in to the English language.

Berlin, July 2002

Ute Effner

Mathias Woydt

1 Introduction and starting situation

Due to their outstanding tribological characteristics, ceramic materials have found wide fields of application which can no longer be excluded in different areas of production and application, [1, 2, 3, 4] and have thus displaced classical materials. The insertion of expensive ceramic is calculated only due to the functional benefits in the system, the longer time intervals for maintenance and the minimization of the operating cost or the performance.

Lubricated Si_3N_4 hybrid ball and roller bearings (ceramic rolling elements and metallic rings) are used at low temperatures, high speeds and start-stop conditions and, for example, represent a standard solution in spindle bearing arrangements of machine tools. Si_3N_4 hybrid ball and roller bearings possess momentarily a market share of approx. 3-5 per cent. Full ceramic ball and roller bearings made of Si_3N_4 have proven themselves under unlubricated operation conditions and at high temperatures [4, 5].

Both full ceramic and hybrid bearings fulfil the expectations placed on them in practice, at high precision requirements and long service life compared with steel under extreme conditions and make possible in some cases undreamt of function benefits.

In corrosive media and where states of deficient lubrication occur, sliding bearings and axial face seals made of the most diverse SiC materials have worked and led to components that are extraordinarily reliable in service [6], since ceramic sliding mating can be wear resistant lubricated by aqueous, acid and alkaline media [7], from which the good market penetration results.

For counter metals the ceramic materials offer protection from adhesive failure during deficient lubrication and under sliding and in principle under rolling stress.

High production costs - especially conditioned with the finishing of outlines with different and variable radii (compare Table 1) - obstruct a broad market penetration of ceramic components in roll-stressed tribosystems. The portion of the machining costs to total costs moves between 15 and 80 per cent [8]; therefore one goal must be the reduction of the machining- costs in order to reduce total production costs with constant reliability of the ceramic components.

Varying characteristic edge zones, which affect the tribological behaviour of the component, result from the different processes of the cutting finishing of the component. Thus the finishing enters directly into the wear behaviour and the wear-conditioned service life of the component, which is an expression for the reliability of the component and/or the safety of the machine. In order to hold down or eliminate the number of processing-conditional faults (defects or internal stresses) to the surface, roll-stressed components are polished. According to current opinion, the philosophy „best as possible!" is considered necessary, since the ceramics possess a low fracture toughness and with a rolling stress it is a matter of periodic stress under high pressure and with large cycle numbers, so that a finishing low in damage is to be selected, because surface defects under mechanical load increase.

Table 1
Portion of the machining costs of ceramic components in the production series.

Component	Portion of the machining costs
Automobile valve made of Si_3N_4	~ 55 %
Ball bearing made of Si_3N_4	~ 70 %
Face seals made of SiC	15 - 30 %
Seals made of Al_2O_3	~ 35 %
Cutting inserts ceramic	~ 30 %
Special sealing ring made of SiC	60 - 80 %
Sliding bearings made of SiC	~ 70 %

The machining conditioned effect on the tribological behaviour under rolling friction can be tested by means of the model wear test, supported by DIN 50324 (or ASTM G99). Thus the circle between the tribological test conditions and the machining parameters and tribological behaviour can be closed.

An aim of the model wear tests is the development of criteria that ensure the reliability for the tribological application of ceramic components with economic finishing in consideration of the intermediate media, the machining parameters and the rate of material removal, i.e., with which with greatest possible rate of material removal the lowest wear rates will be achieved.

2 Tested materials

For the comprehensive test program, the only materials selected are those that are commercially available, have an outstanding market penetration or are characterized by special properties (see Table 2). These are the materials HIP-Si_3N_4 (NBD 200), GPS-Si_3N_4-TiN (EDM), SSiC (EKasic D), GPS-SiC-TiC [9] as well as high-strength HIP-ZrO_2 (htc-PSZA) and liquid phases sintered LPS-SiC (htc-SiC-B). These materials cover a broad spectrum with characteristics such as hardness, E-module, fracture toughness or bending strength, which form an important basis for the model development.

The materials were characterized before the slip-rolling wear test in the „as fired" state by means of light-optical microscopy, acoustic-microscopy, TEM (transmission electron microscopy), SEM (scanning electron microscopy), XRay-diffraction (XRD) and x-ray analysis within the BAM. The physical characteristics of the materials were taken from the data sheets of the manufacturers. At the high-strength ZrO_2 material recently introduced at the market the 4-point flexural strength σ_{4b}, the fracture toughness K_{IC} and the Weibull-modulus were determined within the BAM-V.22 tests. For the material LPS-SiC the hardness of the material was determined at the BAM, since the manufacturer data for this were missing. The characterization of the materials came to the following results:

2.1 HIP-Si_3N_4 (NBD 200)

The selected Si_3N_4 (NBD 200) is used in high-quality hybrid ball and roller bearings. The processing of this material takes place in units which are lined on the inside with Si_3N_4 (NBD 100), so that it cannot come therefore to foreign inclusions in the structure, which is considered to be an outlet source of pitting. The TEM-tests show a structure made of β-Si_3N_4, whereby the grain size lies within the range of 0.1 to 1 µm (compare Fig. 1). This very low grain size of the HIP Si_3N_4 material does not permit light-microscope tests. The large beta-Si_3N_4 grains contain partially sub-grain boundaries. Due to the low glass phase content no amorphous glass phases are formed at the grain boundaries and the grain gores, as this is usual with other sintered Si_3N_4 qualities. The glass phase is generally unfavourable for the rolling stress.

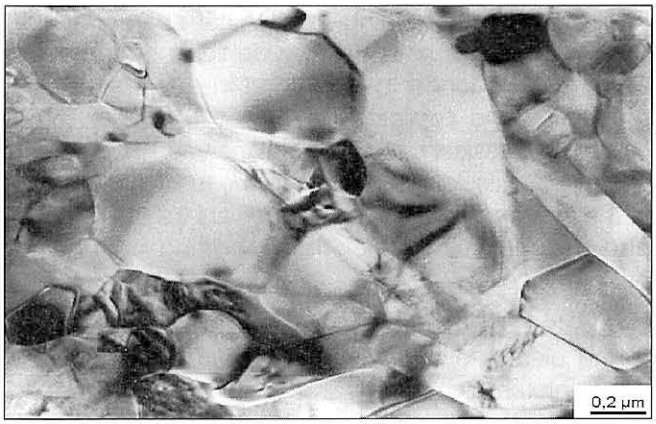

Fig. 1
TEM picture of the HIP-Si_3N_4 material with the columnar β-Si_3N_4 structure

With the very high resolution of TEM, a (100) lattice plane distance of the β-Si_3N_4 of 0.66 Nm was determined (compare Fig. 2). The EDX analysis coupled with the TEM could identify several ferruginous inclusions in fine-grained areas of the material.

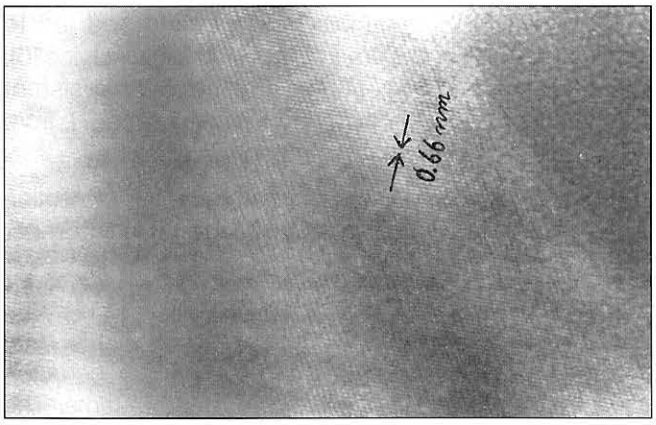

Fig. 2
Highly resolution TEM picture of the material HIP-Si_3N_4

Table 2
Mechanical characteristics of the different tested ceramic materials

Mechanical characteristics	Si_3N_4 [5]	SiC [10]	SiC [11]	Si_3N_4-TiN [10]	ZrO_2 [12]	SiC-TiC [13]
Density ρ[g/cm³]	3,17	3,10	3,22	3,86	5,42	3,79
E-module E [GPa]	309	410	456	300	256	444
Poisson number ν	0,27	0,17	0,14	0,26	0,23	0,18
Hardness, Vickers [GPa]	16,5 [HV 10]	28 [HV 0,5]	25 [HV 0,5]	17 [HV 0,5]	14,5 [HV 0,5]	22,4 [HV 5]
Fracture toughness K_{IC} [MPa*m$^{0.5}$]	6,8	3,2	7,5	7,5	13,9	5,5
Flexural strength σ_{4B} [MPa]	750	410	670	700	1399	490

Due to the low glass phase part the columnar β-Si_3N_4 structure is represented with SEM tests only weakly. This also does not change if the HIP-Si_3N_4 material is etched with NaOH melt 90 seconds at approx. 350° C and coated afterwards with carbon.

The results of the Röntgen-diffraction (XRD) confirm that the largest part of the HIP-Si_3N_4 material consists of β-Si_3N_4 (95.62 Vol.-%), the remaining part (4.38 Vol.-%) of the structure was indicated as Si-0-N-Phase. The x-ray-fluorescence analysis confirms these specifications, which determined following elements and chemical compounds that are contained in the HIP-Si_3N_4 material:

Table 3
Elements and compounds contained in the material HIP-Si_3N_4 in accordance with the x-ray fluorescence analysis

Element/compound	Weight-%
Si	59,30
N	37,30
Al_2O_3	0,11
MgO	1,18
Fe_2O_3	0,50

Thus the part of sintering additives with 1.79 weight-% can be indicated and is slightly over the manufacturer data [5].

With ESCA-tests still additionally the elements C (carbon) and Na (sodium) were accounted for. These measurements could confirm that Al (aluminium) and Mg (magnesium) are oxide-bound and that C is present as carbide-bound. The ferruginous compounds and/or inclusions that have already been detected with the TEM/EDX examination and the X-ray analysis are detectable also by means of ESCA (compare Fig. 3). From the energy shift of the individual trunk levels it can be concluded that the different elements are present in the material bound by oxide, carbide and/or nitride, since a shift is to be recorded in relation to the pure component.

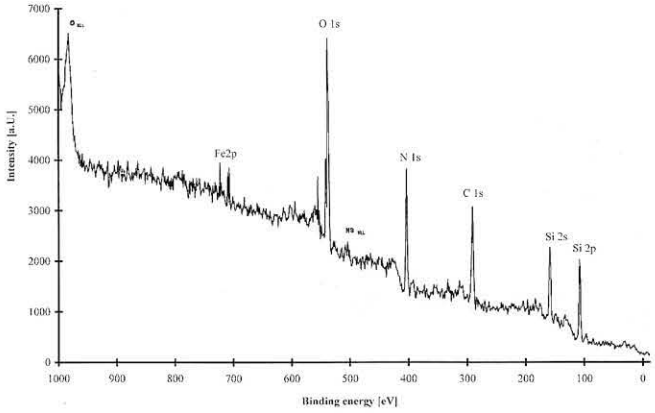

Fig. 3
ESCA measurement of the Si_3N_4 material in the overview. (E_F= 0 eV)

With the acoustic-microscopy (compare Chapter 5) can be tested the pore distribution in the material without destruction. Depending upon selected frequency the penetration depth and thus the surface and/or volume sensitivity of the method vary. The higher the frequency, the nearer the surface is the tested range. The pore content of the Si_3N_4 material is so low that an acousto-microscopic measurement with 1 GHz could not be made, rather the test had to be accomplished at 800 MHz, with which a larger depth range is detected. The test resulted in a pore density of 0.37 percent, whereby all pores belong to the lowest size class (< 33 µm²) that can be dissolved by the acousto-microscope.

The chemical and physical composition of the material causes the mechanical characteristics, which are to be taken from table 2. All of the tests that were accomplished confirm that with the tested HIP-Si_3N_4 quality a material sufficient for high requirements is present. The low pore part and the practically not present glass phase, as well as the low part of sinter additives permit the use of HIP-Si_3N_4, also under rolling stress.

2.2 GPS-Si_3N_4-TiN (EDM)

Components can be fabricated by means of eroding from the gas pressure-sintered Si_3N_4-TiN (EDM) [10]. The TiN phase causes the electric conductivity of the material; thus simpler half-wrought material with complicated geometry can be made from the material by means of electrical discharge machining.

With the TEM tests the material GPS-Si_3N_4-TiN shows a bimodal grain size distribution whereby the large grains consist usually of TiN (see Fig. 4). The grain size of the β-Si_3N_4 grains is comparable with that of the HIP-Si_3N_4 material and is thus between 0.1 and 1 µm. The grain size of the TiN phase is 1 -3 µm. In the TiN phase some dislocations were found. Similar to the material HIP-Si_3N_4, there were also no amorphous grain boundaries observed with the Si_3N_4-TiN material. Due to the low part of sinter additives, amorphous grain boundaries were also not to be expected. The columnar β-Si_3N_4-phase is deposited between the larger TiN grains. With the material Si_3N_4-TiN could be accounted for likewise ferruginous inclusions, which presumably are attributed to the grinding of the ceramic powders in ball mills or similar devices during the production process.

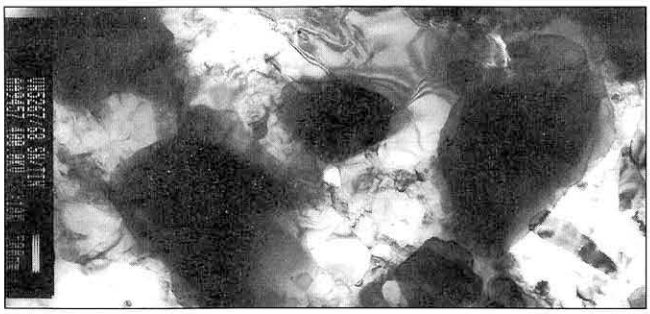

Fig. 4
TEM picture of the material GPS-Si_3N_4-TiN. The large dark grains are the TiN phase

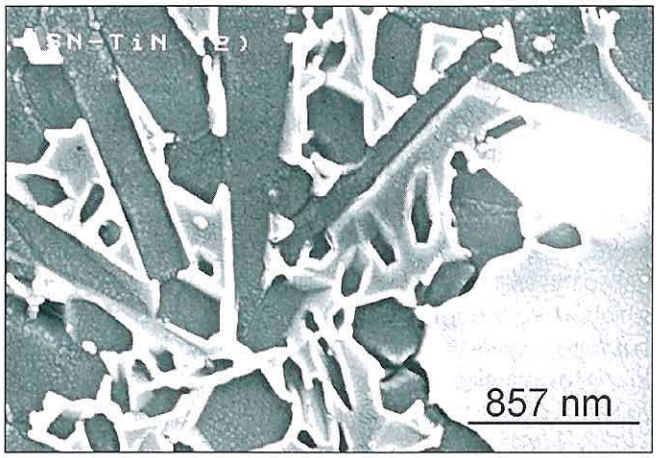

Fig. 5
SEM picture of the material Si_3N_4-TiN;
left: β-Si_3N_4 phase, right: TiN phase

The structure representation by means of the SEM picture (see Fig. 5) clearly shows the columnar structure of the β-Si_3N_4 part, which is represented in the left half of the picture as fan-like; the larger graining of the TiN phase is in the right half of the picture.

By means of the Röntgen diffraction the Si_3N_4 and TiN phases can be well represented separately. A part of 66.66 Vol.-% β-Si_3N_4 phase and a part of 33.34 Vol.-% TiN phase was determined, this results for the ratio of volumes in the material in

$$TiN : \beta\text{-}Si_3N_4 = 1:2.$$

Here it is to be noted however that the weight-% of the individual phases constituted approx. 50 percent in each case. A third phase could not be determined.

The X-ray analysis could determine the following proportions in the material:

In accordance with the material composition from table 4 a part of the sintering additives of 4.41 weight-% results.

With both the light microscopy and the acoustic-microscopy the two-phase state of the GPS-Si_3N_4-TiN material can be well represented. The pores in the material result visually in a slight, acoustic-microscopic although high contrast. In contrast to this, in the optical picture the TiN grains give a high contrast; in the acoustic-microscopic picture they can still be detected, however there is less contrast.

Table 4
Chemical components and compounds of the material Si_3N_4-TiN

Element/Compound	Weight-%
Si	32,30
Ti	33,20
N	29,30
MgO	1,54
Fe_2O_3	2,87

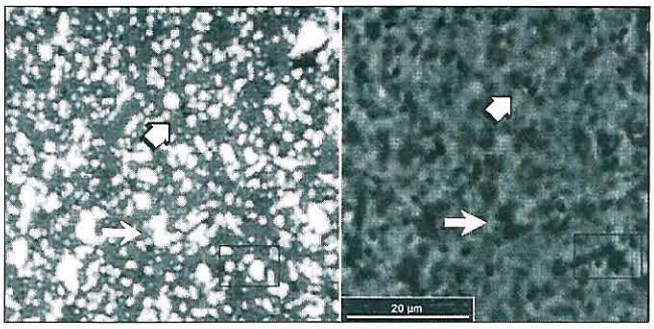

Fig. 6 - Two-phase state of the material GPS-Si_3N_4-TiN. To the left, the light-microscope picture; to the right, the acoustic-microscopic picture at 1,000 MHz
(⬅ = TiN grains, ➡ = pores)

Here it is to be noted that in the acoustic signal the information about a depth expansion is contained.

The mechanical characteristics (compare Table 2] are comparable with those of the material HIP Si_3N_4. However due to the electric-discharge machinability of Si_3N_4-TiN components with complex geometry can also be fabricated from semi-finished products of this material.

2.3 SSiC (EKasic D)

SiC is the most frequently used material in axial face seals and sliding bearings. Even in highly loaded sliding bearings SSiC is an often-used or preferred material. However little is known about the behaviour of this material under slip-rolling, since for this stress its bending strength and fracture toughness are regarded as too low.

The structure of the material SSiC (EKasic D) can be represented in the optical microscope in the transmitted light process (compare Fig. 7), which holds the preparative expenditure within limits, since etching does not supply an additional structure contrast due to the chemical resistance of SiC. For the transmitted light pictures (enlargement: 1000 : 1) with the light-optical microscope through polishing thin sections are produced, which are examined against the light in the microscope. This

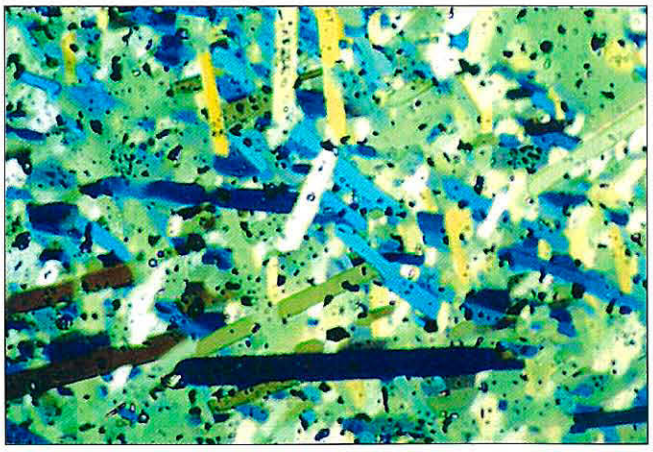

Fig. 7
Light-microscope picture of the material SSiC (EKasic D) by means of transmitted light, enlargement: 1000 : 1

technique was recently developed for the SSiC material and was applied for the first time in the context of this work. The columnar crystals of the SiC structure have a diameter of 4 to 5 µm with a length of approx. 20 to 50 µm. The varying coloring of the columnar SiC crystals depends on the refraction of light during the illumination.

The pores in the material are well visible as black spots in the light-microscope picture. The manufacturer (ESK GmbH) specify for closed porosity a value < 3.5 volume-% [10]. Since the porosity of a material (similar as the grain size) enters the mechanical characteristics, a pore analysis by means of acoustic-microscopy was made. The acoustic-microscopic pictures with different frequencies show that the depth expansion of the pores is quite varied and the total material volume is interspersed with closed pores. The picture with 1000 MHz (compare Fig. 8 above left) supplies no depth information and is similar to the light-microscopic picture of the surface. The picture with 100 MHz (compare Fig. 8 lower right) supplies compared with the picture with 200 MHz (compare Fig. 8 lower left) no new information. A benefit of the acoustic-microscopic test is that the component does not have to be destroyed.

However it is to be noted that not only pores, but also cracks and other defects cause interferences and thus a standardization of this method must take place first.

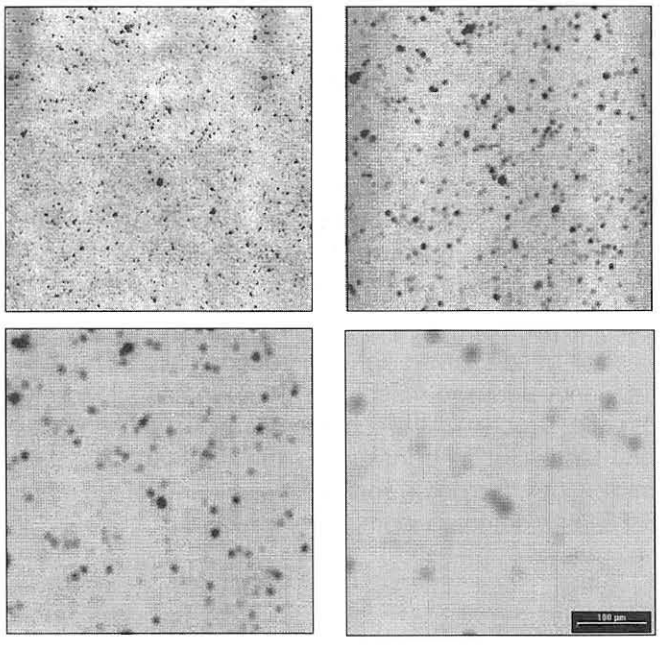

Fig. 8
Acustic-microscope pictures of the material SSiC;
Above: left; 1000 MHz, right: 400 MHz,
Below: left: 200 MHz, right: 100 MHz

The microstructure with a grain size of 15 µm, a bimodal particle size distribution as well as a porosity of 3.5 volume-% in connection with the high E-module will prove however in principle to be unfavourable properties for a slip-rolling stress of this material with an initial Hertzian pressure of 3 GPa.

2.4 GPS-SiC-TiC

With SiC-TiC a material composition was produced through gas pressure-internal, which is likewise machinable by means of electrical discharge. This two-phase composite is with HV5 = 22.5 GPa comparatively „hard". From other tests it was known [14, 15] that TiC increases the wear resistance in the unlubricated operation under sliding as also under rolling stress opposite SSiC. The combination of the materials as well as the higher toughness and low porosity (< 1 percent) let the carbide material without glass phase for the slip-rolling stress appear to be more favourable than pure SiC. The material SiC-TiC was produced and characterized in the BAM [13]. The data for the mechanical characteristics, which were likewise determined at the BAM, are summarized in table 2.

The material contains an approx. 50: 50 percent composition; SiC is contained to 54 weight-%, TiC to 43 weight-%. As sintering additive a weight-percent Al_2O_3 and two weight-% C were used. The material possesses a low porosity with < 1 percent. By means of the acoustic-microscopy it could be determined that the few pores contained in the material exhibit only a slight expansion (approx. 10-30 µm²).

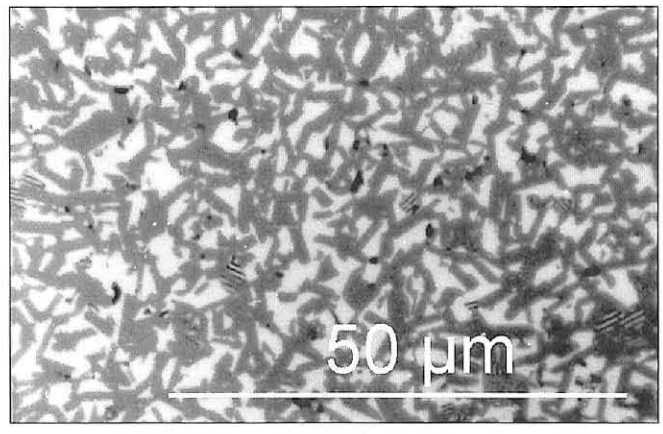

Fig. 9
Light-microscopic picture of the material GPS-SiC-TiC produced and characterized at the BAM

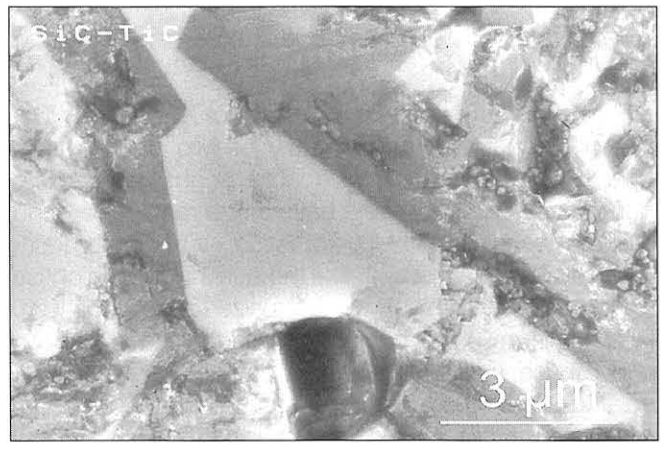

Fig. 10
SEM picture of the material GPS-SiC-TiC; the brighter grains are the TiC phase, the darker grains are the SiC phase

Already in the light-microscopic picture the two-phase state of the material becomes visible. The SiC phase stand out as gray and the TiC phase stands out as white, the pores are visible as black spots.

The SEM tests confirm the results already obtained from the light-microscopic picture. Also in the SEM picture the TiC grains stand out somewhat more brightly. The different phases can be uniquely assigned by means of EDX.

The columnar SiC grains have a size of 1-4 µm, the TiC grains are larger and have an expansion of up to 2-6 µm. The graining of the structure is clearly smaller than that of the pure SiC material, likewise the porosity is lower.

2.5 HIP-ZrO_2 (htc-PSZA)

The HIP-ZrO_2 material newly introduced to the market is particularly interesting due to its bending strength and fracture toughness (see Table 2). The physical characteristics of ZrO_2 materials build a bridge between the extremes of Si_3N_4 and 100Cr6. The most remarkable advantages of ZrO_2 over Si_3N_4 result with the thermal expansion, the flexural strength, the E-module and the fracture toughness, which approximate very strongly the values of 100Cr6 (AISI 51200). This multi-phase ZrO_2 material has a homogeneous particle size distribution with a grain size of 0.7 µm for Al_2O_3 and in the range of 0.4 µm for the Y_2O_3-stabilized ZrO_2 phase [12].

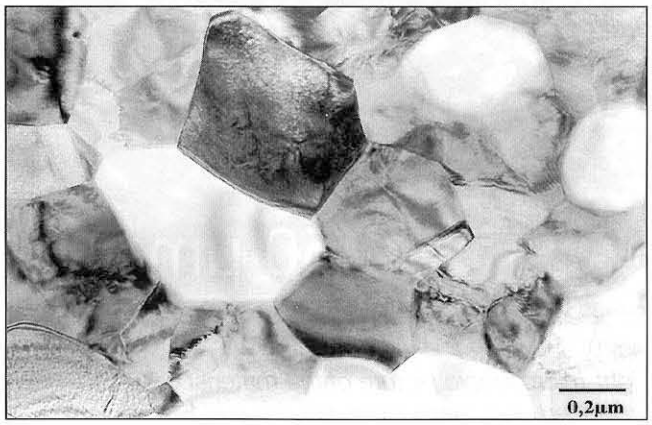

Fig. 11
TEM picture of the structure of the material HIP-ZrO_2

In Fig. 11 the structure of the material ZrO_2 is shown. The material consists predominantly of two phases [12]: corundum and $Y_{0,15}Zr_{0,85}O_{1,93}$. The bright grains were identified as corundum and have a size range of around 0.7 µm. The grains of the cubic, $Y_{0,15}Zr_{0,85}O_{1,93}$-phase (dark grains in Fig. 11) are exactly like the aluminum oxide phase of isometric habitus and exhibit a size range of 0.4 µm. The aluminum oxide phase is embedded in the zircon oxide phase, which is to be regarded as matrix material. Isolated ZrO_2 is present in the material as the third phase; baddelyite is present in the monoclinic phase, which shows a typical twin accommodation. This pure ZrO_2 phase is present in such a low volume in the material that it is not relevant for the total material. The phase composition can be affected by thermal treatment.

The material exhibits no glassy grain boundaries; it is, however, high crystallogaphical defects and distortions and shows adaptative dislocation transfers. The material is extremely brittle in the thinned-out form and contains strong internal stresses, so that already the lowest heating process in the electron microscope leads to the cracking.

The hot isostatically pressed ZrO_2 quality exhibits according to manufacturer data a 4-point flexural strength of σ_{4Bb} = 1,800 MPa. Since this material with the high strength is new to the market and the strength level depends on the thermal treatment, the manufacturer data was verified. The tests resulted in a 4-point flexural strength of σ_{4Bb} = 1,399 MPa + - 40 MPa, which is under the manufacturer data [12]. For the Weibull-parameter according to the Maximum Likelihood method the result was m = 23,07.

The phases of the structure could be confirmed by means of the x-ray diffraction (XRD). The reflexes of the different phases overlay partially, which makes an evaluation more difficult, nevertheless the different phases can be assigned.

The defect in the R-value is < 3. As result of the measurement can be secured:

Al_2O_3 is present as corundum (rhombic and/or hexagonal);

Yttrium is present after this measurement not as Y_2O_3, but rather dissolved in ZrO_2 as cubic $Y_{0,15}Zr_{0,85}O_{1,93}$;

ZrO_2 is present here only in orthorhombic form, due to the HIP production process, rearranging into the orthorhombic phase can result if the conditions T ≈ 950° C and P > 10 GPa occur [13].

The x-ray analysis indicates the proportion in percent, which agrees with the previous results of measurement. The following chemical elements in the material were determined, whereby was calculated the oxygen content over the oxide form of the different components.

The fine microstructure of the HIP-Al_2O_3-ZrO_2 (htc-PSZA) cannot be dissolved light-microscopically. The high frequency acoustic-microscopy likewise cannot dissolve the ZrO_2 structure in the sub-micron range with the special ball lens. But in contrast to the light and electron microscopy, the pores and inclusions (dark) of the material can be detected (compare Fig. 12).

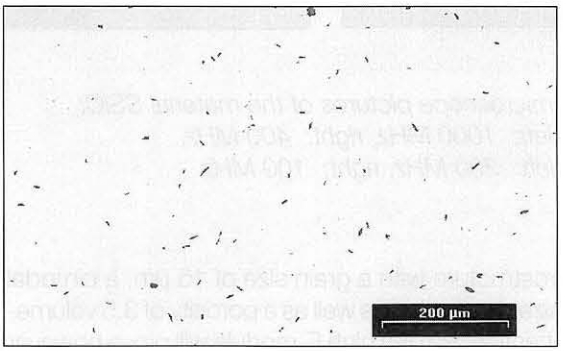

Fig. 12
Acoustic-microscopic picture; 1 GHz; Inclusions and pores (dark)

Table 5
Chemical components in the material HIP-ZrO_2 in accordance with the X-ray analysis

Element/ compound	weight-%
Zr	47,4000
O	29,8000
Al	12,8000
Y	4,6000
Rb	0,1670
Si	0,0678
S	0,0638

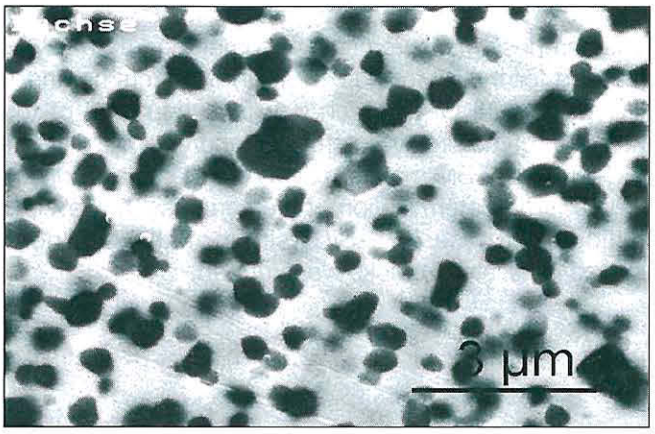

Fig. 13
SEM picture of ZrO_2; dark spots Al_2O_3; bright area ZrO_2

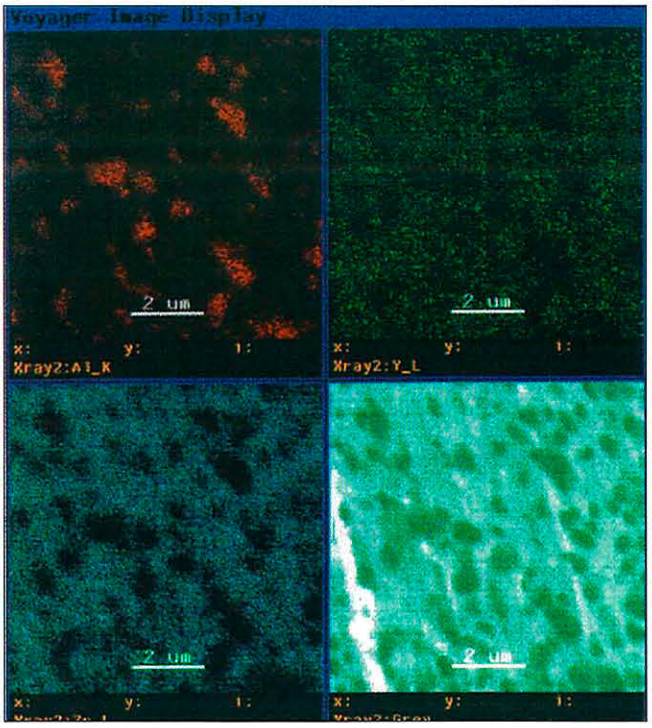

Fig. 14
EDX test of the different component distributions; upper left: Al, upper right: Y, lower left: Zr, lower right: Gray scale representation

A two-phase structure shows only the SEM picture. Due to the difference in the ordinal number, the bright matrix can be assigned to the ZrO_2 and the dark inclusions can be assigned to the Al_2O_3.

The EDX tests, which can be accomplished in situ with the SEM tests, assign uniquely the two-phase structure to the Al_2O_3 and ZrO_2 phases of the material. Both phases can also be separated chemically. Yttrium is also not to be observed here as individual phase, which confirms the results of the Röntgen diffraction analysis. It is however predominantly dissolved in the ZrO_2 grid, this can however not be dissolved by the EDX.

Since the material-physical characteristics of ZrO_2 are partly comparable with those of steel [17], the technical designer can integrate ZrO_2 relatively trouble-free into existing constructions. Thus press fits and plays barely change due to temperature loads. Likewise ZrO_2 can be classified under the ceramics as relatively impact-resistant.

Similarly as is known with Si_3N_4, [18, 19, 20], it can be concluded from more recent tests that certain zirconium dioxide qualities possess a fatigue strength. Unfortunately ZrO_2 materials did not work because of their phase instability with high temperature applications and humidity [21].

2.6 LPS SiC (htc-SiC-B)

The abbreviation LPS stands for liquid phases sintered and was introduced for this material for the distinction of the simply sintered SiC (SSiC) [22]. This material was absorbed in the test program in order to possibly test a silicon carbide material more suitable for the slip-rolling stress. Also the LPS-SiC contains a glass phase part, which generally affects the rolling load in an unfavourable way.

The mechanical material data for LPS-SiC are to be found in table 2. A testing of some of the mechanical sizes by means of acoustic-microscopy supplied for the E-module the value E = 454 GPa and for the Poisson's number the value $\nu = 0.157$. The verified measured variables lie in the range of the manufacturer data.

A representation of the structure could be achieved by means of light microscopy. Here was used the transmitted light process. From the LPS-SiC sample a thin section was manufactured and this was treated with the process of modified Murakami etching [23]. The modified Murakami etching was used for the preparation, since by means of this process a detection of both α-SiC and β-SiC can take place. The available material was subjected to 30 minutes of the etching solution. This time, however, depends on the sinter additives contained in the material and the grain size of the material [23].

From the light-microscope tests (compare Fig. 15) it is to be recognized that to a large extent the material consists of polygonal α-SiC grains with a grain size of 0.5 - 0.6 µm with narrow grains and 20-24 µm with broad grains. Around the α-SiC-matrix β-SiC-grains are added on a small part. Thus this structure differs substantially from that of the SSiC with its columnar crystallites made out of α-SiC.

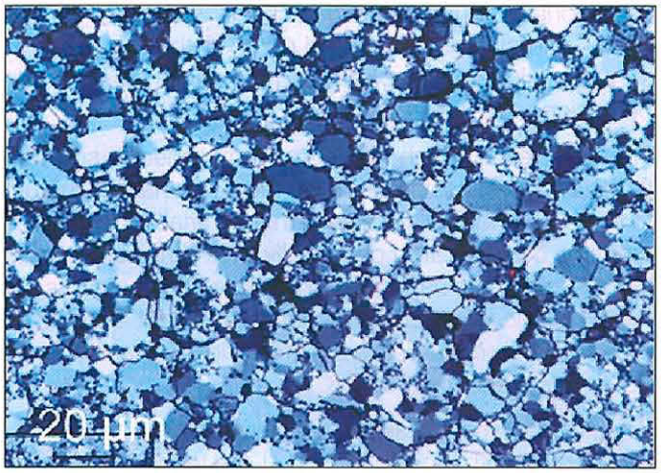

Fig. 15
Structure representation of the material LPS-SiC with the light-microscope in transmitted light mode

The tests by means of x-ray diffraction show that the structure of the material LPS-SiC to 77 weight-% consists of hexagonal α-SiC and to approx. 20 weight-% of cubic β-SiC. The remaining approx. 3 weight-% is formed from materials of the sinter process materials, which represent finally the glass phase of the material. Since the portion of other substances in the material is ≤ 5 %, by means of x-ray diffraction no statement can be met about which chemical compounds it concerns thereby.

Through an X-ray analysis the components of the glass phase part can be identified particularly as aluminum and iron. Furthermore vanadium, titanium and sulfur are detectable in low amounts; zirconium is present in traces. Iron, vanadium and titanium can be found more frequently than traces in sintered materials, which is due to the grinding process in the powder milling. Al_2O_3 is a usual sinter aid. A quantitative test could not be accomplished by means of Röntgen fluorescence, since no reference material was present.

It could be determined from the tests that the glass phase part is approx. 3 percent. This is over the value of for example, Si_3N_4, which exhibits only a very low glass phase part of ≤ 1 % and is a typical material for the rolling load.

The hardness measurements accomplished at the BAM resulted for the material LPS-SiC in a Vickers hardness [HV 0.5] of 25 GPa, which is within the range of the hardness of the simply sintered SiC and/or of the material SiC-TiC, i.e. all SiC materials show comparable hardness values. The determination of the hardness, however, is difficult with the LPS-SiC, since at the hardness impressions lateral cracks were formed.

3 Experimental

The experimental conditions were kept constant with the total slip-rolling wear tests, in order to permit a reproducibility of the results.

3.1 Machine

All tribological slip-rolling wear tests were accomplished with a twin-disk tribometer of the type Amsler [24]. In the testing device two test specimens (one disk is cylindrical and one spherical) in each case are mounted at one of the two shaft ends and stressed at their lateral surfaces (see Fig. 16). The rotation speeds of the two shafts differ by approx. 10 percent. For a sample change the upper shaft supported in a rocker can be taken off.

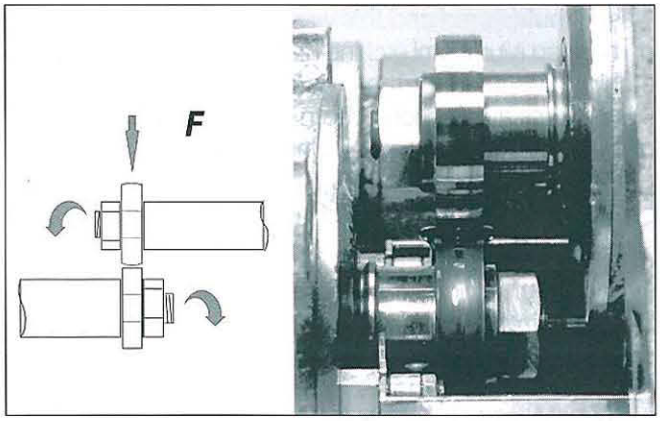

Fig. 16
Calibration set-up in the Amsler-Tribometer for the slip-rolling stress (left: schematic, right: photographic)

For the preparation of the tribological rolling abrasion tests, the Amsler tribometer used was modified. A revolution counter was installed, whereby on the inner toothed disk flywheel of the test equipment inside a strip reflex transparency was stuck, so that with an optical sensor with subsequently added counter fixed in direct proximity, the number of rotations / cycles of the subsample, which is always the cylindrical sample, can be determined. Due to this measure the exact number of cycles and/or the resulting slide path could be determined.

Table 6
Test conditions in twin-disk tribometer of the type Amsler

Stress conditions	Parameters
Type of movement	slip-rolling, rolling with 10 % slip
Initial Hertzian pressure P_0	3 GPa; 1,5 GPa (SSiC)
Rotational speed	386 rpm/ 347 rpm
Sliding speed v_{diff}	0,085 m/s
Test duration n_{ges}	$2 * 10^6$ (→$2 * 10^7$)
Sliding distance s	26.390 m (→263.900 m)
Ambient temperature T	RT (≈23°C)
Lubrication	Paraffinic oil, water

For the tribological tests by means of rolling abrasion the following close-to-applications parameter were selected (see Table 6).

The normal force is applied by means of a spring, the upper rocker with the spherical test specimen against the lower shaft and the cylindrical test specimen is pressed.

3.2 The interfacial media

As interfacial media for the slip-rolling tests unadditivated paraffinic oil and/or distilled water was used. The unadditivated paraffinic oil as intermediate media was used also for the avoidance of hot-spot conditioned wear mechanisms. This paraffinic oil is already used with failure load tests for the system „cam/ tappet" [25].

No additives that could also affect friction and wear behaviour are added to the paraffinic oil. The reduction of friction and wear with ceramic/ceramic mating through the addition of lubricating oil additives depends on the additives used and on the length of the chains of the chemical compounds [26]. The paraffinic oil of the firm Merck is dispersed under the designation ,,paraffinic oil viscous „ and exhibits a dynamic viscosity at 20° C from 110-230 mPa* as well as a cinematic viscosity at 40°C from > 34.5 cSt [27]. The de-ionized water was used as contrast to the paraffinic oil, since in chemistry and equipment construction, as well as in the machine-building industry, aqueous media also occurs. Also here it was made certain that there were no additives present that could influence wear.

With the intermediate media used, the effect of the „Rehbinder"-effect [28] on the surface of the material to be checked is to be considered. The nature of the Rehbinder effect consists of the fact that the surface energy of the solid and concomitantly its strength under the effect of an interfacial media is reduced. The interfacial media lowers the surface energy of the solid very clearly if both materials are related chemically with one another [29]. The Rehbinder effect is significant in the area of material fatigue, if macroscopic cracks come from microcracks or if cracking and/or pitting result. The fatigue of a material can be forced due to surface-active interfacial media; in order to avoid this, interfacial media and/or lubricants are selected, which contain the least possible amount of surface-active substances [29].

Since the interfacial media selected with the tests accomplished here do not contain any additives, is to be assumed at the beginning of the tests that the surface activity is low and thus abrasion-pumping effects could outcrop in a smaller frame.

With the rolling abrasion tests accomplished in water with the materials Si_3N_4-TiN, ZrO_2 and SiC, it was shown, however, that a fatigue wear with outbreaks led to the failure of the material and these are thus not suitable for lubrication with water under rolling stress. A cause here could be the surface-active effect of water, which promotes the cracking. Thus, for example, with the material Si_3N_4-TiN, the TiN phase in water over titanium hydroxide dissolves and in the material ZrO_2, the Y_2O_3 is extracted as hydroxide $Y(OH)_3$, which leads to material outbreaks and to the failure of the material.

3.3 Samples for the slip-rolling

For the slip- rolling tests ceramic test specimens of the same kind were always used, i.e. both rolling members always consisted of the same material and the function areas were usually also finished according to the same process. The test specimens were supplied by the manufacturers in accordance with geometry in Fig. 17.

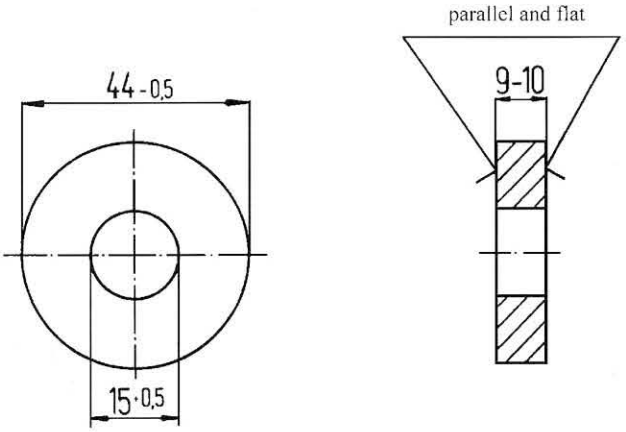

Fig. 17
Test specimen geometry before the finishing

The test parameters and geometry were selected in such a way that the edge zones of the material surfaces in the area of the fatigue are stressed. For example, with the geometry and the material properties of HIP-Si_3N_4 used, as well as with an adjusted load of F_N = 1,005 N, a Hertzian elastic contact width of 1.2 mm and a radial flattening of 0.5 to 2 µm result. This track width is visible with the eye after the tests on the sample surfaces in each case, even if the wear track widths in some cases are smaller.

The selected radius of 21 mm with the round test specimens is selected from the geometry in such a way that the stresses take place predominantly in a light edge zone volume and thus a better statement about the treating-conditioned effects can be made. The radial wear lengths are less than 3 µm per test specimen. The second test specimen has a flat or rectangular profile. Thus with the flat and round test specimens, defined conditions result at the beginning of the test due to the spot contact.

According to statements made by Adachi and Hokkirigawa [30], for the material Si_3N_4, a slip of ≥10 % with the slip-rolling lies within the range of the high-wear condition of the function area. This can also be said of a critical slip, which is, however, pressure-independent.

3.4 Theoretical notes for interpretation of test results

For the evaluation of the measured standard sizes only a relatively low theoretical expenditure is necessary. The measured tribological sizes are the friction coefficient f and the wear rate/coefficient K_v.

The friction coefficient f can be determined over the torque of the flywheel, divided by the adjusted normal force and the radius of the test specimen.

The wear rate is calculated as follows:

Formula I $$k_v = \frac{W_V}{F_N * s} \quad [mm^3/Nm]$$

with the wear volume W_v [mm³], the normal force F_N [N] and the sliding distance s [m].

In order to achieve a reproducibility of the results between different engineering ceramics, an equal initial surface pressure was selected, so that as variable parameters, only the surface finishing and the material were changed with the tests.

The different normal force to be adjusted with the different ceramic materials results in accordance with the Hertzian formula [31] (compare Formula II) with the same surface pressure (compare Table 6) in connection with the mechanical characteristics (E-Moduli E and Poisson numbers ν, compare Table 2). According to experience, the pressure in comparison to the normal force in the tribo-contact for the material must be regarded as the more significant size. For this reason this was also selected as constant.

The surface pressure F_N results in accordance with the Hertzian Formula from:

Formula II

$$F_N = \pi^3 m^3 n^3 \frac{1}{6(B + A)^2} (k_1 + k_2)^2 P_0^3 \text{ [N]}$$

In formula II the parameters m, n, B and A denote sizes dependent on the specimen configuration. In the present case, the following applies to the test specimens with the slip-rolling: m = 1.276; n = 0.8045 and (B+A) = 1/14 [mm^{-1}]; (k_1+k_2) is calculated with formula III, in which the mechanical characteristics of the material from table 2 enter.

Formula III $$(k_1 + k_2) = \frac{2(1 - \nu^2)}{E} \quad [mm^2/N]$$

In formula III E denotes the Elasticity module and ν denotes the Poisson number.

If formula III is used in formula II, results according to formula II the normal force F_N [N] (compare Table 7) in each case to be adjusted for the different monolithic ceramic materials.

Due to the results of the rolling resistance tests on the material SiC with an initial Hertzian pressure of P_0 = 3 GPa and an associated normal force of F_N = 665 N, the initial Hertzian pressure was halved and lowered to P_0 = 1.5 GPa, which resulted in a normal force of F_N = 250 N. The material SSiC proved suited for the rolling resistance only under the modified settings. Same could be observed for the material LPS-SiC, for which the initial Hertzian pressure was likewise reduced by half. With P_0 = 1.5 GPa, the normal force F_N = 205 N resulted.

Since the results obtained on the ceramic materials should be compared with the in practice widely spread and tested roller and ball bearing steel 100Cr6, some tests were accomplished under the conditions specified above also with test specimens from this material. Since the normal force to be maximally adjusted at the Amsler tribometer is F_N = 2,000 N, only an initial Hertzian pressure of P_0 = 2 GPa was achieved.

Table 7
Normal force for the different ceramic materials with an initial Hertzian pressure of P_0 = 3 GPa

Material	Si_3N_4	SSiC	LPS-SiC	Si_3N_4-TiN	SiC-TiC	ZrO_2	100Cr6H
Normal force F_N [N]; (P_0 = 3 GPa)	1,005	665	548	1,150	563	1,575	2,000$
Normal force F_N [N]; (P_0 = 1,5 GPa)		250*	205*				

* *The initial Hertzian surface pressures for the different SiC qualities must be lowered*
$ *F_N = 2,000 N is the maximally adjustable normal force of the test equipment, therefore resulted for 100Cr6H/AISI 52100 a surface pressure of P_0 = 2 GPa*

4 Machining techniques of the test specimens

Before the slip-rolling tests the work pieces, which were supplied in the „as fired" state by the ceramic manufacturer, were by means of the finishing procedures of grinding, honing, lapping or polishing at the Institute for Machine Tools and Finishing Technique (IWF) of the Technical University Braunschweig (Prof. Drs. E. Westkämper), D-38106 Braunschweig, finished and exhibited thus varying outer surfaces zones and surface morphologies. The finishing took place in each case in a „rough" and a „fine" specification [32] for each of the manufacturing procedures. Per material thus eight tests per medium resulted. For each individual tribological test, in each case recently finished test specimens were used.

Grinding the samples took place on a CNC-internal-cylindrical-grinder of the type Overbeck 600 IR, whose machine-own control permits the processing of five shafts. The manufacture of the two component geometries differed here only by an adapted programming of the grinding machine. The samples were machined with a cutting velocity of v_c = 30 m/s. Grinding wheels of the specification D64 VSS 2813 DK 1AC C140 were used with the „rough" finishing. With „fine" finishing the specification D15 C100 B61 was used.

A model test stand [33], upon which two component geometries were created by different apparatures, was used for the honing. The model test stand was developed at the IWF in Braunschweig and taken into operation. At this model device both sample geometries could be fabricated. Cutting velocity and honing angle were with honing v_c= 1 m/s and α = 25°. For „rough" honing, the honing performing specification 030/710/6/75 was used; with ,,fine" honing was used honing performing of the specification D7/512/1/100.

In order to be able to lap and polish the cylindrical and toroidal lateral surfaces of the ceramic samples, a special construction was necessary [34]. The samples were pushed vertically on the buffing wheel and could unreel freely by a turning bearing (compare Fig. 18). For the toroidal samples a groove with the required radius was pivoted in the buffing wheel. Since this groove could be straightened only at large expenditure, the toroidal samples were swivelled back and forth. In this way the radius groove wore out uniformly. By free unreeling of the samples an erosion from contortion of the lapping grains came off; the lapping grains were pressed into the surface of the work pieces and brought out material particles.

In order to reinforce the erosion process, the coils were placed measured diagonally around the helix angle a from the tangential direction. Thus a slip motion between coil and buffing wheel in radial direction was created. In this way grains, which settle occasionally in the buffing wheel surface, caused an additional erosion by cutting grains.

A suitable apparatus positioned the samples on the buffing wheel and created by means of an adjustable weight the necessary contact pressure. Since here, in contrast to plane-polishing, it is a matter of a line contact, the application forces were clearly higher. With an estimation of the physical width of the contact surface resulted contact pressure of 1.3 to 13.8 N/mm². With plane-polishing usual values are around 0.05 N/mm².

The samples were lapped in this way and partially polished afterwards. In each case a „rough" specification and a „fine" specification were selected. As lapping grain, boron carbide with average grain size of 30 and 7 µm was used. It was mixed up in the ratio 1:2 with water. For polishing, diamond grain with 3 and 1 µm grain size was used. The polishing suspension was mixed with water and glycerine.

In Fig. 19 are represented the allowance for the individual treating steps. Starting situation was always a pre-ground surface. It was guaranteed by the sequence of the different finishing methods that the edge zone created was affected only by the final manufacturing process [34]. With the very finely worked function surfaces (fine polishing) a shorter operating time could be achieved by the process applied here.

The treating specifications of the finishing of the function surfaces of the ceramic rolling members are to be inferred in summary from table 8.

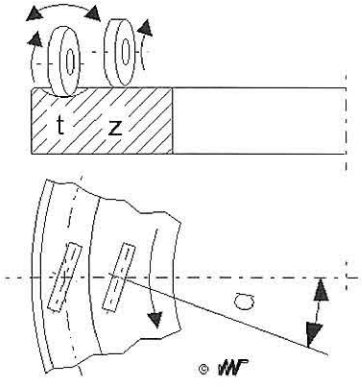

Fig. 18
Cinematic arrangement of the test specimens on the buffing wheel during the surface finishing;
t: toroidal coil,
z: cylindrical coil,
a: helix angle

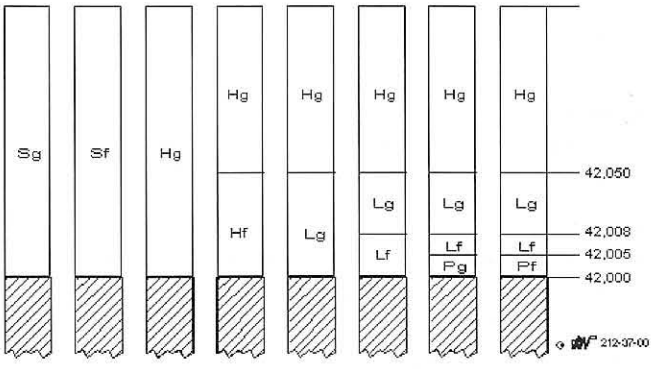

Fig. 19
Allowances of the finishing steps with the different process chains. The abbreviations mean: Manufacturing process: S: Grinding, H: Honing, L: Lapping, P: Polishing, as well as g: rough and f: fine

Table 8
Treating specifications with the finishing of the function surfaces of the rolling samples at the IWF of the TU Braunschweig [32]

Grinding:		Lapping:	
Grain size	D126, D 64, D15	Lapping grain	B 30, B 7, F 240
Diamond concentration	25 Vol.-%	Normal force	2 N
Binding	ceramic	Lapping medium	water with additives, grain to water 1:3 by vol.
Cutting velocity	30 m/s		
Cooling lubricant	Oil, Variocat G 500	Lapping-grinding speed	0,6 m/s
Honing:		Polishing:	
Grain size	D30, D7	Polishing grain	D 3, D1
Diamond concentration	25 Vol.-%	Normal force	3 N
Binding	ceramic	Polishing medium with glycerine admixture	aqueous suspension
Contact pressure	$p_n = 3$ N/mm^2		
Tangential honing speed	$v_t = 1$ m/s	Polishing grinding speed	0,6 m/s
Axial honing speed	$v_a = 0{,}2$ m/s		
Cooling lubricant	Oil, Honilo 930		

5 Acousto-microscopy / Non destructive testing

In the context of this work the acousto-microscopy for the characterisation of tribological stressed test specimens was developed and its informative capability was verified.

It had been assumed in the apron that with the acousto-microscopy treating-caused surface defects at and beneath the surface as well as defects originating tribologically in the wear tracks can be detected non-destructive.

5.1 Principle of acousto-microscopy

The principle of the acousto-microscopy involves a special echo process. The sample, which lies in ,,field of vision „ of the lens, is sensed by the acoustic lens point for point and the resulting picture is built up electronically. The wave outgoing from the focus is broken at the sample surface or in the sample volume; in addition, on irregular structures, as for example, cracks, the wave is scattered, bent, in some cases absorbed and reflected.

Special acoustic lenses with large aperture and beam widths from 60° to 100° cause the conversion of a section of the acoustic wave into a Rayleigh wave (surface wave). At the piezoelectric converter (compare Fig. 20) a signal originates which is composed through the interference of the reflected rays [35]. This signal is sensitive to a change of the (sound) path as well as the speed of sound (running time). Local changes in the sample material cause a change of the speed of sound and thus act on the signal contents; this is represented as image contrast. The photometric light-dark contrasts thus permit references to mechanical-elastic parameters of the sample material [36].

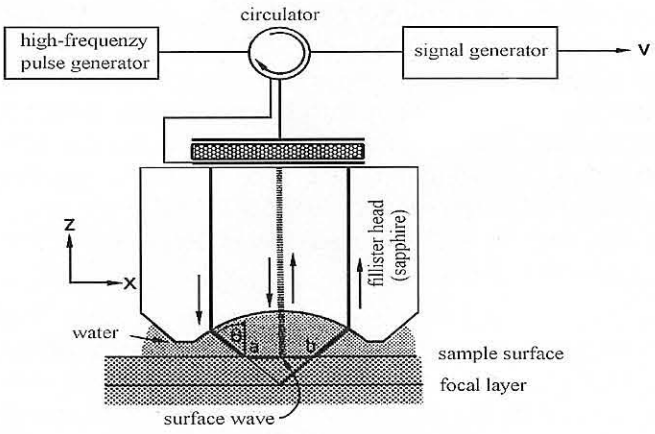

Fig. 20
Schematic representation of the sample arrangement and of the path of rays in the acousto-microscope.

The penetrating power of the acoustic waves is dependent on the irradiated wavelength, the greater the irradiated frequency, the nearer the surface can be observed.

5.2 Advancement of the measuring method

The tests for the characterization of the probes showed that with the measurement of parameters that are important for the application, such as focus tube length, focus tube diameter and probe spectrum of the reflector used and the length of the probe cable, the measurement results can have a crucial effect. For the planned acousto-microscopic tests new wide-band probes inclusive of the

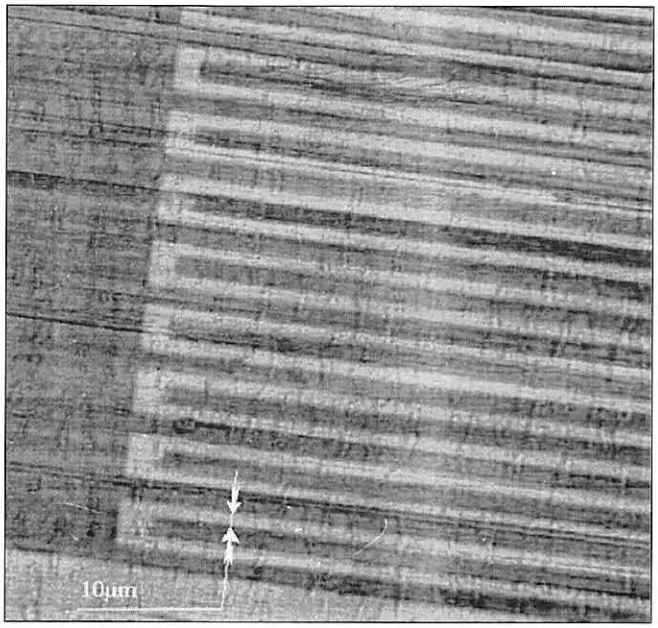

Fig. 21
PVDF-foil with structured gold contacts

secondary electronics had to be developed, since for this there were no commercial offers available.

The middle frequencies of the probes were at 7.5 MHz and the bandwidth was 10 MHz. For this tests with PVDF foils were done (compare Fig. 21), which permit the treating with the conventional steps of the microelectronics. The transparencies are between 5 and 50 µm thick. With them ultrasonic waves to over 100 MHz can be incited, which is dependant on the concrete transparency strength. The tested foils were 40 µm thick and coated with 100 nm gold. The electromechanical coupling factor corresponds to approximately that of the zircondioxide. Due to the low acoustic quality of the material, the converters possess a large bandwidth. For the field use in the impulse reflection method, the high tension strain is substantial.

In order to achieve the desired loss reduction, a special matching circuit had to be realized, so that an effective charge is possible in the inspection technique. With the same technology a phase-sensitive converter was developed and built for the acousto-microscope. Moreover a 32-Element-Array was planned, whose acoustically active structure was produced with the photolithography.

For the generation of the complex structures on the transparencies, the standard photolithography is used. With this it is possible to create on the transparency, structure widths of less than 10 µm and lower edge roughness. The contacting of the guidance tracks on the transparency with external electric connections happens at present with printed circuit board plugs or with conductive epoxy resin.

The PVDF foil is used as piezoelectric converter, since it combines the characteristics of a large transformation bandwidth and a lighter mechanical shape and management. Thus the transparency is exceptionally suitable to also realize more complicated converter surfaces and structures. It affects disadvantageously the high electric impedance and the lower electromechanical couple factor compared with other converter materials. These disadvantages can be compensated, however, within certain limits by more complex electronic arrangements.

One of the tasks was the characterisation of the (non-flat) lateral surfaces of the rolling samples by means of acousto-microscopy; for this reason an advancement of the acoustic lens had to take place, since the use of dynamically balanced acoustic lenses does not permit the dissolution of direction-controlled material properties.

In the following the results of the probe (lens)development and the electronic circuit concept are represented. In Fig. 22 the schematic construction of such a lens is shown. A point-focused radiation pattern is realized through this construction. Segmenting the oscillator and the epoxy resin stratum into four sectors divides the lens into right-angled to each other, completely independent radiation ducts.

With the technological means available, focal lengths between 5 and 20 mm can be set with a beam width to 80°. The lenses can be used in the frequency range of 5 to 50 MHz without new adjustment. By the realization of a curved converter area, acoustic focusing means in the path of rays can be dispensed with. Are omitted suitable lens echoes, which would affect the interference level noticeably.

For the operation of the sector lens, the construction of a transmit channel and two separate receiving channels was provided and realized. An HF burst is used as exciting signal for the sectors working as transmitters.

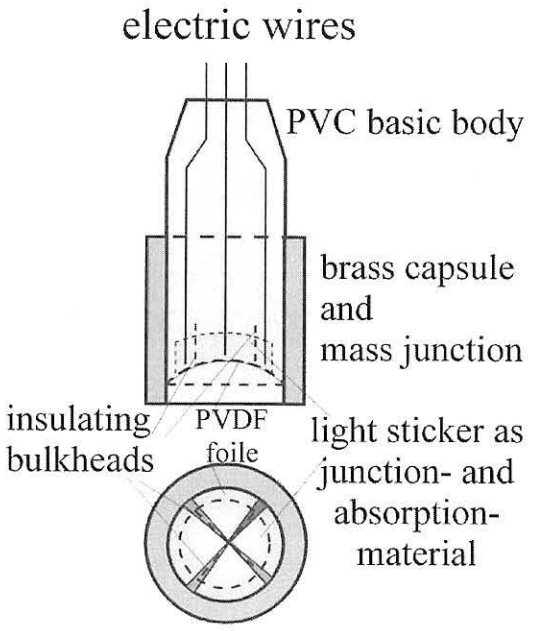

Fig. 22
Schematic construction of a sector lens

Its generation takes over an HF generator, an electronic switch and a square-wave generator. The required 20 V of peak voltage are applied by subsequent reinforcement in a power amplifier. The high impedance of the transparency requires special adapting amplifiers and measures for the compensation of capacitive loads. Although the lens system permits high bandwidths, a band limitation results on the already set frequency range here. Over a delay unit, a second duct of the square-wave generator and corresponding HF switches are filtered temporally cross talk and other interferences. The resulting information signal is continued to reinforce low-noise, used in parallel and over a digitization to the screen layout.

A control computer takes over the controlling of the mechanical cross table and the computational image editing. Thus its own acousto microscope resulted, which permits some new measurement principles apart from the conventional mode of operation. Measuring speed is limited at present by the used cross table to approximately two minutes for 200 x 200 pixels.

By integration of an axis of rotation into the test assembly the measurement of cylindrical surfaces became possible, whereby the function area under the measuring lens to be measured is rotated away. With the construction of the sector lens (see Fig. 22) and the development of the pertinent measuring technology, the selective representation of structures with treating-conditioned preferred orientation is a success. In a measuring course transversal cracks and longitudinal grooves can be selected at the same time over separate ducts. In contrast to the conventional ultrasonic microscopy, here the surface is no longer illustrated, but rather an accurate position of the defects is determined. With a large work distance of approx. 2 cm this process is suitable for a surface inspection that can be automated after treatment processes and adaptable with corresponding manipulator guide at complicated surface forms.

One of the benefits of the ultrasonic microscopy is the low preparative expenditure before the tests, i.e., the samples to be tested can be built in without reduction. The exclusive detecting of defects is possible by means of fading in and out of the background signals. Large areas can be tested by unreeling the lateral surface and from this results thus a good synopsis of the structures and defects of the function area.

6 Model representations for the slip-rolling wear

In the context of the task, wear mechanisms are to be regarded as consequence of the tribological stress and of the finishing operations. The aim is that the material is machined free of sub-surface damages during the finishing, so that the wear rates remain small during the tribological operation.

6.1 Wear mechanisms

The wear mechanisms describe the interaction between basic and counter specimens during the tribological stress. The different mechanisms that influence the friction and wear processes are adhesion, tribo-oxidation, abrasion and fatigue. These different mechanisms are represented schematically in Fig. 23 and are described in DIN 50320 [37].

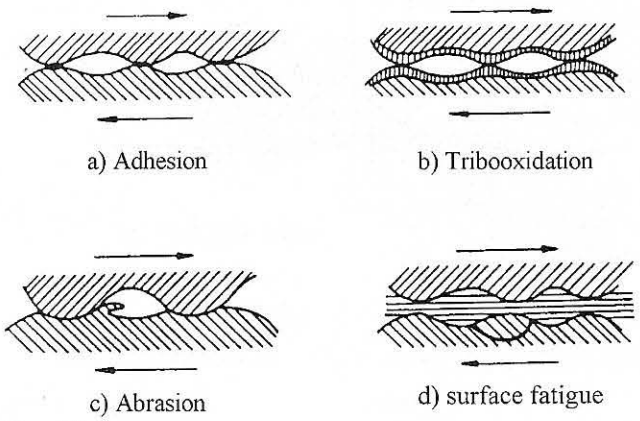

Fig. 23
Schematic representation of the different wear mechanisms

In the following these mechanisms are described briefly and are thereby particularly examined on the mechanisms with ceramic tribo contacts:

a) With the adhesion it comes to formation and separation of atomic bindings (micro welding) between the two triboelements.
With ceramic materials the tendancy to adhesion is very low due to the ionic and/or covalent bindings. The required surface energy for cracking of these kinds of binding is substantially higher than, for example, for metallic bindings. The low tendancy to micro welding becomes favourable also through the small microcontact area resulting from the high hardness and the high E-module. Moreover, with the materials SiC and Si_3N_4 these substances possess no melting point, but they do possess a decomposition temperature, and the plastic ductility is reduced.

b) The tribo-oxidation is a tribologically enhanced chemical reaction of both specimens with components of the lubricant or the environment medium.
Both oxide and especially non-oxide ceramic materials are subject both under dry friction as well as under lubricated conditions to the tribologically caused chemical changes of their surfaces. With these materials usually light, passive reaction layers form. Thus with ceramic materials, smaller layer thicknesses, which are due to a tribo-oxidation, are to be expected than with metallic materials.

c) With the abrasion there is a cutting, ploughing and a micro-machine cutting of the basic specimen from hard surfaces asperities of the counter specimen or from particles in the interfacial media.
The processes with the abrasive wear can be categorized according to K.-H. Gahr [38] as follows:

Micro-ploughing
occurs with ceramic materials only at high temperatures or high contact pressures. The mechanism is justified on the effect of an individual abrasive particle and leads only to plastic deforming and not to material removal.

Micro-cutting
here in the ideal case a splinter/debries with the same volume as the resulted furrow forms.

Micro-chamfering
is with ceramic materials the prevailing mechanism and is characterized by breaking out of larger abrasion particles than the resulted furrow forms. The brittleness and the low plastic ductility of these materials result in increased lateral cracking as well as crack growth in the area of high stress concentrations and finally break-outs low in deformations of abrasion particles at the workpiece surface.

Surface fatigue
The surface fatigue is the result of cracking and crack growth up to separating of particles due to cyclic mechanical loads. These stresses are effective in the surface areas of the two bodies. The areas of conflict result due to a mechanical surface load or in the unlubricated operation from conversion of the friction loss power into heat, from which an elongation of the sub-surface area and therefore residual stresses result. Internal defects, jumps in the material properties between two or more phases and internal stresses in the material favor the surface fatigue.

6.2 The wear mechanisms of ceramic materials

The high hardness and the high E-module as well as the small contact area and the type of chemical binding of ceramic materials affect the low inclination to adhesion.

The ionic or covalent bindings of the ceramic materials are chemically very stable and contribute thus to the fact that these substances chemically are not reactive or only slightly reactive. Opposite the tribo-oxidation with metals the mostly oxidic reaction strata are softer than their substrate.

The low fracture toughness of engineering ceramics and the low plastic ductility cause a fatigue of the material due to formation and propagation of cracks. Thus the surface ruin is a relevant wear mechanism, also in the case of the dry friction or under water lubrication. On the other hand recently with Si_3N_4 and ZrO_2 duration vibration resistances have become known, so that ceramics also below a certain voltage can be contortion-firm.

The formation and propagation of cracks is involved also in the abrasion processes and can favor a separating of particles from the surface range. Due to the low plastic deformation of engineering ceramic materials the micro chamfering is the most occurring abrasive wear mechanism.

6.3 Wear mechanisms during processing

Also during the finishing of ceramic components the previously mentioned wear mechanisms and thus their effect on the surface and the zones near the surface are to be considered.

During processing workpiece and tool form a tribological system consisting of the workpiece as basic body and the tool as counter-body. It leads to a material removal with effects on the edge zone with the counter-body and to an abrasion of the basic body [39]. Thus during processing the known wear mechanisms occur according to DIN 50320 [37].

By the example of the grinding treating it is to be clarified how the wear mechanism comes with ceramic materials and thus an erosion of the material becomes possible.

The grinding grain moves in Fig. 24 from left to the right. First it comes to a flexible deformation of the material, then follows the cracking, as microcracks form in the material surface. Further it leads to a plastic deformation. The grinding grain is scratched into the surface. Due to the brittleness of the ceramics, splinter fragments rip out [39]. Here it is to be recognized that it does not come to a removing splinter as with metallic materials, which are very plastic ductile.

The test results achieved are regarded among other things also concerning the rate of material removal during the finishing. This rate of material removal is a usual size for the material removal in [mm³] during processing in relation to the time required for it in [s].

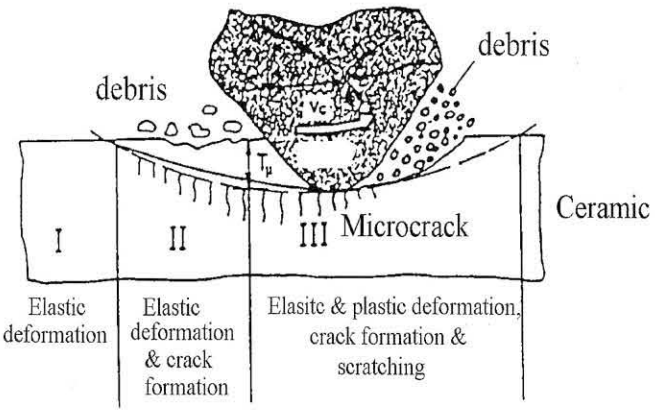

Fig. 24
Wear mechanisms during the grinding machining

7 Test results

With the slip-rolling tests in the context of this work the same kind of engineering ceramics were always used and the tribological surfaces were also usually finished in the same finishing process. The different materials used are described in detail in chapter 2. The machining of the tribological area is treated in chapter 4 and is listed in the overview in table 8.

Before the beginning of the tribological tests the roughness parameters of C.L.A. (R_a) and R_z were determined according to DIN 4768 [40] and R_{vk} and R_{pk}, according to DIN 4776 [41] (now as DIN EN ISO 13565-2:1998) as well as the outline profiles for the quantitative determination of the wear rates.

In order to be able to make a statement about the treating-conditioned effect on slip-rolling wear behaviour, several manufacturing processes were used for each material, which produced varying roughnesses and morphologies of the function areas. Statements about the effect of machining could be made by this procedure. With some materials it could be shown that a ,,the best as possible" machining does not consequently lead to the lowest wear rates.

The test series were accomplished with different interfacial media in order to be able to also consider the effect of the interfacial media on the wear and fatigue behavior. As interfacial media paraffin oil without additives or de-ionized water was used. Some the materials are not suitable for a water lubrication, therefore these test series up to some few tests were not continued any further.

The widely varied test program permits a purposeful statement on how the suitable material for a good and economical wear behaviour should be machined.

The test results are represented arranged in the following according to the different materials with a closing comparison of different engineering ceramics. In the unit all result sizes for each individual tribological test are listed in tabular form in the annex.

7.1 HIP-Si_3N_4 (NBD 200)

The material description for HIP-Si_3N_4 (NBD 200) is to be found in chapter 2.1.

7.1.1 Tests in paraffinic oil

For the rolling wear tests of HIP-Si_3N_4 in paraffinic oil the same type processed rolling members were used. Due to the good slip-rolling behaviour of the material a comprehensive testing program was accomplished. The machine settings of the test series are to be inferred from chapter 3.1.

7.1.1.1 Friction

The coefficients of friction can be documented dependent on the contortion/revolutions numbers (see Fig. 25). From Fig. 25 it is to be clearly recognized that the friction coefficient for the individual tribological test varies only slightly from the beginning of the test up to its end by a revolution number of $n = 2*10^6$. Altogether regarded the coefficients of friction lie also only in a narrow range from $f = 0.04$ to around $f = 0.12$. The roughly polished test specimens, which exhibit a relatively rough function surface, show also the highest friction coefficient over the total duration of the test. The lapped and polished sample surfaces exhibit a middle friction value, while the honed show the lowest friction values.

Already with the coefficients of friction it shows up that with the material HIP-Si_3N_4 under rolling friction in paraffinic oil the finest finishing also does not lead to the lowest coefficients of friction.

The almost constant friction values for the respective treating parameters let it be assumed that in all cases an „individual roughness" sets or originates itself automatically. Initial surface roughness is dependent on the manufacturing process, thus the manufacturing process affects the occurring friction.

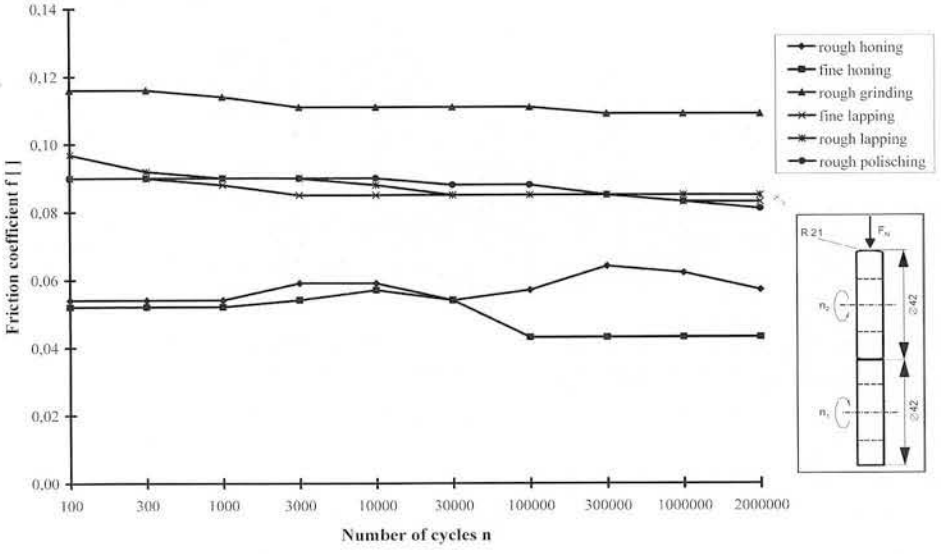

Fig. 25
Coefficient of friction of the number of revolutions for the material HIP-Si_3N_4 with slip-rolling friction in paraffinic oil

7.1.1.2 Wear

Generally the wear rate of the material HIP-Si_3N_4 with the slip-rolling friction in paraffinic oil is low and lies depending upon the kind of finishing of the surfaces between values of 0.06 and 30.2 x 10^{-9} [mm^3/Nm] for the individual test specimens. The wear rate increases with increasing initial surface roughness, i.e. with increasingly rougher finishing process, which also means that the rate of material removal for the processes used here increases.

For material HIP-Si_3N_4 it is valid that the lower the wear rate/coefficient, the finer the finishing process. However the wear rates becomes only slightly lower from the manufacturing processes of the fine honing or precision grinding for polishing. This means that the polishing treatment can be dispensed with if a slightly higher wear coefficient for the application is acceptable during running-in, e.g. gears and cams.

The spread of the wear rates with the spherical test specimens is larger than with the cylindrical, which however is on the more complicated process of the finishing, and thus on the usually higher initial surface roughnesses of the spherical surfaces. Even the coarse processing procedures, such as coarse grinding and honing show a low wear value. In Figure 26 it is evident that the wear rate for rate of metal removal of Q_w is ≤ 0.02 m^3/s exhibits an low-wear regime and in its value only slightly varied.

Gardos and Hardisty [42] bring back the low wear of the material HIP-Si_3N_4 (NBD 200) under lubrication with paraffinic oil and others to the low part of glass phase. Further, through their studies they were able to determine a connection between the mechanical characteristics of the material HIP-Si_3N_4 and the erosion rate with the finishing [42], which likewise represents a tribological stress (compare also chapter 6.3).

The adjusted surface roughness is directly dependent on the finishing. Thus it is also possible to determine surface roughness as base factor concerning the wear rate. In Fig. 27 it is clearly evident that the wear rate increases with increasing surface roughness.

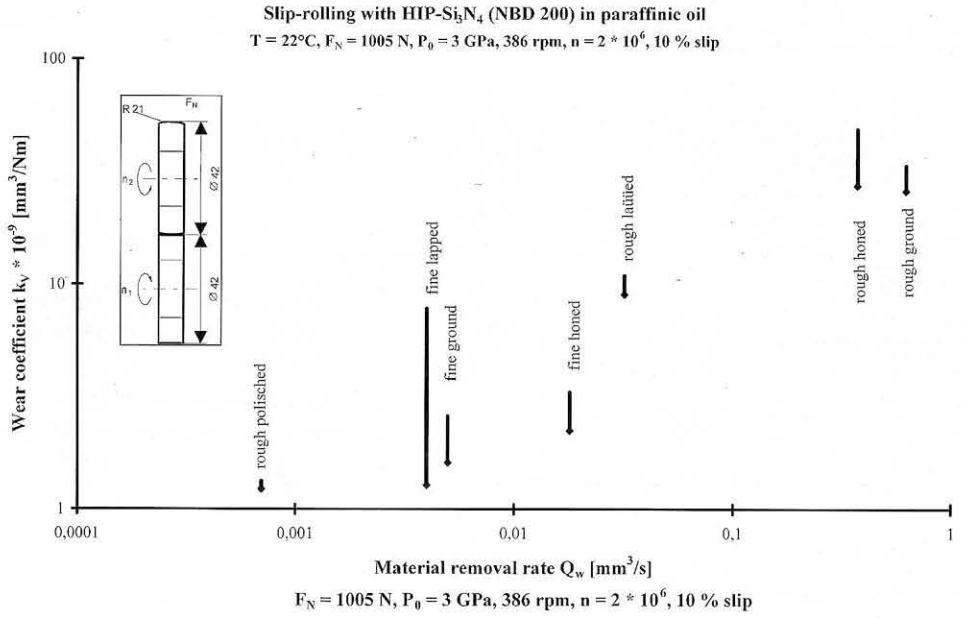

Fig. 26
Total wear coefficients of the tribo-system for the material HIP-Si_3N_4 in dependence on material removal rate

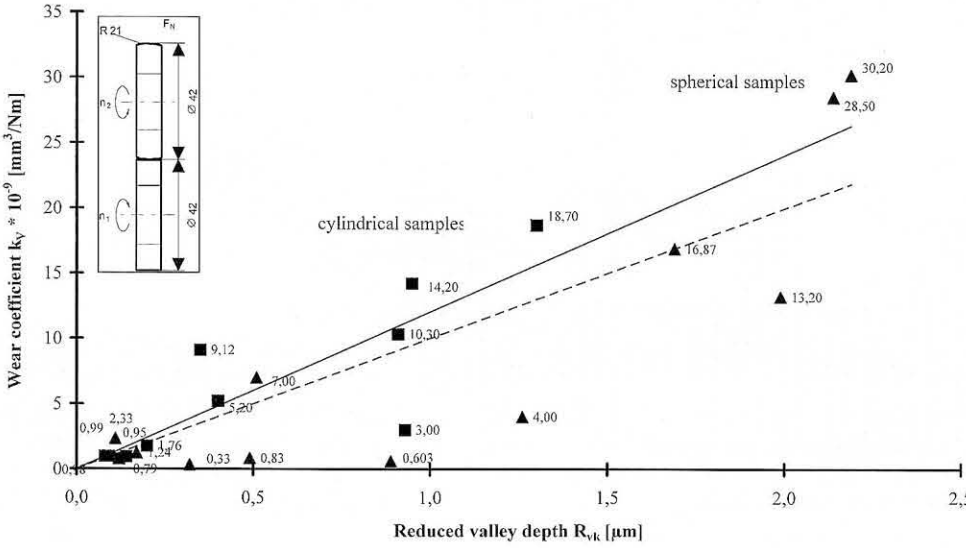

Fig. 27
Wear rates of HIP-Si_3N_4 under slip-rolling friction in paraffinic oil as function of the filtered reduced scoring depth R_{vk} [41]

Here it is also clearly recognizable that the scattering of the wear rates of the spherical test specimens is broader than those the cylindrical.

The different relations of the wear coefficient with other evaluation sizes shows that the manufacturing processes can always be correlated with roughnesses achieved and thus a direct statement about an optimal finishing of the surfaces can be made.

7.1.1.3 Surface roughnesses

The surface roughnesses are - as described above - directly connected with the finishing process of the surfaces used. The roughnesses were measured before the tribological stress and partly in the trace of the cylindrical test specimen.

If the roughness characteristic values of the reduced peak height R_{pk} and reduced valley depth R_{vk} are regarded before the tribological stress, then it is to be stated that the reduced valley depth R_{vk} exhibits a better correlation to the wear of the component. The occurring scattering of the values (compare Fig. 28) points to the fact that the filtered roughness characteristic values would have to be adapted in accordance with DIN 4776 for ceramic components. A better correlation results with the unfiltered roughness characteristic values P_{vk} [32], which is near R = 1. The filtered reduced valley depth R_{vk} points only to a correlation coefficient of R = 0.47 (compare Fig. 28).

If the roughness characteristic values of the mean peak-to-valley height R_z [40] and the average roughness C.L.A. [40] are regarded before and after the tribological load, it can be recognized in Fig. 29 that for roughly worked surfaces, i. e. a rough surface, the surface roughness in the trace is smoothed by the tribological load. However if the function areas are already relatively smooth after the finishing, then the tribological operation has only a slight or no effect on the roughness characteristic values.

For an initial surface roughness of $R_z \leq 0.5$ µm and $R_a \leq 0.2$ µm, no significant changes of surface roughness are determined after the tribological tests. On the other hand the surfaces with an initially higher roughness exhibit a kind of subsequent free „surface machining" through the intake or running-in.

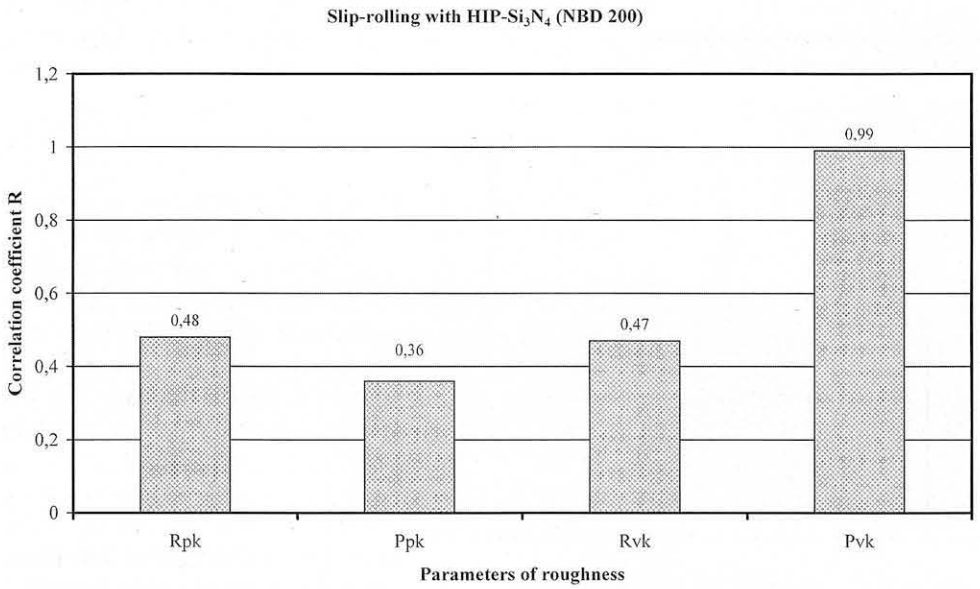

Fig. 28
Correlation between the wear coefficients k_v and the filtered (R_{pk}) and unfiltered (P_{pk}) reduced peak height as well as the filtered (R_{vk}) and unfiltered (P_{vk}) reduced valley depth

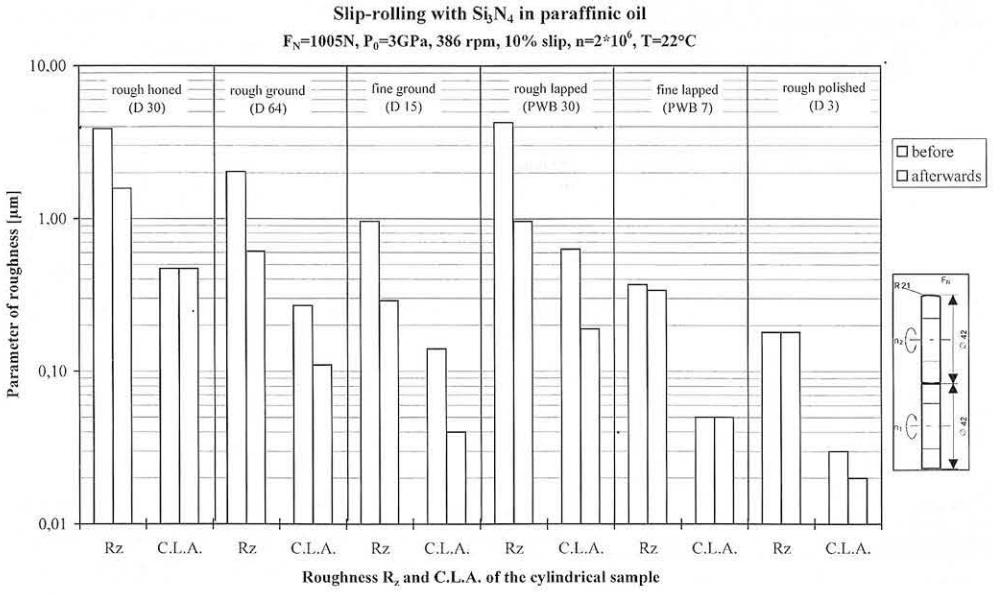

Fig. 29
Roughnesses of the respective cylindrical test specimen before and after the tribological rolling stress of the material HIP-Si_3N_4 in paraffinic oil

Generally the favorable tribological running-in behaviour of HIP-Si_3N_4 in paraffinic oil can be regarded, used and inserted as free „machining" if this permits the construction of the component.

7.1.1.4 Surface analytics

For the rolling tests in paraffinic oil, the SEM picture (see Fig. 30), for example, with a roughly lapped sample, clearly shows that the surface roughness in the track decreases.

Strong enlargements in the SEM, however, also show that these apparently smooth surfaces exhibit fine cracks in the track (see Fig. 31). These fine cracks indicate thereupon that in the case of a continued further tribological load of the rolling mating over a crack growth, damage of the function area could result (compare Fig. 36). Likewise this can be already a reference to slip-rolling wear behaviour under water lubrication, which is discussed in chapter 7.1.2.

Since the glassy phase in the material HIP-Si_3N_4 is low, chemical changes of the material in the rolling wear track are not tobe expected and also not accounted for.

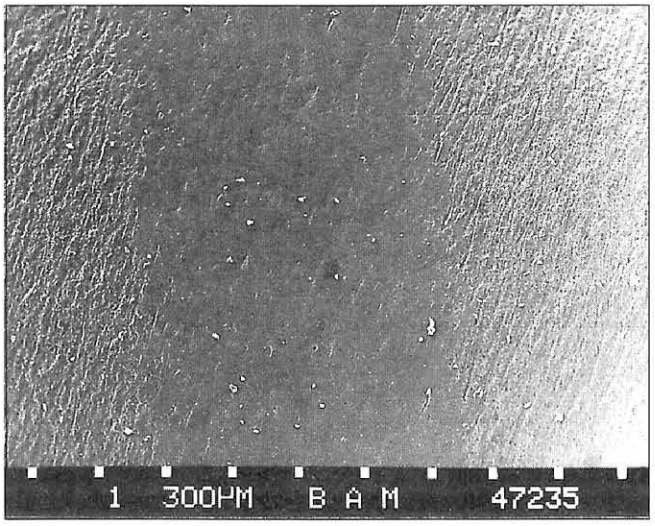

Fig. 30
HIP-Si_3N_4 roughly lapped after the slip-rolling tests in paraffinic oil

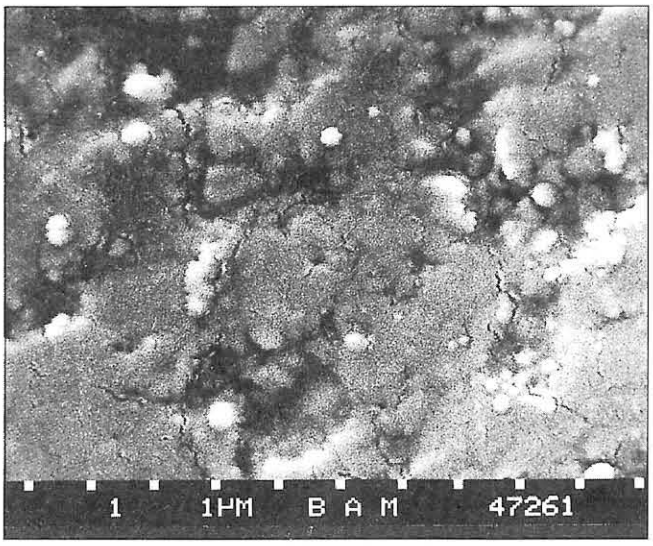

Fig. 31
Fine cracks pull through the slip-rolling track of a finely honed sampling after the slip-rolling tests in paraffinic oil.

7.1.2 Tests in water

The material HIP-Si_3N_4 proves under the rolling tests in water to be relatively stable, so that a test series can be accomplished. The machine settings are to be inferred from chapter 3.1.

7.1.2.1 Friction

The same type of HIP-Si_3N_4 test specimens show a reduction of the friction coefficient during the rolling test. The greater the initial roughness of the function areas at the beginning of the tribological load was, the more reduced the friction was. This is to be attributed to the fact that during the tribological load a kind of additional „processing" of the material in the wear track results. The wear track is after the tribological load always shining and at first sight appears to be „polished". Due to the reduction of roughness in the track and the erosion of the roughness points, the initial pressure in the course of the test (from one point to a line contact) decreases, the friction between the rolling members decreases.

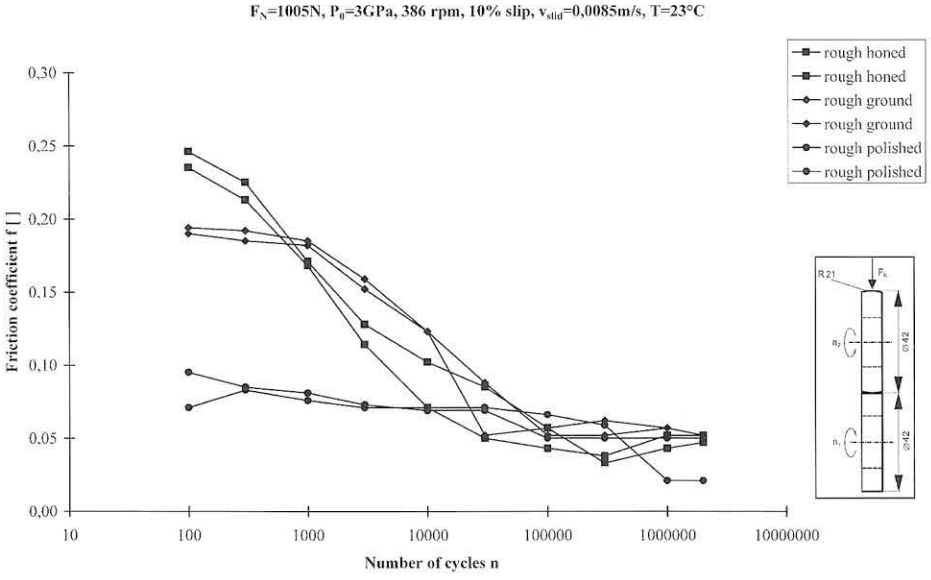

Fig. 32
Slip-rolling of HIP-Si_3N_4 in water

With this test series, the friction coefficient decreases up to a value of f = 0.05, which lies in the same range as with the tribological tests with paraffin oil lubrication.

With the tests with water-lubrication the initial coefficients of friction are clearly dependent on initial surface roughness and thus on the applied finishing process. The finely worked samples exhibit a lower initial value, in addition, a lower reduction of the coefficient of friction in the process of the stress (compare Fig. 32).

7.1.2.2 Wear

The wear rates of the material HIP-Si_3N_4 in water is approximately two orders of magnitude higher than under paraffinic oil lubrication. It is a tendency to recognize that is dependent on the finishing (compare Fig. 33). The more finely the function areas of the rolling members were worked, the lower the wear rate.

With the rolling friction with water lubrication, friction and wear show an evenly running-in behaviour. For this selected intermediate media a good and thus smoothly worked function area is of importance, for that reason here a machining according to the principle „the best as possible" has duration.

7.1.2.3 Surface roughnesses

If the mean peak-to-valley height R_z and the average roughness C.L.A. before and after the tribological stress are regarded, it is to be recognized (compare Fig. 34) that the slip-rolling results in a smoothing of the surfaces.

Contrary to the rolling tests in paraffinic oil, surface roughness decreases with the rolling test in water also with the finely worked surfaces, like the polished function areas. Thus no value can be indicated for which the surface roughness values remain almost constant, as this is possible for the tests in paraffinic oil.

Since surface roughness under the tribological load decreases, this can be regarded as „no cost", additional machining of the surfaces. This can take into account the technical designer also, if an increase of the tolerances in the component is allowed.

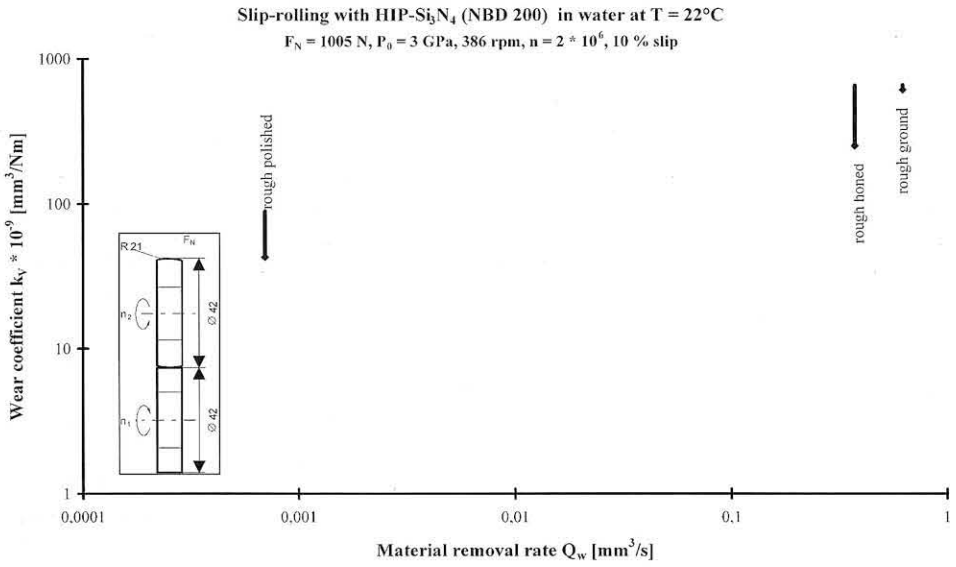

Fig. 33
Wear rates with HIP-Si_3N_4 in water.

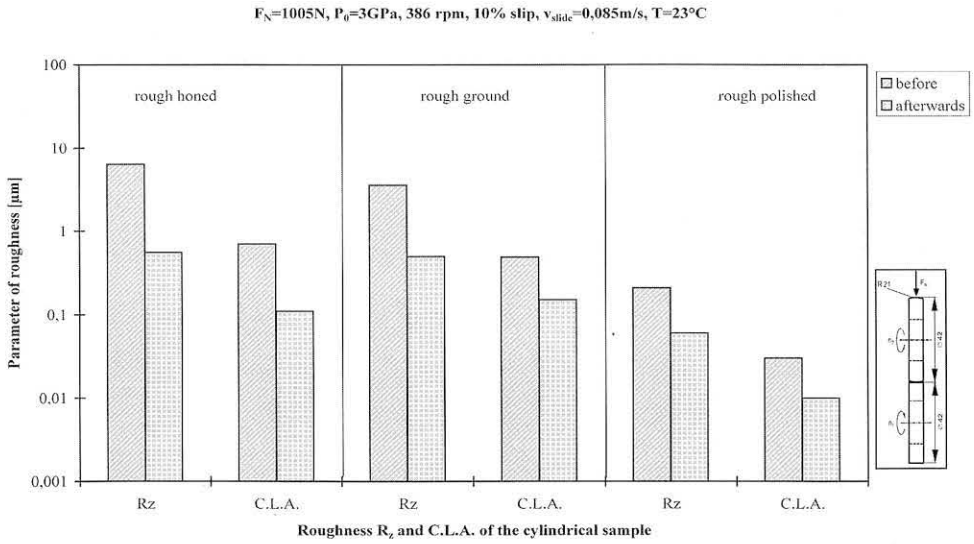

Fig. 34
Roughness characteristic values before and after the tribological tests of HIP-Si_3N_4 under slip-rolling with water lubrication

7.1.2.4 Surface analytics

Also under water lubrication there is no chemically detectable change in the wear track from the rolling load. However, here the cracking is further progressed as with the tests in paraffinic oil. From the rolling load crack networks resulted in the wear tracks, in some cases small material particles broke out as the material surface (compare Fig. 35). With a further tribological load it would come to pitting and material failure.

In Fig. 35 the resulted cracks are clearly recognizable, in addition, the smoothed areas in the wear track. Also after 2 million contortions the crack growth is still relatively low, so that the material HIP-Si_3N_4 can be used within a certain framework also with water as interfacial media.

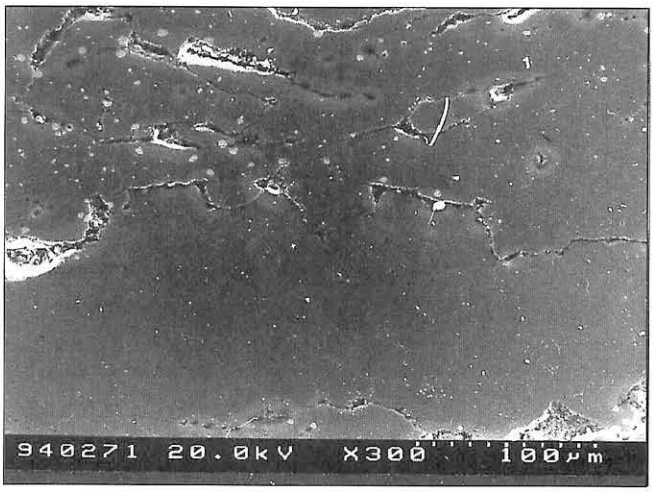

Fig. 35
SEM picture of a roughly honed sample after the slip-rolling stress in water.

At the beginning of the test, this roughly honed sample surface exhibited roughness characteristic values of R_z = 6.4 µm and C.L.A. = 0.71 µm, after the tribological stress the values were at R_z = 0.56 µm and C.L.A. = 0.11 µm. After n = $2*10^6$ revolutions, an wear rate of $k_v = 3.27 * 10^{-7}$ [mm^3/Nm] resulted. In the transverse cross section (see Fig. 36) the resulting crack system inside and below the sub-surface of the wear track can be clearly recognized. This crack network would lead in the case of a further load to a sharp rise in wear.

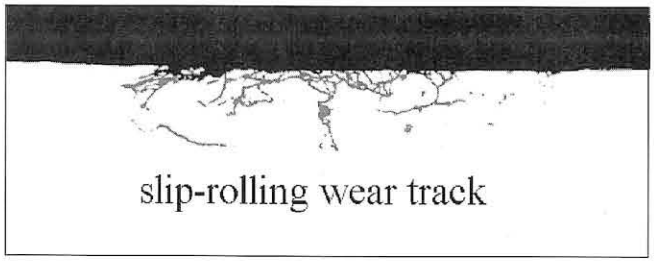

Fig. 36
Transverse cross section of the wear track of a roughly honed HIP-Si_3N_4 sample after n = $2 * 10^{-6}$ revolutions under water lubrication

The acousto-microscopy can account for the resulting crack network also in the material volumes, without - as with transverse cross section - the rolling member having to be divided and prepared. The technical procedure of this measuring method is described in chapter 5, to which one refers. From the V(z) curve the local speed of sound can be determined, which changes proportionally to occurring mechanical stresses.

The speeds of sound and representations of the distribution of velocity over the tribo-trace that were further used resulted from evaluation of the V(z)-curves at the suitable positions. The relative measurement uncertainty is 10^{-4}. With a bundle diameter in the 10°-µm range treating-conditional voltages can be quantitatively acquired over the fluctuations of the speed of sound locally referred in the µm-range.

With the roughly honed HIP-Si_3N_4 sample a deep outbreak as well as some further structures can be recognized in the light-microscope picture (see Fig. 37). A compound between these structures is not to be determined light-microscopically. The acousto-microscopic picture at 1000 MHz (see Fig. 38) shows in outlines the process of some superficial cracks. At 400 MHz (see Fig. 39) the shape of the cracks under the surface is to be pursued clearly. The strong luminance contrast in this area could be expression for the mechanical stresses built up with the rolling and their local distribution. Determination of internal stresses by XRD confirm this statement that a general (wider and integrated over larger depths) rise of the compression stress at the surface after rolling load is present.

The semi-quantitative stress analysis in the micro-range by evaluation of sound speeds by means of the acousto-microscopy supplies more differentiated statements about the lateral power distribution in comparison to Röntgen (XRD) scattering. In Fig. 40 are marked measuring positions. Increased local sound speeds (here 6814 m/s) as a sign of compression stresses occur only at positions 7 and 8 in Fig. 40 in direct neighborhood of cracks, which reach to the surface. In the bright wide zone the voltages in the seized highest surface layer are disassembled by the lateral crack which is under it and correspond to those in the surrounding field (here 6809 to 6811 m/s). The measurements of the speed of sound were accomplished at 1000 MHz, the seized depth range is at approx. 2.5 to 3 µm.

With the observation at 400 MHz (see Fig. 39) against it a depth range to 7.5 µm is evaluated. Thus the lateral crack can be located on a depth around 3 µm, while the voltage-afflicted zone remains under it.

These tests show that by the slip-rolling mechanical stresses in the ceramic material build themselves up, which disassemble themselves by the formation of crack again. The crackss can be pursued in the volume material. This crack growth leads finally to cracking of material and thus to pitting and to the material failure.

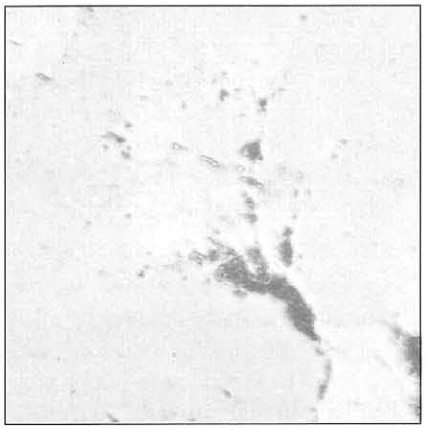

Fig. 37
Light-microscope picture of the crack area

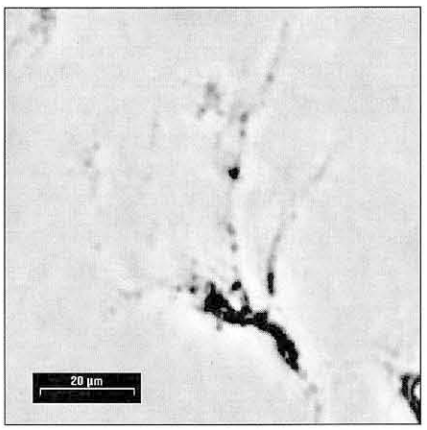

Fig. 38
Picture at 1000 MHz

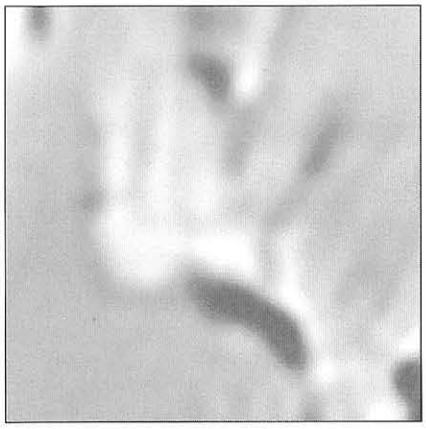

Fig. 39
Crack area at 400 MHz (recognizable the lateral crack area)

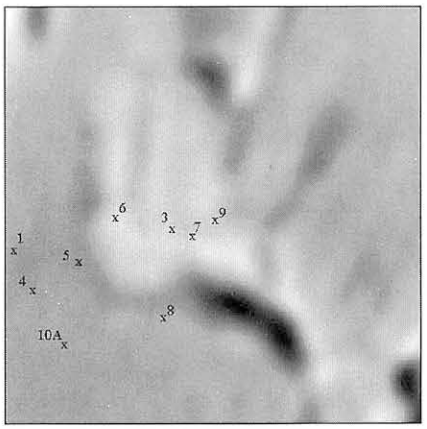

Fig. 40
Measuring points for the stress analysis over the speed of sound

7.1.3 Summary of the tests at the material HIP-Si_3N_4

The material HIP-Si_3N_4, (NBD 200) is suitable for the rolling stress both with the interfacial media paraffin oil and also limited with water. Here it is to be noted however that lubrication with water results earlier in material failure and thus the components in the field use would have to be exchanged sooner.

The wear rates of HIP-Si_3N_4 with the lubrication with paraffinic oil are within the range of 10^{-9} [mm^3/Nm], with a lubrication with water the wear rates are higher by two orders of magnitude within the range of 10^{-7} [mm^3/Nm].

For HIP-Si_3N_4 in paraffin oil lubrication a good correlation R of the wear rate/coefficient k_v could be determined with the unfiltered reduced scoring depth P_{vk}. This points to the fact that for ceramic materials probably new and/or changed roughness characteristic values would have to be determined and would have to be defined by a standardization.

For roughly worked function areas at values of $R_z \geq 0.5$ µm and C.L.A. ≥ 0.2 µm, it comes to a smoothing of the surface through the intake with rolling stress under paraffinic oil, which can be used as free „machining process", if a certain clearance increase is acceptable through the running-in.

With revolution numbers of n =2 * 10^{-6}, with paraffinic oil as interfacial media, fine cracks in the surface of the material show up. If water is used as intermediate material, the stresses brought in by slip-rolling stress disassemble themselves in the form of a crack network. With the acousto-microscope the resulting crack network is without destruction in the material reservoir detectable. From this it can be predicted that with a further tribological load of the component there would result a clod-shaped popping of the material and thus the failure of the component.

The wear behaviour of HIP-Si_3N_4 depends on the finishing of the functional surface area. The best worked areas (polished) show the lowest wear rates, however more roughly finished areas (for example, finely honed) show only slightly higher wear rates. Also less finely finished functional areas can be used by this wear behaviour. This would reduce substantially the costs of the finishing with the component fabrication.

7.2 GPS-Si_3N_4-TiN (EDM)

The complete test results with the material GPS-Si_3N_4-TiN are to be found in the appendix. This composite material was selected for the rolling abrasion studies since it concerns an material machinable by means of electrical discharge machining (EDM). This group of materials permits a machining of half-wrought material with complex surface geometry. The description of the material can be found in chapter 2.2 and the machine settings can be found in chapter 3.1.

7.2.1 Tests in paraffinic oil

The EDM material GPS-Si_3N_4-TiN permits a comprehensive analyser for the rolling friction in paraffin oil (see Appendix).

7.2.1.1 Friction

With the material GPS-Si_3N_4-TiN, for the friction coefficient, the treating of the function area is of secondary importance, if paraffin oil is used as interfacial media (see Fig. 41).

The friction coefficient changes over the test duration only insignificantly and it lies within the range of 0.11 to 0.08 for all tested surfaces. Scattering between the individual coefficient of friction values is also low for all modes o machining and over the total test duration.

7.2.1.2 Wear

The wear rates for the GPS-Si_3N_4-TiN test specimen is in the lower 10^{-9} [mm^3/Nm] range, between 0.1 and 10 * 10^{-9} [mm^3/Nm]. The rougher finishing procedures, as for example, rough honing or lapping, show the higher wear rates (see Fig. 42). The finer manufacturing processes can always be selected, if low wear rates are demanded. Also the polished test specimens show a wear rates that lies in the same range, as for example, with the fine lapping or fine honing.

The experimental results with GPS-Si_3N_4-TiN in paraffin oil show that also manufacturing processes for the finishing of components can be selected which exhibit a larger rate of material removal than, for example, polishing. The polished rolling members do exhibit the smallest wear rates; however, the wear rates here are still in a similar order of magnitude. Thus here likewise - similarly as with the material HIP-Si_3N_4 - rougher finishing processes can be used.

7.2.1.3 Surface roughnesses

For the rolling friction in paraffin oil, the material GPS-Si_3N_4-TIN shows a similar dependence as already discussed with the material HIP-Si_3N_4. The decrease of the surface roughnesses is to be noted for roughly finished function areas. If by means of the finishing of the function areas, surface roughnesses of $R_z \leq 0.2$ µm and C.L.A. ≤ 0.02 µm are achieved, the surface roughness of the function

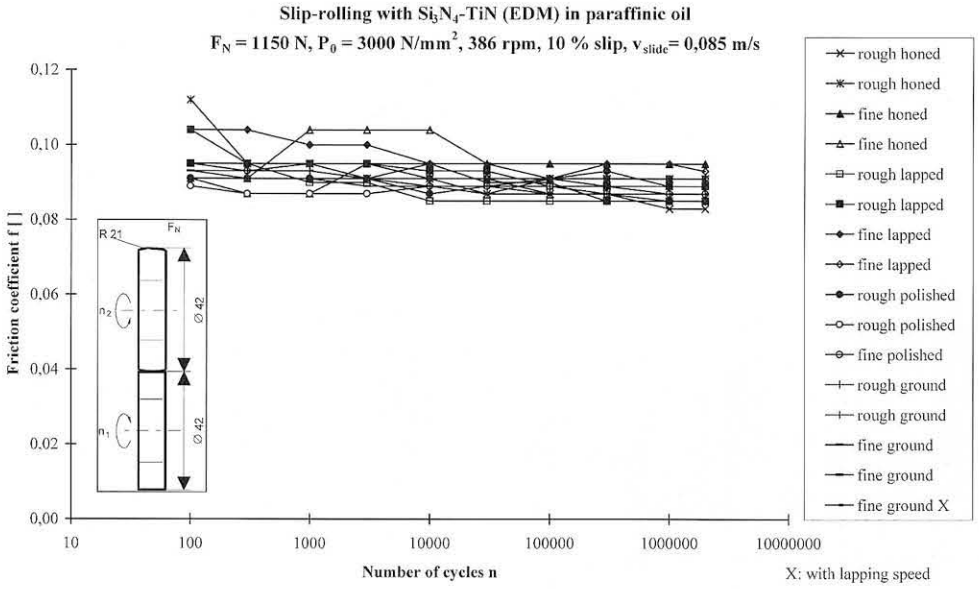

Fig. 41
Slip-rolling with GPS-Si_3N_4-TiN in paraffinic oil.

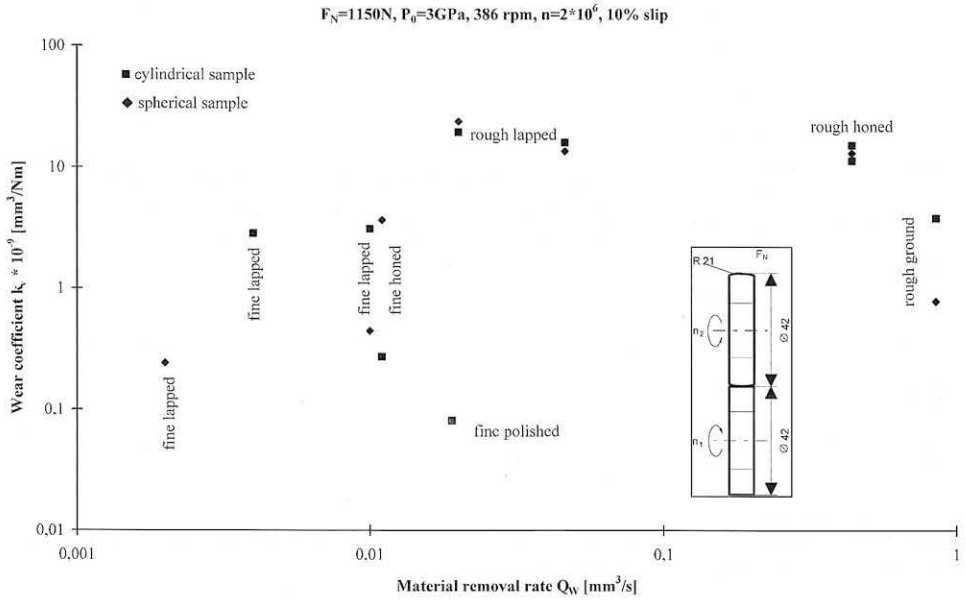

Fig. 42
Slip-rolling with GPS-Si_3N_4-TiN in paraffinic oil;
wear coefficient as a function of the rate of meaterial removal during processing

area through the tribological load does not change anymore or it changes only slightly (see Fig. 43).

If a clearance increase of the component is admissible, then also here the self running-in behaviour of the material can be used as „free of cost" manufacturing process and thus a complex and cost-intensive finishing process such as, for example, fine polishing can be done without.

The wear rate shows a clear dependence on the reduced valley depth R_{vk} (compare Fig. 44). The larger the amount of the reduced scoring depth, i.e. also, the rougher the manufacturing process, the higher also the wear rate. Here a direct dependence between wear and surface roughness is recognizable.

From the behaviour with respect to the surface roughnesses of the material GPS-Si_3N_4-TiN, it can be derived that depending upon desired area of application the material can be worked in such a way that surface roughness, wear factor and running-in behaviour optimally can be matched one on the other. If it can come to a clearance increase through the running-in and if the wear coefficient is in the lower 10^{-9} [mm^3/N] range, then finishing processes such as fine honing or fine lapping are sufficient.

7.2.1.4 Surface analytics

The tribological stressed surfaces in the SEM picture clearly show the two-phase state of the material and the smoothing in the wear track. By means of EDX the increased appearing parts of the surface can be identified as TiN phase (compare Fig. 45).

This increased concentration in the function area may have been caused by a carry-over of the TiN phase by the rolling load. Also tests in the AFM confirm a topographic increase of the function area. Although the load carrying part of the function area consists particularly of the pure TiN phase, the material shows a good wear behaviour under the rolling load.

7.2.2 Tests in water

The material Si_3N_4-TiN shows a bad wear behaviour under slip-rolling with water as interfacial media, since water

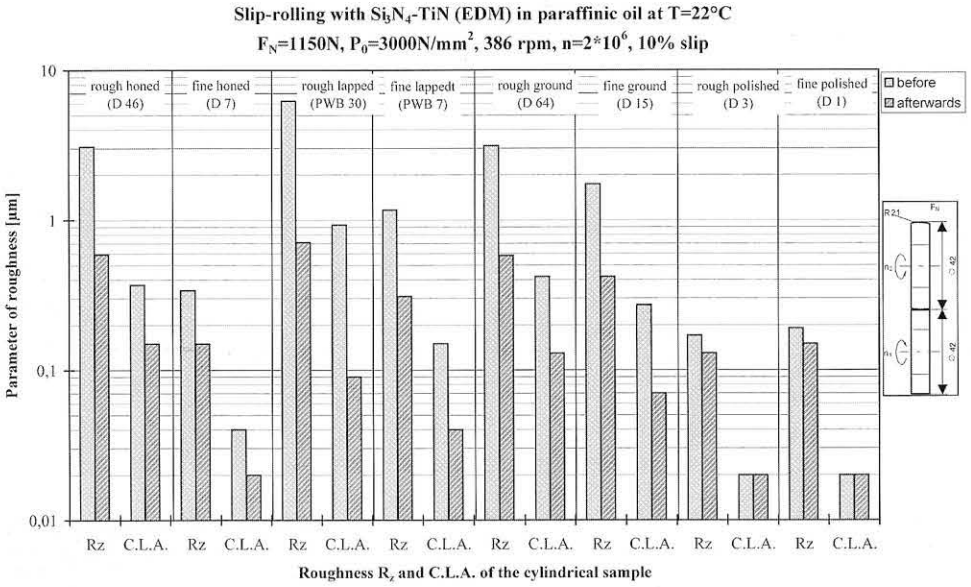

Fig. 43
Roughness parameters for the material GPS-Si_3N_4-TiN before and after the slip-rolling stress

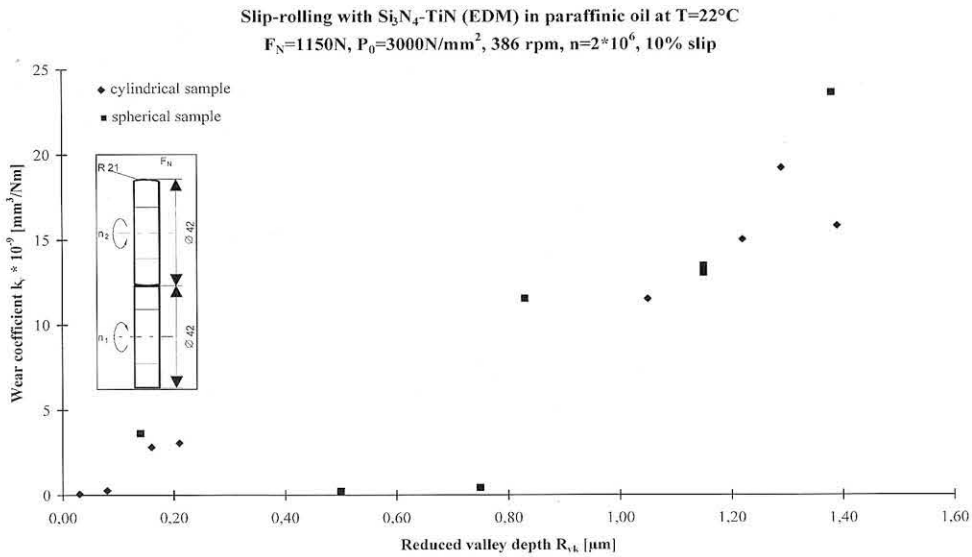

Fig. 44
Slip-rolling of GPS-Si_3N_4-TiN in paraffinic oil; wear coefficient as a function of the reduced valley depth R_{vk}

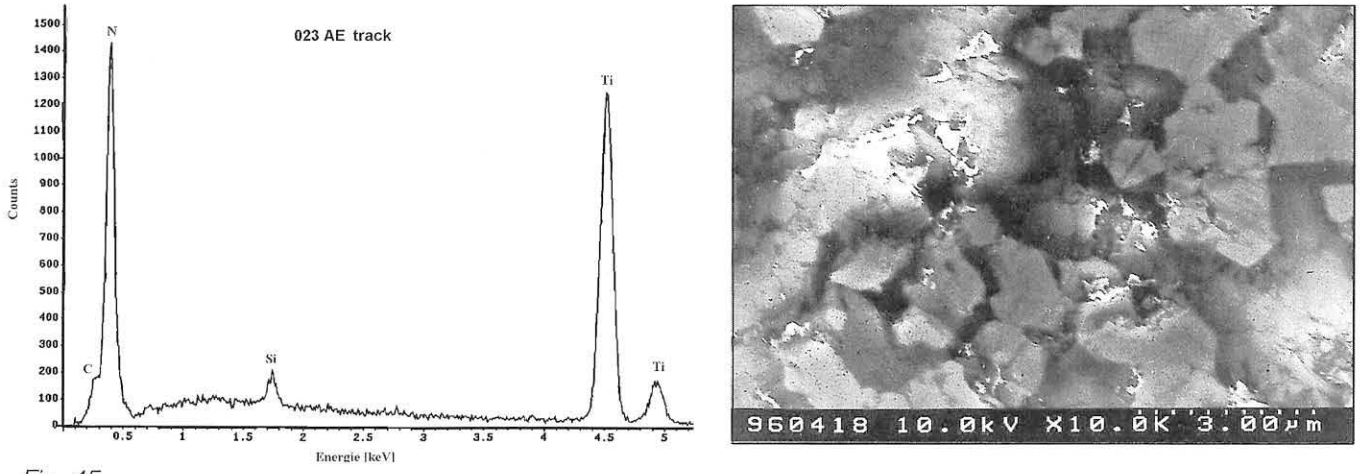

Fig. 45
EDX spectrum (left) of the higher part of the surface (see Fig. right) in the wear track of a roughly polished GPS-Si_3N_4-TiN sample after the rolling abrasion in paraffin oil

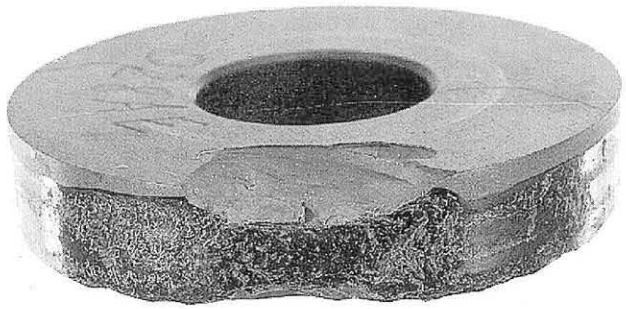

Fig. 46
*Light-microscope picture of a roughly lapped Si_3N_4-TiN sample after the rolling abrasion under water lubrication according to a revolution number of n approximately equal 1 * 10^{-6}*

dissolves TiN over titanium hydroxide. Thus it comes to pitting, wide outbreaks and material failure of the sample by breaking (compare Fig. 46). Thus the material Si_3N_4-TiN is not suitable for lubrication with aqueous media, independent of the finishing. For this reason this test series was not continued any further (see Appendix).

Dissolving the TiN phase can be accounted for also by means of EDX. The tests in the rolling trace showed that the silicon nitride part increased opposite the unloaded sample, however the TiN part dropped (compare Fig. 47).

Due to the tests it can be stated that the material GPS-Si_3N_4-TiN is unsuitable for the rolling friction under water lubrication.

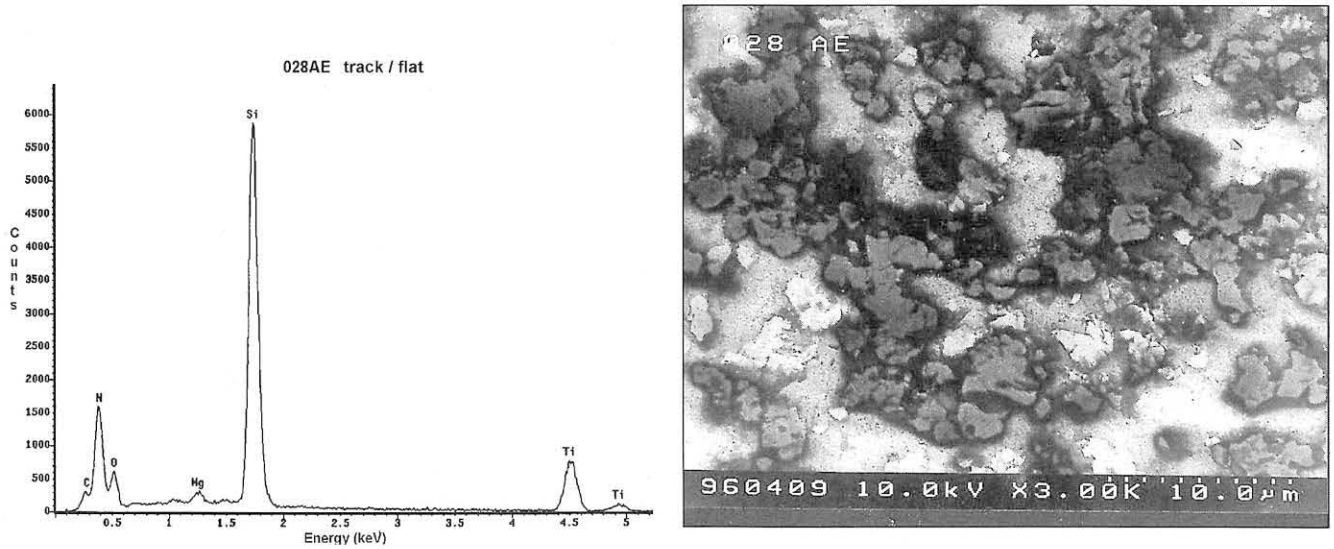

Fig. 47
EDX spectrum (left) in the wear track of a roughly lapped GPS-Si_3N_4-TiN sample after the slip-rolling in water, SEM picture right

7.2.3 Summary of the tests on the material GPS-Si_3N_4-TiN

For the slip-rolling with paraffin oil the material GPS-Si_3N_4-TiN shows up as suitable as interfacial media. The wear rates lie in the lower 10^{-9} [mm^3/Nm] range. The friction coefficient changes over the test duration only insignificantly.

If surface roughnessess of $R_z \leq 0.2$ µm and C.L.A. ≤ 0.02 µm are achieved by means of the finishing of the function areas, the surface roughness of the function area does not change or changes only slightly from the tribological load. The intake behaviour can be used as „free of cost" additional manufacturing process.

Good results are achieved also for finishing processes such as fine lapping or fine honing. Thus a costly and time-intensive finishing of the function area, for example, by means of fine polishing, can be done without.

The material Si_3N_4-TiN is not suitable for lubrication with aqueous media, independent of the finishing, since water dissolves TiN as titanium hydroxide. This behaviour leads to pitting, wide outbreaks and material failure of the sample through break.

7.3 SSiC (EKasic D)

The material SSiC (EKasic D), which was introduced to the market and which is good for sliding bearings and seals was tested under slip-rolling stress. First the same test conditions were used as for HIP-Si_3N_4 in ball and roller bearings.

7.3.1 Tests in paraffinic oil

The tests in paraffinic oil revealed that an initial load of the material SSiC with a initial Hertzian pressure of $P_0 = 3$ GPa is too high, therefore the Hertzian pressure was lowered to the half value $P_0 = 1.5$ GPa, which led to a normal force of $F_N = 250$ N (for this see also chapters 3.4).

7.3.1.1 Friction

The value of the friction coefficient decreases with the quantity of contortions. Nearly all values lie in a range from $0.15 \geq f \geq 0.07$. A roughly lapped rolling mating and with polishing finished test specimens exhibited a clearly higher friction coefficient, which lies at the beginning of the tribological load between 0.17 and 0.23 and on values between 0.17 and 0.14 during the stress drops.

The friction coefficients for the sample mating, which were tested with a Hertzian pressure of $P_0 = 1.5$ GPa, lie in the range between 0.15 and 0.09. This corresponds to the major part of the values achieved with $P_0 = 3$ GPa. This behaviour gives grounds for the assumption that the friction value is determined rather over the intake behaviour of the material as over the pressure and/or normal force applied.

For the material SSiC no connection between friction value and surface finishing can be derived.

7.3.1.2 Wear

The wear coefficient of the material SSiC shows a behaviour that is inversely proportional to that which was observed for the materials Si_3N_4-TiN and Si_3N_4. The wear rates increases with the refinement of the finishing process, if the initial Hertzian pressure as with the remaining tested materials is $P_0 = 3$ GPa.

In the case of an initial Hertzian pressure of $P_0 = 3$ GPa, the fine finishing processes prove to be unfavourable for the rolling abrasion load. Here processes such as fine honing or fine grinding show a substantially better wear behaviour (compare Fig. 49). With the finer processes such as polishing and fine lapping, conical cracks result in the abrasion track, whereby it leads with a further continued rolling load to pitting.

Due to this wear behaviour of the material SSiC, the initial Hertzian pressure was halved and set to $P_0 = 1.5$ GPa, which according to formula II (see Chapter 3.4) resulted in a normal force of $F_N = 250$ N.

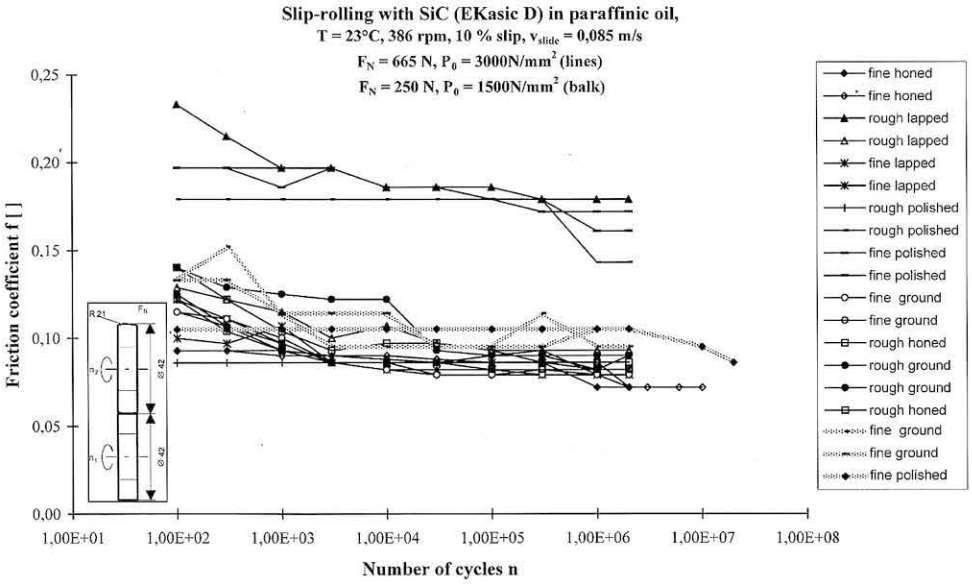

Fig. 48
Friction coefficient as a function of the number of revolutions for the material SSiC under rolling friction in paraffinic oil

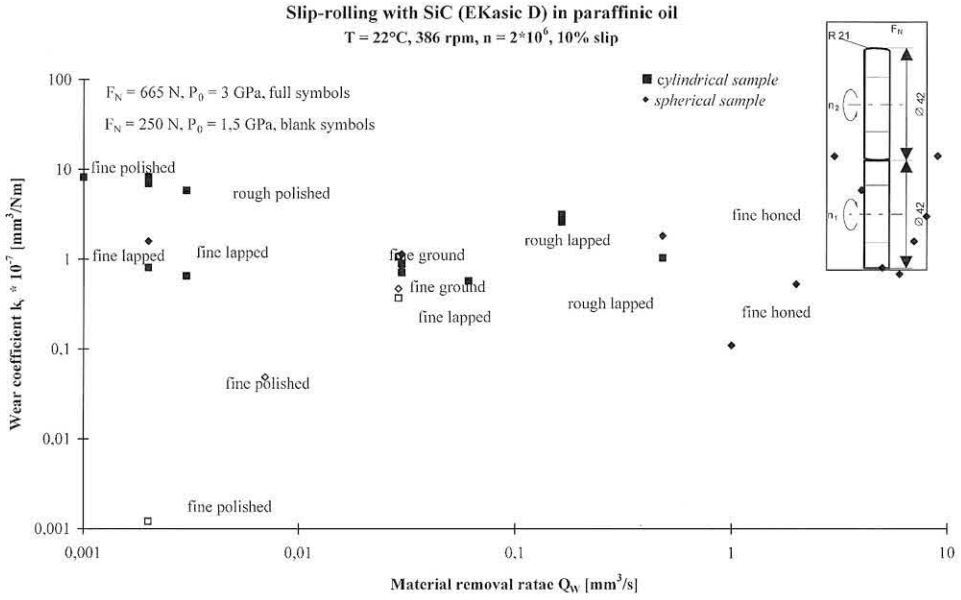

Fig. 49
Slip-rolling friction of SSiC in paraffinic oil; wear coefficient as a function of the rate of material removal with the finishing of the function areas

At 1.5 GPa the material SSiC proves to be ,,rolling fatigue resistant" under the rolling stress. The finely polished test specimens exhibit a low wear rate in the range of 37 to $110*10^{-9}$ mm³/Nm. The polished surfaces show wear rates of 0.12 to $5*10^{-9}$ mm³/Nm, if the number of revolutions is $n = 30*10^6$, after $n = 2*10^6$ cycles no wear rate is assignable, since it is too low, in order to be detected by means of profilometric method (see also for this the appendix).

As an upshot for the wear behaviour of the material SSiC under rolling friction in paraffin oil, it can be noted that with an initial Hertzian pressure of $P_0 = 3$ GPa the material is suitable only with rough finishing process such as fine honing or precision grinding for the rolling load. With a lower initial Hertz surface pressure of $P_0 = 1.5$ GPa the material is suitable for the slip-rolling, here it is generally recommended however, that the fine finishing processes such as polishing be selected in order to achieve a good wear behaviour comparable with Si_3N_4 within the range $< 10^{-10}$ mm³/Nm.

7.3.1.3 Surface roughnesses

The wear rate is not only dependent from the material removal rate, but also clearly dependent from the initial surface roughness.

As can be seen in Fig. 50, the values for the averaged roughness height and the middle roughness height for the polished surface rise after the tribological test. This behaviour in the wear track also suggests a higher wear coefficient.

At the reduced valley depth R_{vk} it can be clearly recognized (compare Fig. 51) that the smaller this surface roughness characteristic value becomes, the higher the wear rate becomes. This permits the statement that for the material SSiC with an initial Hertzian pressure of $P_0 = 3$ GPa, a low surface roughness unfavorable for the wear behaviour results. No surface roughnesses of $R_{vk} \leq 0.3$ µm should be created by means of the finishing, if the component made from SSiC is to be used for the slip-rolling.

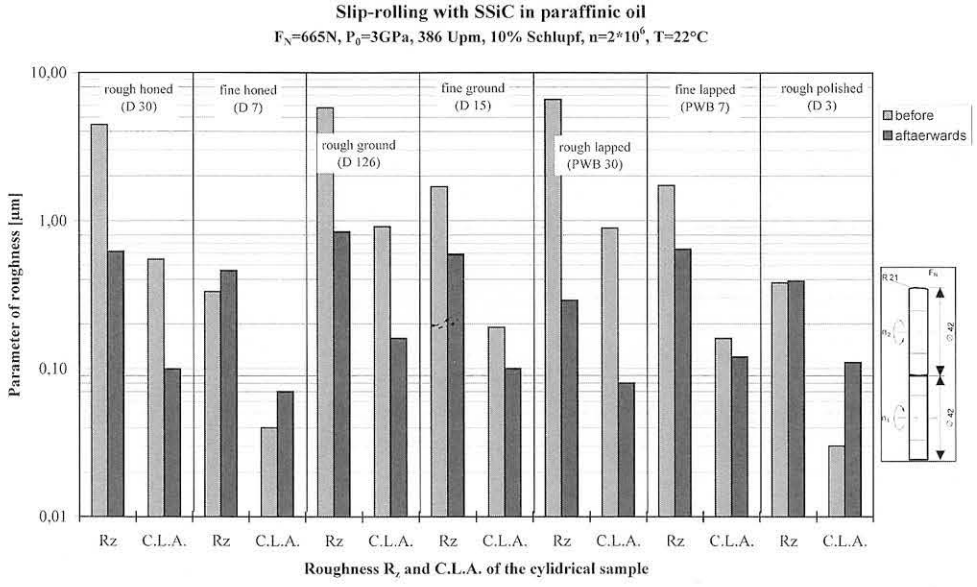

Fig. 50
Roughness characteristic values before and after the tribological test for the material SSiC in paraffinic oil

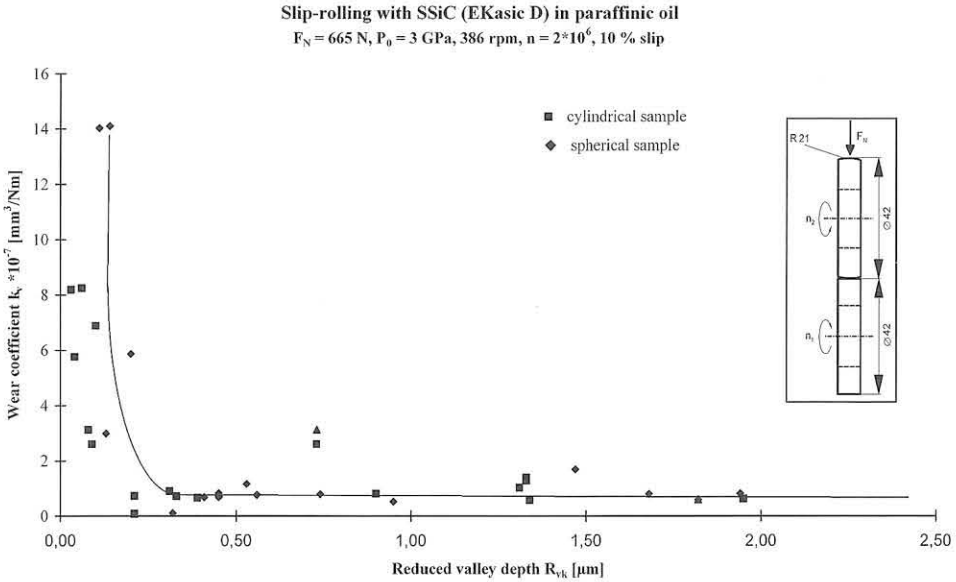

Fig. 51
Wear coefficient k_v as a function of the reduced valley depth R_{vk} with the rolling load of the material SSiC in paraffin oil

7.3.1.4 Surface analytics

The formation of cracks of the material can already be observed with the optical microscope, wherefore more sensitive processes such as REM could be done without.

It is clearly recognizable in the light-microscope pictures (see Fig. 52) that the tribologically stressed slip-rolling track of the roughly honed function area exhibits no damages from cracking. Still partially visible here is the scoring that resulted from the treating.

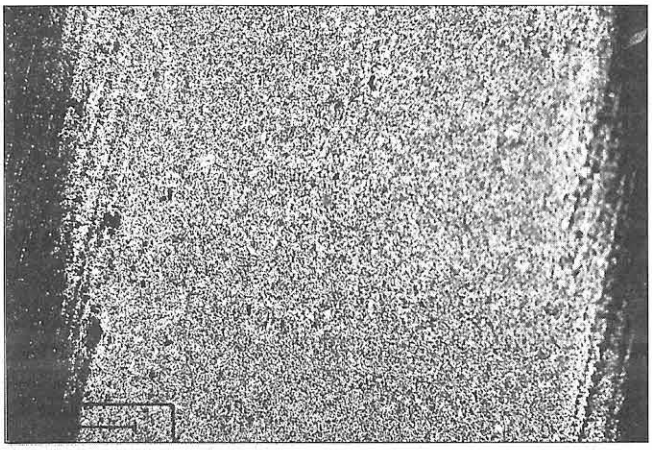

Fig. 52
Light microscopic picture of a roughly honed SSiC sample after slip-rolling stress in paraffinic oil

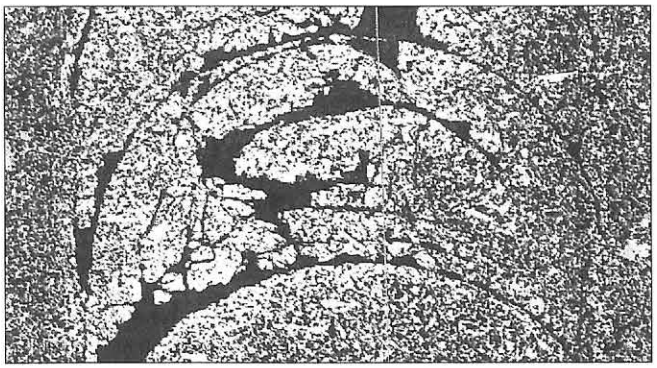

Fig. 53
Light microscopic picture of a roughly polished SiC sample after the slip-rolling stress in paraffinic oil

In contrast to the roughly honed surface the roughly polished function area shows a conical cracking in „classic form" with cracking (see Fig. 53). This visual proof clarifies the bad wear behaviour of the finely worked SSiC test specimens and the increase of surface roughness during the rolling load.

By means of the acousto microscopy information from the volume of the material is available underneath the surface. The advancement of the micro-acoustic measurement principle was applied to the interests of the characterization by slip-rolling test specimens. Micro-defects can also be detected in large areas. Through integration of an axis of rotation into the test assembly the measurement of cylindrical surfaces for rolling load has become possible, whereby the function area under the measuring lens to be measured is rotated away.

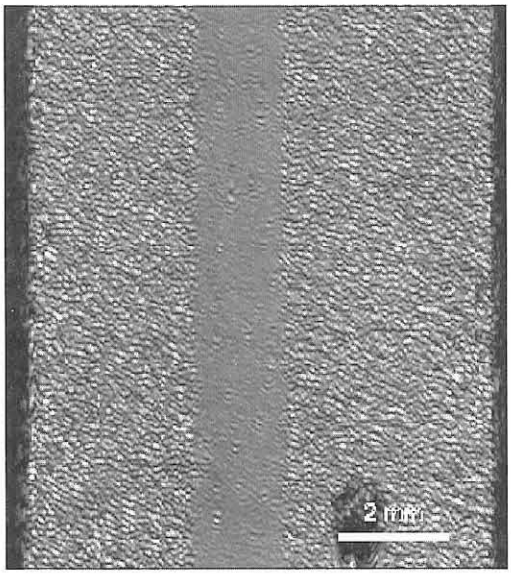

Fig. 54
Scattering signal at f=5 mm, ultrasonic microscopy on a roughly lapped SiC sample surface after the slip-rolling stress

In Fig. 54 the effect of the surface roughness with a roughly lapped sample is not switched off. These tests were accomplished with a short-focus (f = 5 mm) lens. Clearly visible are the ghost linesthrough the lapping of the function area as well as the wear track after the slip-rolling stress. The slip-rolling stress leads to a smoothing of the wear track. Thus the background signal in the wear track is reduced and a material-conditioned defect density of 1.7 cm^{-2} remains. In order to be able to detect a larger range, the cylindrical outer casing was unreeled under the lens.

The figures 55 and 56 show acousto-microscopic pictures of a polished surface after the rolling load; it concerns the same sample as in Fig. 53.

Disturbances in Fig. 55 can also be observed in the light-microscope picture (see Fig. 53) as cracks and outbreaks. In contrast to the light microscopy already disturbed areas are visible during the ultrasonic test apart from the wear track as internal stresses. These disturbances indicate thereupon that here also a further tribological load to would lead to cracking and to pitting.

The horizontal and vertical crack structures in the slip-rolling track in Fig. 56 are not detectable by light-microscope. The area shown exhibits still no pitting light-microscopically. Disturbances of the function area already shown with the ultrasonic microscopy also clearly show the internal stressed of the process.

The tests with the acousto microscopy show again clearly that the roughly worked function area (roughly lapped) exhibits fewer defects in the wear track. The polished rolling sample clearly shows scattering signals after the rolling load. Even the starting material fatigue can be accounted for with the acousto microscopy.

7.3.2 Tests in water

After the tests in paraffinic oil, bad results for the tests in water were likewise to be expected, which was also confirmed and is why this test series after a few tests was broken off.

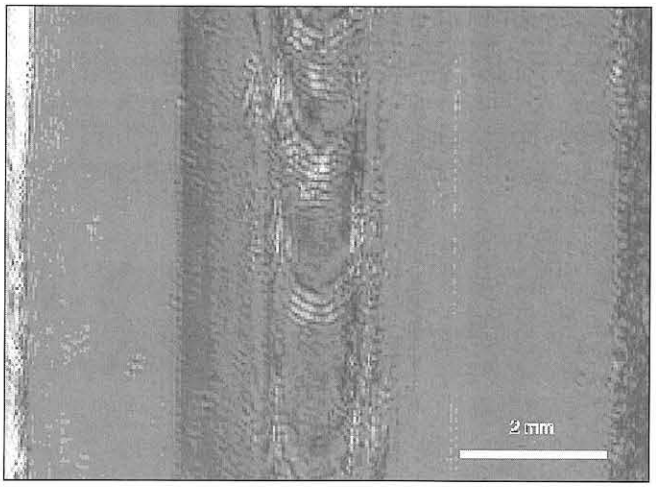

Fig. 55
Strongly disturbed area of a polished SiC rolling sample after the tribological slip-rolling tests, ultrasonic microscopy, 40 MHz

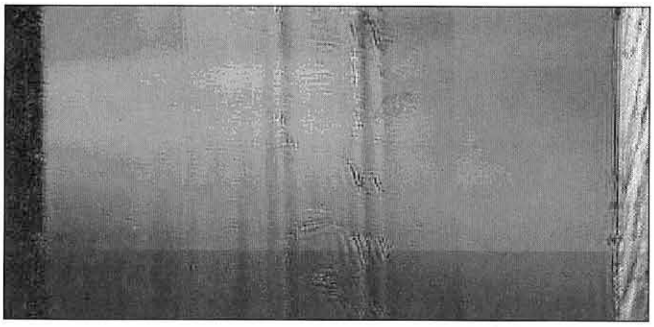

Fig. 56
Areas of starting material fatigue on a polished SiC slip-rolling sample after the tribological tests, ultrasonic microscopy, 40 MHz

7.3.2.1 Friction

The tests were accomplished with finely honed samples, which exhibited an acceptable wear rates in paraffinic oil.

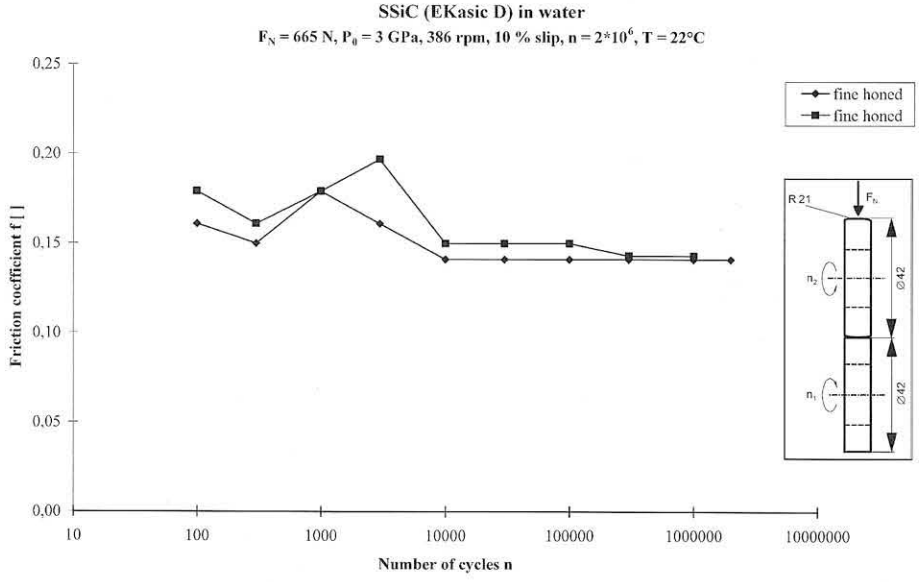

Fig. 57
Friction coefficient as a function of the number of revolutions for the material SSiC under slip-rolling friction in water

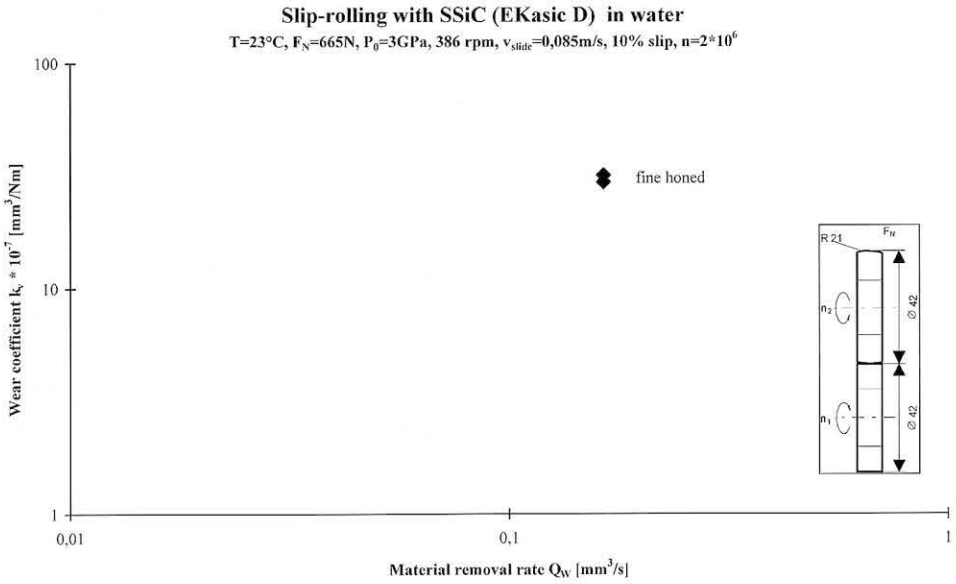

Fig. 58
Slip-rolling of SSiC in water; wear coefficient as a function of the rate of material removal

The friction coefficient f is with the rolling friction in water with $0.2 \geq f \geq 0.14$ usually higher than in paraffinic oil. After the running-in and the dropping of the friction values it comes to a rise and to a repeated dropping with an approximation to a constant value.

7.3.2.2 Wear

With the tests in water the wear for the spherical sample surfaces was not assignable, it could only wear rates for the cylindrical test specimens be indicated due to pitting (compare Fig. 58).

Since this material exhibited an unfavorable slip-rolling wear behaviour under water lubrication, only two tests were accomplished with finely honed sample mating.

The wear rates are higher than for the polished test specimens under rolling friction in paraffin oil. Thus the material SSiC with an initial Hertzian pressure of $P_0 = 3$ GPa for the slip-rolling load is not suitable. In the tribological wear track it comes to the education of conical cracks, to cracking and to the material failure.

Due to these first results of the slip-rolling abrasion tests of SSiC in water the test series was not continued any further.

7.3.3 Summary of the tests with the material SSiC (EKasic D)

The material SSiC is generally applicable for the slip- rolling, if the initial Hertzian surface pressure adapted at $P_0 \leq 1.5$ GPa is selected.

With a higher load of the rolling members a treating „as good as possible" does not prove to be practical, since the polished function areas show worse wear behaviour than, for example, polished test specimens. The finer the finishing and/or the lower the roughness characteristic values (for example, the reduced valley depth R_{vk}), the greater the wear rate through the slip-rolling stress.

The finely worked function areas show just as the test specimens in water lubrication a material failure from formation of conical cracks and pitting.

The material SSiC can be used for the rolling abrasion, if the Hertzian pressure is adapted (for example, $P_0 = 1.5$ GPa) and the finishing processes create surface roughnesses of $R_{vk} \geq 0.3$ µm.

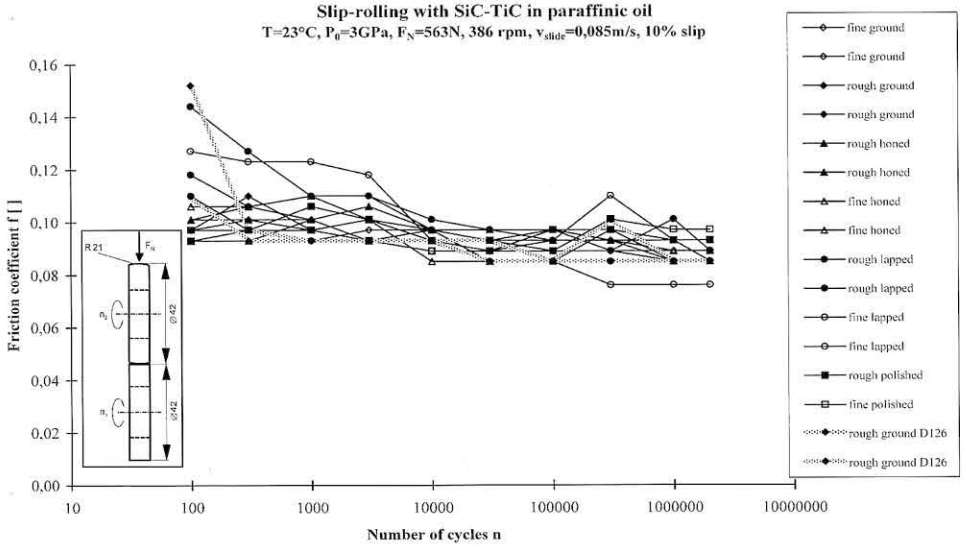

Fig. 59
Slip-rolling friction with SiC-TiC in paraffinic oil; the friction coefficient f as a function of the number of revolutions n

7.4 GPS-SiC-TiC

The SiC-TiC slip-rolling samples were produced and characterized at the BAM (see Chapter 2.4). SiC-TiC is also suited for EDM machining.

7.4.1 Tests in paraffinic oil

With the material GPS-SiC-TiC a comprehensive series of measurements could be accomplished (see Appendix). The machine settings are to be reread in chapter 3.1.

7.4.1.1 Friction

The friction coefficient with the tests in paraffin oil exhibits only slight fluctuations over the total test duration, likewise the differences between the individual finishing processes are not significant (compare Fig. 59). All friction values range at the beginning of the tribological load within the range of f = 0.16 to 0.09 and approach at the end of the slip-rolling wear test the value f = 0.08.

After an running-in phase all friction values, independently of the respective finishing of the function area, even out to an almost constant value. Thus after approx. 10,000 revolutions, nearly all friction values fall within the range of f = 0.10 to f = 0.09 (see Fig. 59).

7.4.1.2 Wear

As already described in chapter 2.4, the TiC part increases the wear resistance of this material developed in the BAM of opposite pure SiC. Due to the additionally higher tenacity and lower porosity, this material combination appears more favorable for the slip-rolling stress.

The wear rate for the material GPS-SiC-TiC is higher than for the silicon nitride materials, within the range of $1 * 10^{-9}$ to $1 * 10^{-6}$ [mm³/Nm]. For the rolling stress the lapped samples are less suitable. Beside the polished function areas the finely polished test specimens exhibit a favorable wear behaviour. Thus it can also be assumed with this material that the device „best as possible" is not always suitable.

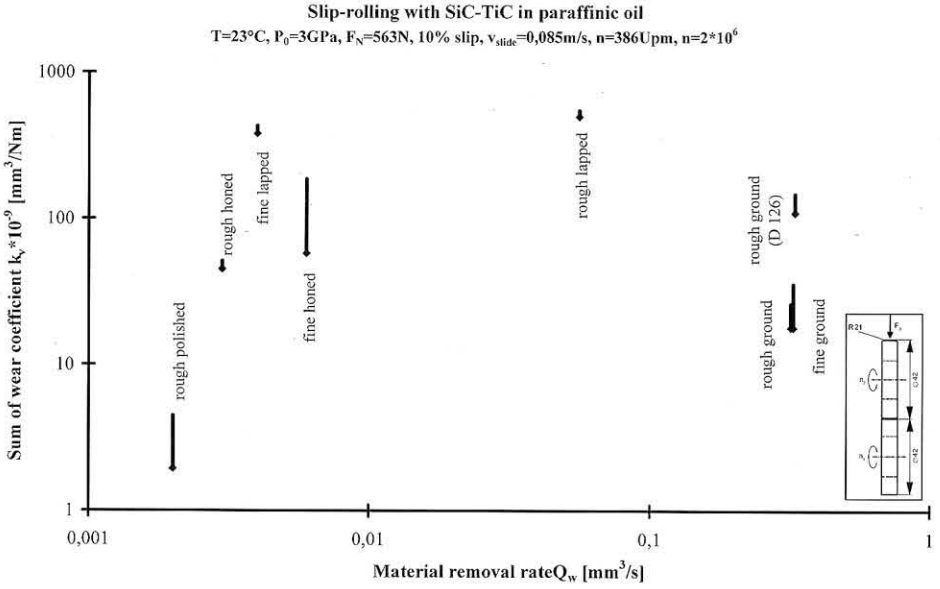

Fig. 60
Wear coefficient k_v as a function of the rate of material removal with the finishing for the material SiC-TiC

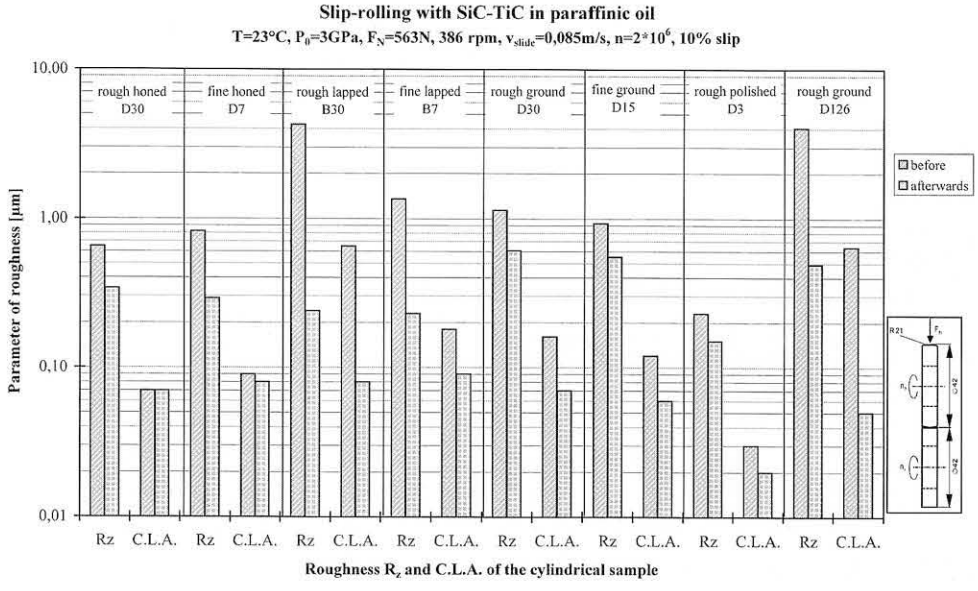

Fig. 61
Roughness characteristic values before and after the tribological stress for the material GPS-SiC-TiC in paraffinic oil

7.4.1.3 Surface roughnesses

The material GPS-SiC-TiC does not show as clearly as other materials the behaviour that the surface roughness of the function area settles down to a value. The averaged roughness R_z reduce only to values of approx. $0.15 \leq R_z \leq 0.6$ µm (compare Fig. 61), but a significant final value for the averaged roughness is not to be recognized. It behaves similarly with the mean peak-to-valley height C.L.A. of the function areas, which adapts itself to values of approx. 0.06 less than or greater than C.L.A. less than or greater than 0.09 (compare Fig. 61).

In Fig. 61 it is good to recognize that there is the largest wear with the running-in behaviour with the lapped function areas. The polished surfaces, however, show a slighter change of the roughness characteristic value amounts. Thus, since they exhibit also a low wear rate, the polished function areas can be regarded as suitable for the rolling load. The finishing process grinding - above all precision grinding - seems to be the most favorable process for the finishing of the SiC-TiC surfaces.

If the reduced valley depth R_{vk} of the GPS-SiC-TiC functional surface is regarded, then it is to be stated that for the cylindrical test specimens there is a wear high condition for a reduced valley depth of $R_{vk} \geq 0.3$ µm; for the spherical test specimens a more complex process of the wear rate appears. On the one hand there is a higher wear rate for Rvk ≥ 1.2 µm and on the other hand the wear rate for values around R_{vk} approximately equal 0.4 µm increases (compare Fig. 62). These R_{vk} values refer with the spherical samples to sample surfaces worked with lapping.

7.4.1.4 Surface analytics

The wear track of a roughly polished sample shows in the SEM picture that the roughness asperities were smoothed by the rolling load (see Fig. 63, left). Individual structure grains were chamfered from the material. The outbreaks of structure grains are to be determined reinforced with the lapped sample (compare Fig. 63, right) which explains the higher wear rate as well as the higher roughness characteristic values after the tribological load.

The two-phase consitution of the material is still well recognizable also after the tribological slip-rolling load.

7.4.2 Tests in water

The material GPS-SiC-TiC can also be used for the slip-rolling stress under water lubrication. Contrary to the TiN phase of the material GPS-Si_3N_4-TiN, the TiC phase is more hydraulically stable, so that there is no material failure with an adapted slip-rolling load.

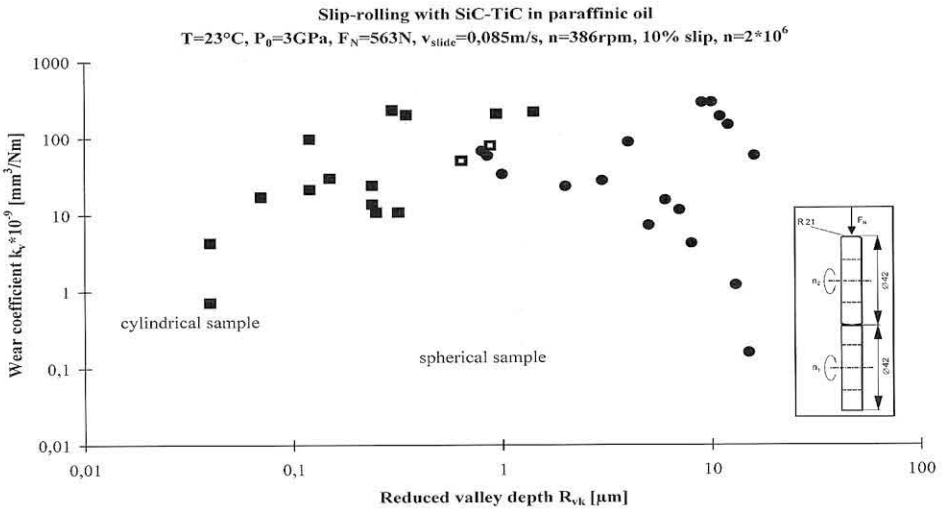

Fig. 62
Wear rate k_v of two sample geometries as a function of the reduced valley depth R_{vk} for the material GPS-SiC-TiC

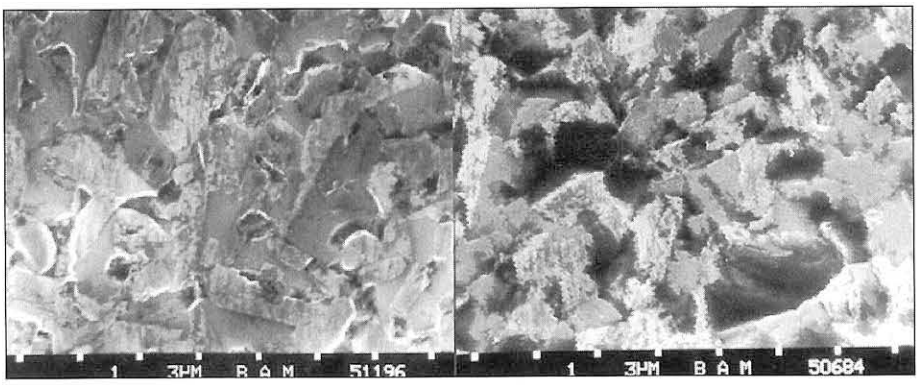

Fig. 63
SEM pictures of the wear track of GPS-SiC-TiC test specimens;
left: roughly polished;
right: roughly lapped

7.4.2.1 Friction

The material SiC-TiC shows a rise of the coefficients of friction under slip-rolling friction in water through the flow. Starting from a revolution number of approx. n ≈ 10,000 the coefficient of friction remains approximately constantly at a value of f ≈ 0.17. The final value of the friction coefficient with the rolling wear tests is independent of the finishing of the function areas of the test specimens.

The initial friction values vary depending upon the type of finishing of the rolling members, the polished test specimens exhibit an initial value of approx. f ≈ 0.1, the roughly worked samples exhibit a value of f ≈ 0.13. The beginning and final values do not show a marked difference concerning the finishing of the function areas.

Such a difference is to be determined only in the process of the friction values. The roughly worked test specimens show an uninterrupted rise of the coefficients of friction with increasing revolution number. On the other hand, the increase of the friction coefficient with the finely finished rolling members is larger up to values at approx. f ≈ 0.2, which then in turn decreases to larger contortion numbers again and which achieve the same value as roughly worked function areas.

7.4.2.2 Wear

The wear coefficient k_v lies for the material SiC-TiC under slip-rolling friction in water within the range of $k_v = 2 * 10^{-7}$ to $k_v = 12 * 10^{-7}$ mm³/Nm and is proportional to the rate of material removal Q_w with the surface finishing of the function area. To the material SiC-TiC applies: The finer the finishing process, the lower is also the wear rate. However it is to be here also noted that between the roughly polished rolling members and the roughly ground slip-rolling members, only a slight difference of the wear rates is to be noted.

Due to the wear behaviour of SiC-TiC under slip-rolling friction in water, the default can be made also here that a very fine finishing brings hardly a gain for wear behaviour. Thus the structural member can be worked even with rougher processes, without it coming to substantial losses in the reliability of the component.

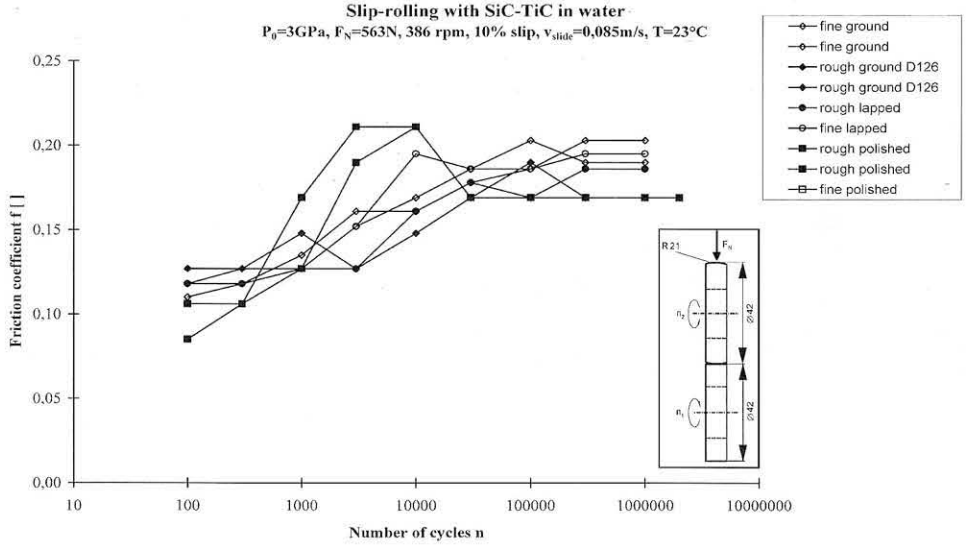

Fig. 64
Friction coefficient as a function of the number of revolutions for the material SiC-TiC in water

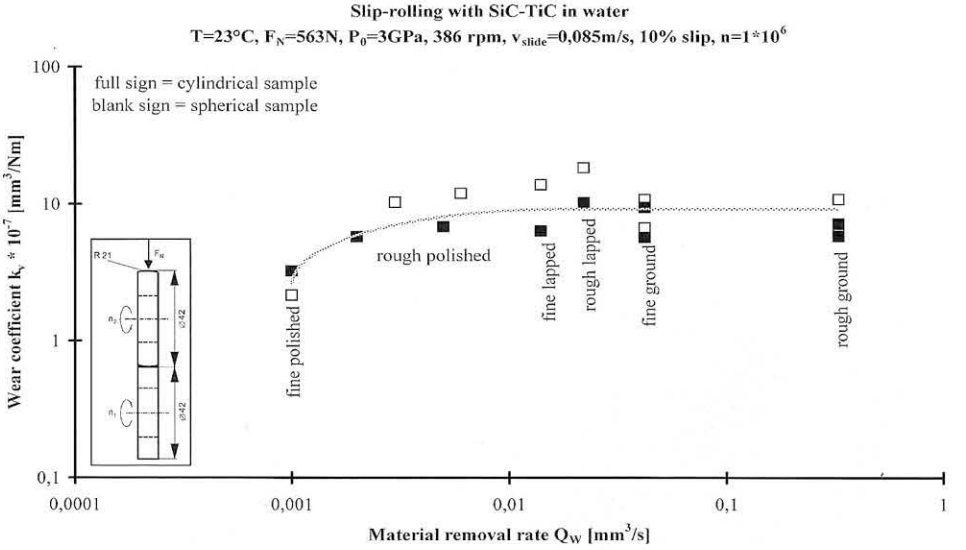

Fig. 65
Wear coefficient k_v as a function of the rate of material removal Q_w during the surface finishing for the material SiC-TiC under slip-rolling wear

7.4.2.3 Surface roughnesses

The averaged roughness R_z and the mean peak-to-valley height C.L.A. before and after the tribological slip-rolling stress show that the finely worked surfaces exhibit an increase of surface roughnesses in the wear track after a million revolutions.

The roughly worked function areas decrease in their surface roughness under the slip-rolling load. A light reduction of roughnesses is to be observed with the roughly polished sample, if this achieves a revolution number of two million. All workings show the same values for the roughness characteristic values after the tribological rolling load, i.e., it adjusts a process roughness under the tribological load.

The wear coefficient as a function of the reduced valley depth R_{vk} before the tribological rolling load shows clearly that a dependence on the finishing for the slip-rolling wear in water plays only a subordinated role.

7.4.2.4 Surface analytics

Surface analytics permit a study of the causes for wear behaviour.

The REM pictures show clearly a change of the component surface through the tribological slip-rolling load in water (compare Fig. 68 a). In Fig. 68 a) on the left, the tribo-track is to be seen and on the right in the figure, the unloaded sample surface on which more structures are visible, which originate from the grinding finishing. This smoothing of the track is also known from the analysis of surface roughnesses before and after the rolling load (compare Fig. 66). If the track with a high resolution (V = 1:5,000) is seen, then it is to be recognized that the apparently smooth trace is interspersed with cracks. These cracks cause the material at the surface to become detached in clod-shaped form. The brightly represented material in Fig. 68 b) is oxidic. In the SEM oxides (non-conducting) appear bright through the loading.

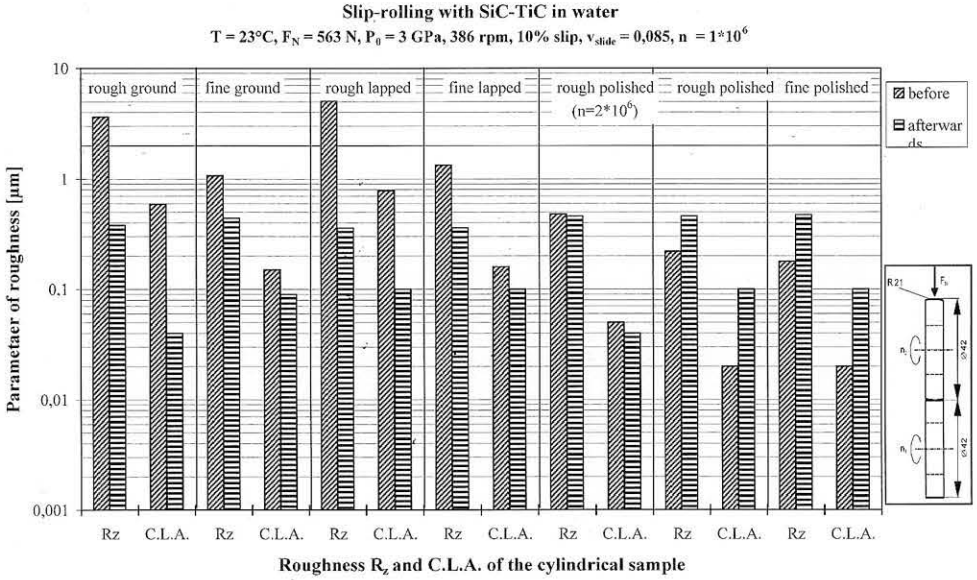

Fig. 66
Roughness characteristic values C.L.A. and R_z before and after the tribological rolling load in water for the material SiC-TiC

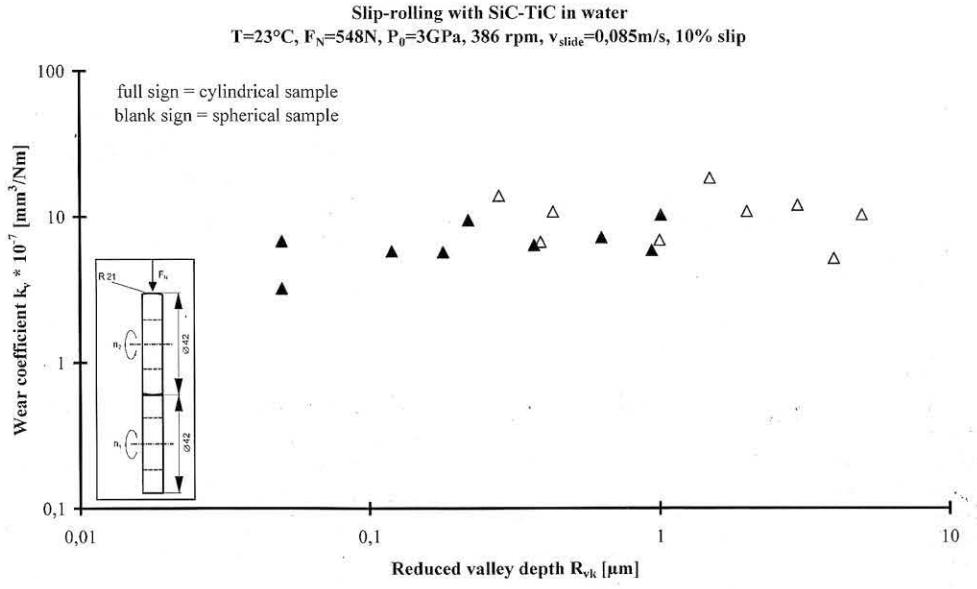

Fig. 67
Wear coefficient as a function of the reduced scoring depth for the material SiC-TiC

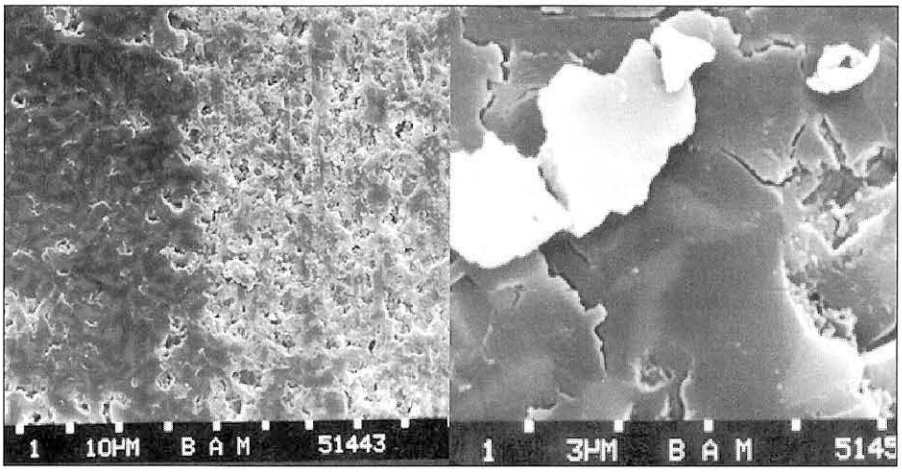

Fig. 68
SEM pictures of a roughly polished sample after the slip-rolling load in water;
a) left: V = 1:1.000,
b) right: V = 1: 5.000

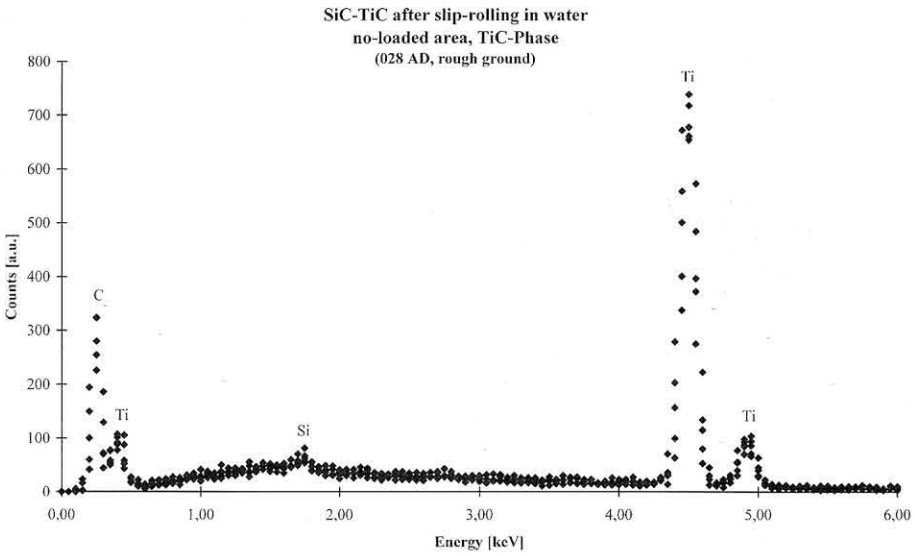

Fig. 69
EDX spectrum of the TiC phase of the unloaded roughly polished SiC-TiC slip-rolling sample

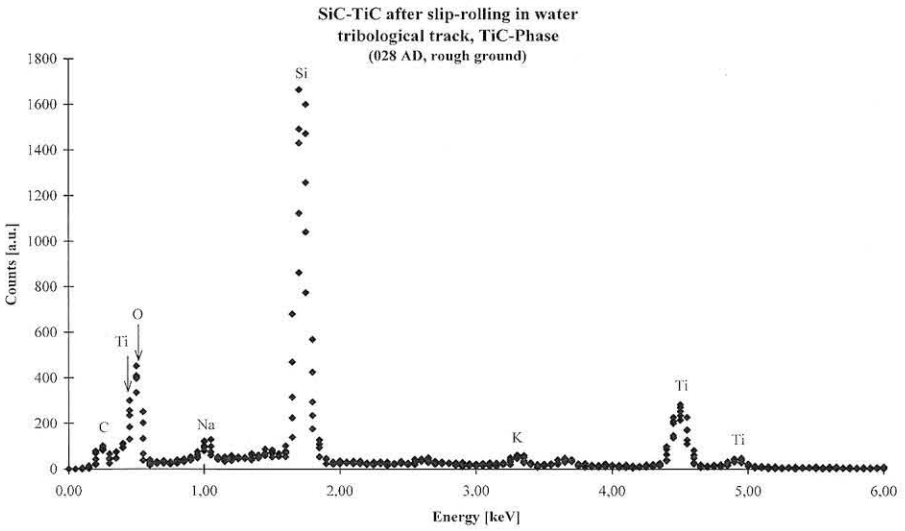

Fig. 70
EDX spectrum of the TiC phase in the trace of the roughly ground SiC-TiC slip-rolling sample

In the EDX spectrum of the unloaded SiC-TiC sample, the pure TiC phase can be clearly recognized (see Fig. 69).

The still weakly detectable Si signal is to be due to stray radiation. The spectrum shows a distribution of the components, which is to be expected.

In Fig. 70 the change of the distribution of the elements in the track opposite the unloaded surface (Fig. 69) is clearly recognizable. Although the TiC phase was detected here, the Ti-signal opposite the unloaded sample is substantially smaller. The clearly recognizable oxygen peak suggests an oxidic compound.

The formation of a TiO_xC_y phase affects the wear favorably in so far as the Ti phase is not so strongly hydrolyzed that it results in a failure by break, as for example, with the material GPS-Si_3N_4-TiN.

7.4.3 Summary of the tests on the GPS-SiC-TiC

The material GPS-SiC-TiC for the slip-rolling stress is generally suitable, both with paraffin oil and with water and intermediate media.

The tests in paraffin oil show a better slip-rolling wear behaviour than the pure SiC material. A uniform smoothing of the function area by the running-in behaviour of the material is not to be determined.

Lapped function areas show a worse wear behaviour than for example ground. Grinding, above all, the precision grinding, seems to be for this material the method of the finishing, the good wear rates and a positive running-in behaviour effectuation.

With the tests in water a certain stability in relation to the water lubrication is to be emphasized, it comes to a hydrolysis of the TiC in water, which, however, does not negatively affect rolling wear behaviour in such a manner that it comes to a failure by material outbreaks.

Thus the material SiC-TiC shows up also in the comparison with other materials as a material suitable for the slip-rolling abrasion.

7.5 HIP-ZrO_2 (htc-PSZA)

HIP-ZrO_2 material, recently introduced to the market, possesses a high strength and no glass phase, which lets it appear to be favorable for the rolling load. The material and its mechanical characteristics are represented in more detail in chapter 2.5.

7.5.1 Tests in paraffinic oil

With paraffinic oil as interfacial media, the material HIP ZrO_2 proves to be favorable for the slip-rolling friction. Thus an extensive testing program could be accomplished (see Appendix); this also always means that many different kinds of finishing could be tested.

7.5.1.1 Friction

The friction coefficient lies for all kinds of finishing within the range of f = 0.105 to f = 0.065. After an initial dropping of the friction coefficient, it approaches a constant value with increasing number of contortions. At the friction value no dependence on the kind of the finishing of the function area could be observed (compare Fig. 71}. Most rolling samples at the end of the tribological load exhibited a friction coefficient within the range of f = 0.08.

7.5.1.2 Wear

The material HIP-ZrO_2 proved to be very wear resistant and thus also shows low wear rates within the range of $k_v \leq 10 * 10^{-9}$ mm³/Nm (see Fig. 72). With very finely finished sample surfaces, the wear rate could sometimes no longer be determined, since it lay below the resolution. So with the finely lapped rolling members, an wear rate could be determined only at the spherical samples. The polished function areas exhibited an wear rate so low that this could be determined at none of the specimens (also not by means of the AFM).

With the material HIP-ZrO_2, the wear rate is reduced with the refinement of the finishing, however it is to be considered for the technical designer whether such a low wear as it can be achieved with polished or finely lapped samples is necessary for the application of the component. Even roughly worked function areas (as for example, roughly ground or roughly honed surfaces) show a low wear value. Very good wear results can be achieved also with the finishing processes, precision grinding or fine honing. These finishing processes exhibit a higher rate of material removal than finer processes, as for example, polishing, which could minimize the costs with the component manufacture.

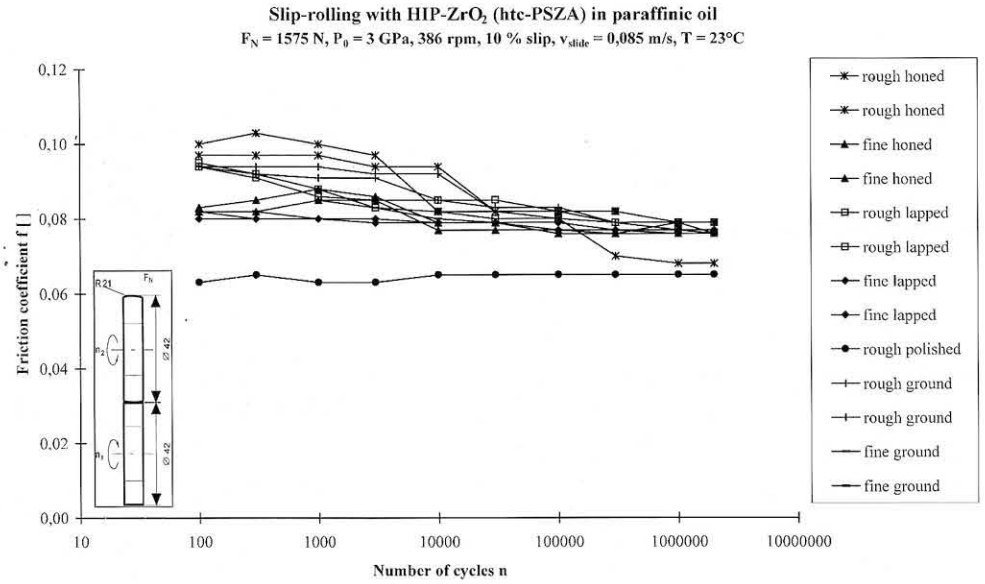

Fig. 71
Friction coefficient as a function of the number of revolutions for the material HIP ZrO_2 under rolling friction in paraffinic oil

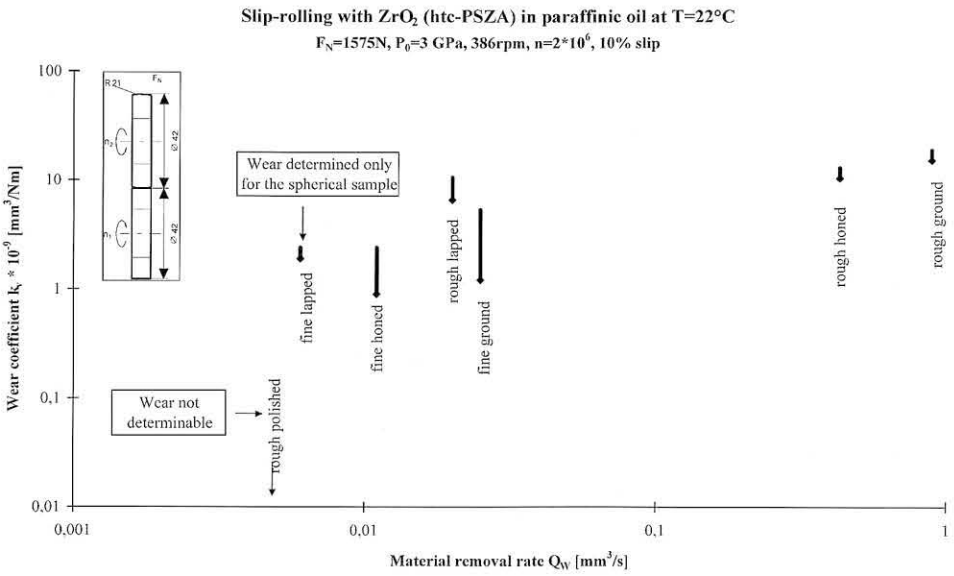

Fig. 72
Wear coefficient as a function of the rate of material removal with processing of the material HIP-ZrO_2

Due to the favorable wear behaviour of the HIP-ZrO_2 slip-rolling body, this material is a good alternative to the HIP-Si_3N_4 introduced well at the market. Particularly since with ZrO_2 the wear coefficients can assume values smaller than 10^{-10} mm³/Nm.

7.5.1.3 Surface roughnesses

During the course with the slip-rolling wear it comes to a smoothing of surface roughness. Above all the roughness asperities are cleared away, which clarifies the averaged roughness R_z and the mean peak-to-valley height C.L.A. before and after the tribological stress in Fig. 73. For applications that permit a low clearance increase, as, for example, tooth profiles or cams, the possibility thus exists of doing without an optimum finishing of the function area of the component. In the other cases polished areas must be used. With the roughly polished samples no wear rate could be determined profilometrically also according to a contortion number of n = 2 * 10^7. For this finishing process also no change of the surface roughnesses could be accounted for by means of the stylus profilometer (Hommel Tester) or AFMs. For the other processes for the finishing of the function areas, a reduction of the surface roughnesses through the rolling load is shown.

The reduction of the roughness characteristic values for the material HIP-ZrO_2 is independent of the surface finishing. Even with low values for R_z and C.L.A. before the tribological stress, the values are still reduced under the slip-rolling load. A reduction of surface roughness is to be noted, if the averaged roughness height $R_z \geq 0.2$ µm and the mean peak-to-valley height C.L.A. ≥ 0.02 µm.

If the wear coefficient k_v is regarded as a function of the reduced valley depth R_{vk}, then it is to be stated that for values of $R_{vk} \leq 0.2$ µm, there is a reduction of the wear rates. With the surface finishing, the values of the reduced scoring depth of $R_{vk} \leq 0.2$ µm can be achieved with the following processes: fine honing, precision grinding, fine lapping as well as polishing.

Also with the material HIP-ZrO_2 good results of the wear rates can be achieved, if manufacturing processes of the function area are used which do not correspond to the slogan „best as possible".

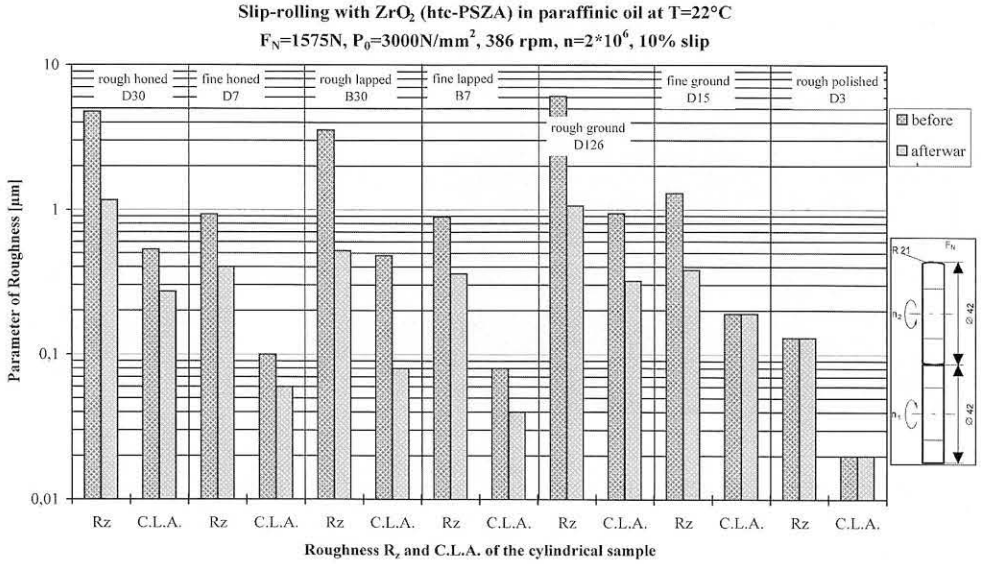

Fig. 73
Roughnesses of the cylindrical HIP-ZrO_2 samples before and after tribological slip-rolling stress in paraffinic oil

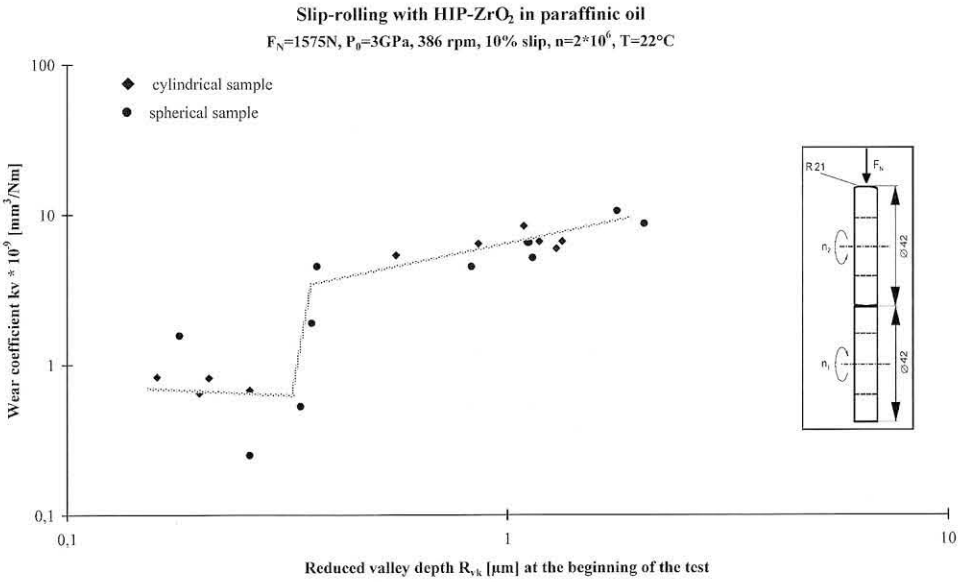

Fig. 74
Wear coefficient k_v as a function of the reduced valley depth R_{vk} before beginning of test for the material HiP-ZrO_2 under slip-rolling stress in paraffinic oil

7.5.1.4 Surface analytics

The ultrasonic-microscopic tests accomplished according to standard were concentrated on areas within which still no damage of the stressed function area could be diagnosed using the light microscopy.

In Fig. 75 a roughly polished HIP-ZrO_2 sample surface is shown. In the centre of the picture the wear tarck that resulted from the slip-rolling load is visible. In the track a surface smoothing that occurred because of the tribological stress. The smoothing of the surface appears with the ultrasonic microscopy through the lower scattering level of the ultrasonic waves in the wear track in relation to the roughly ground unloaded environment.

The smoothing points likewise to a low wear rate and shows also "optically" the result of the test of the roughness characteristic values C.L.A. and R_z before and after the tribological rolling load.

The smoothing of the polished function area by the rolling load in paraffin oil is so slight that it is not detectable with the conventional methods.

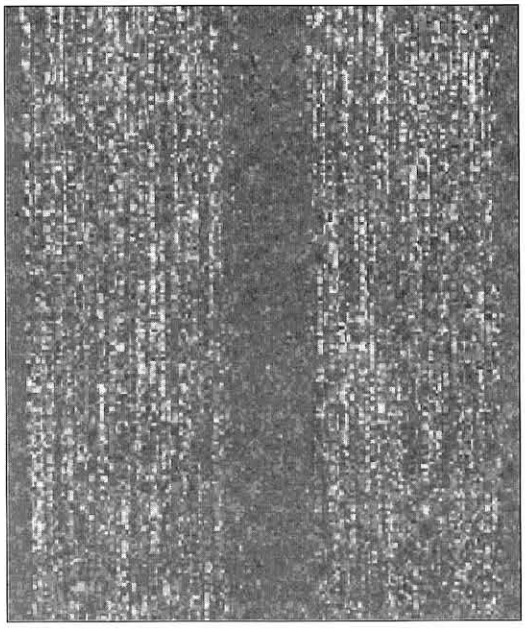

Fig. 75
Ultrasonic microscopy on a roughly ground HIP-ZrO_2 sample surface after the rolling load with 2 million revolutions in paraffinic oil

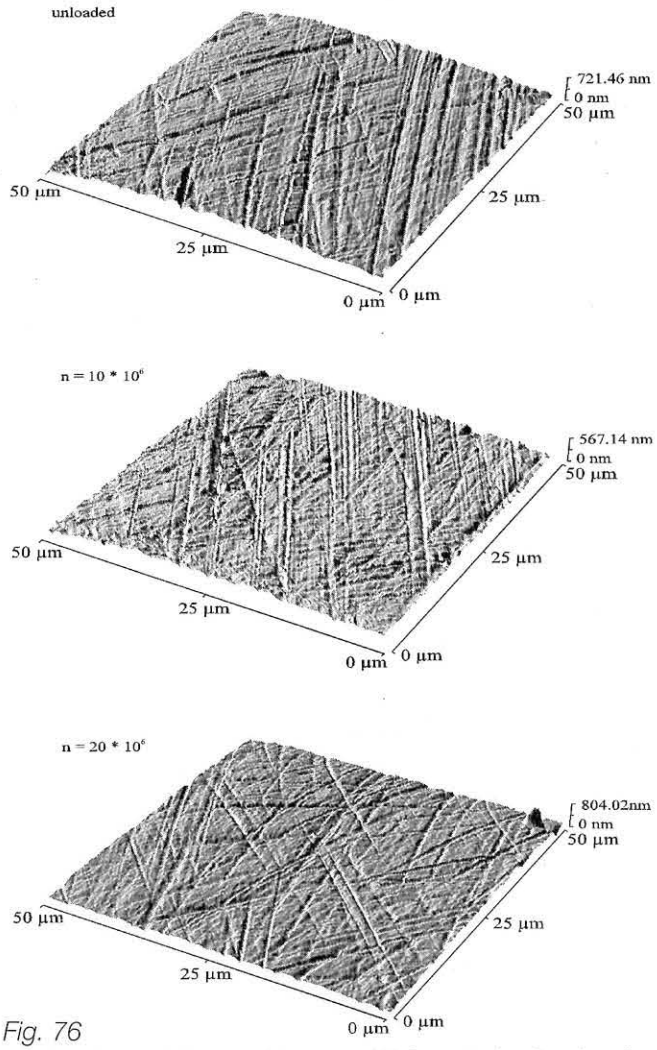

Fig. 76
*AFM pictures of the roughly ground ZrO_2 sample after the slip-rolling stress in paraffinic oil, from above downwards: unloaded surface and after n = 10 * 10^{-6} and n = 20 * 10^{-6} revolutions*

The roughly polished ZrO_2 surface in paraffinic oil exhibits an wear rate that can no longer be determined profilometrically, since this lies below the measuring accuracy. Only tests with the AFM (atomic force microscope) permit a statement about the change of the surface in the wear track under the slip-rolling stress. In the AFM pictures a weak smoothing of the charged surface can be seen (see Fig. 76); even the ghost lines from polishing have remained visible. Thus this material can also be used for long-term applications in paraffinic oil.

7.5.2 Tests in water

The material HIP-ZrO_2 has proved to be unsuitable for use in water. For this reason only two tribological tests were accomplished (see Appendix). For these tests a roughly worked rolling mating (roughly honed) and a finely finished sample mating (roughly polished) were selected.

7.5.2.1 Friction

During the rolling stress in water the friction coefficient increases without interruption with increasing revolution number, so that only low revolution numbers of 10,000 and/or 30,000 could be achieved (compare Fig. 77). Here it is to be differentiated how the sample was finished. The finely finished sample mating achieves a higher revolution number. The revolution numbers achieved depends on the friction value, which is still technically possible for the Amsler tribometer. At a friction value of f = 0.4, the equipment disconnected automatically, so that there is no damage of the machine components.

The uninterrupted increase of the friction value can be explained by the increasing pitting. With the material HIP-ZrO_2 high shear stresses occur through the rising friction coefficient. In addition the hydrothermal resistance of ZrO_2 is insufficient, since the Y_2O_3 in water is extracted as hydroxide $Y(OH)_3$ [43].

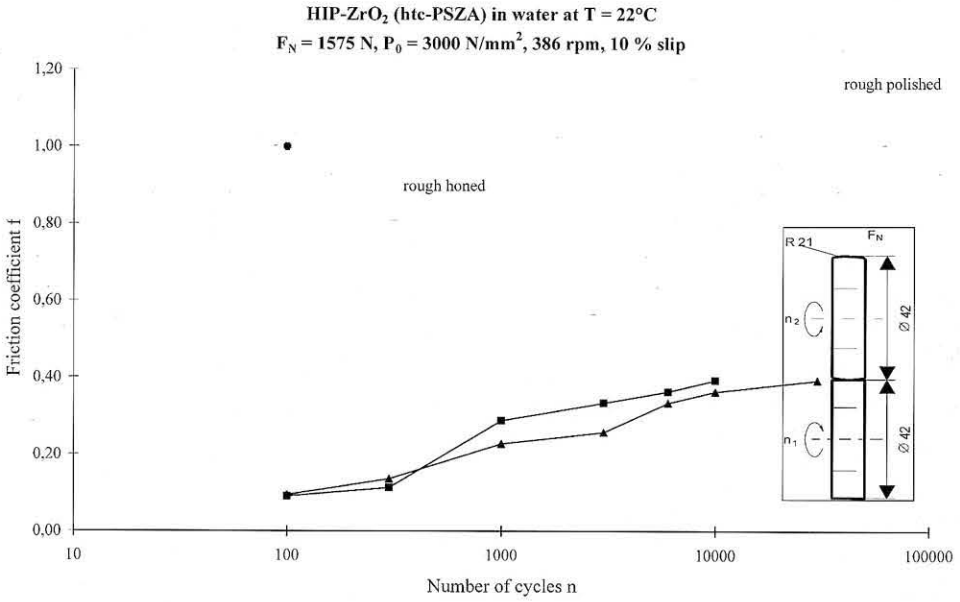

Fig. 77
Process of the friction values f with the number of revolutions n for the material HIP-ZrO_2 in water

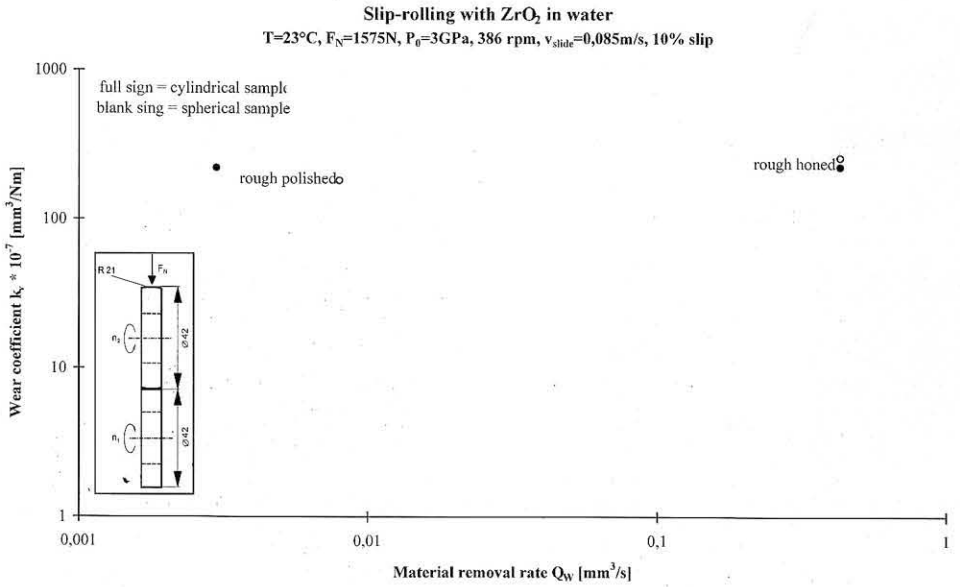

Fig. 78
Wear coefficient as a function of the rate of metal removal with the surface finishing for the material HIP-ZrO_2 in water

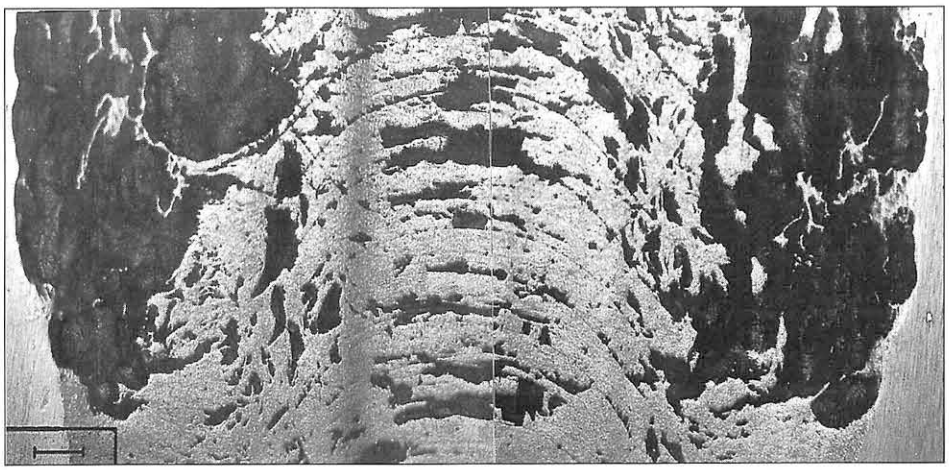

Fig. 79
Light-microscope picture of a roughly polished ZrO_2 sample after the slip-rolling stress in water

7.5.2.2 Wear

As the friction values already suggest, the material HIP-ZrO_2 for the slip-rolling friction shows up in water as wear-unresistant.

The wear coefficient k_v with the tested test specimens is at $k_v \approx 2*10^{-5}$ mm³/Nm; however it is to be considered that the revolution numbers achieved are varying for the different finishing processes. The roughly honed rolling mating achieves the same wear rate as the roughly polished, however with 20,000 fewer revolution. This shows also that a fine finishing of the function area is more favourable here, although the material is not suitable as such for the rolling friction in water.

7.5.2.3 Surface analytics

With the slip-rolling stress of HIP-ZrO_2 in water, high shear stresses with rising friction coefficient occur, which leads to pitting. This is caused due to the insufficient hydrothermal resistance of the Y_2O_3 stabilized ZrO_2 material.

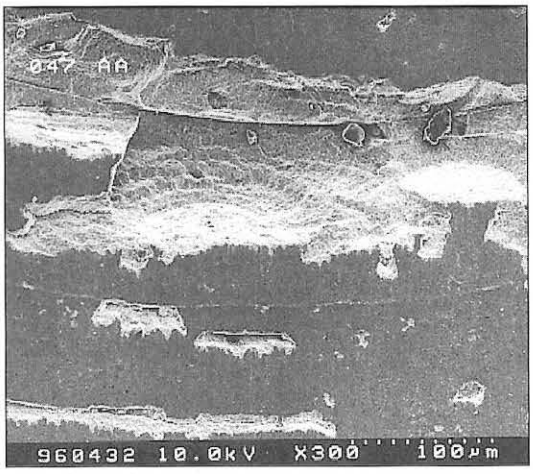

Fig. 80
SEM picture of a roughly polished ZrO_2 sample after the slip-rolling stress in water

In Fig. 79 it is clearly visible that there is pitting. The wear track is characterized by conical cracks and material outbreaks, whereby the cracks are found in the centre of the wear track, the wide outbreaks against it rather in the edge of the track.

In the REM picture it is to be recognized that there are material outbreaks along the conical crack lines; clod-shaped flakings occur. Thus the material HIP-ZrO_2 is not suitable for an application of rolling with water as intermediate material.

7.5.3 Summary of the tests on the material HIP-ZrO_2

The slip-rolling wear tests on the material HIP-ZrO_2 in paraffin oil and in water show very different results.

In paraffin oil the material HIP-ZrO_2 proves to be tribologically very stable and well suited for the rolling stress. The determined wear rates are very low and lie in the lower 10^{-9} to 10^{-10} range for k_v [mm³/Nm]. With very finely finished function areas, hardly any change in the wear track can be determined also after 20 million contortions. In water, however, the material HIP-ZrO_2 proves to be unsuitable, because it lacks hydrothermal resistance for the slip-rolling wear.

7.6 LPS-SiC (SiC-B)

With the liquid phase sintered (LPS) SiC tests were first accomplished under slip-rolling load in paraffinic oil.

7.6.1 Tests in paraffinic oil

After the first slip-rolling wear tests with an initial Hertzian pressure of $P_0 = 3$ GPa, it turned out that also the material LPS-SiC appeared to be not very suitable for the slip-rolling load with such a high surface pressure. A test with the high surface pressure of $P_0 = 3$ GPa was terminated after a revolution number of one million. Therefore, with the following tests, similar to the tests on the material SSiC, an initial Hertzian surface pressure of $P_0 = 1.5$ GPa was selected, which resulted in a normal force of $F_N = 205$ N in accordance with the Hertzian formula (compare Table 7).

7.6.1.1 Friction

The friction coefficient changes for the roughly finished function areas more strongly than for the finely finished. However it is also to be remarked that the roughly polished rolling members were tested with the twice as high initial Hertzian pressure of P_0 = 3 GPa. Between the roughly and finely lapped surfaces is after the intake, however, no more difference with respect to the coefficient of friction is recognizable (see Fig. 81). The roughly polished test specimens exhibit a friction behaviour different from the other rolling members.

Dropping of the friction coefficient with increasing number of contortions is more pronounced with the test specimens with larger initial Hertzian pressure, it exhibits a lower final value of the friction coefficient around $\Delta f \approx 0.05$.

Only with the polished rolling members is to be noted a rise of the friction coefficient with increasing revolution number.

7.6.1.2 Wear

The wear rate shows a strong dependence on the rate of material removal, i.e. on the type of selected finishing and thus also on the surface roughness of the test specimens (compare Fig. 82). For the material LPS-SiC the difference between the fine finishing processes (polishing) and the rougher processes (grinding, lapping) is striking, the wear rate is higher for the rougher processes by a factor of 100. The rougher processes, such as grinding, honing and lapping, show under the slip-rolling stress similar wear rates with $k_v \approx 1 * 10^{-7}$ mm³/Nm. The polished rolling samples show an wear rate of $k_v \approx 1 * 10^{-9}$ mm³/Nm, which is in the range for materials that are usually used for slip-rolling wear, as, for example, HIP-Si_3N_4.

The roughly polished test specimens were tested with an initial Hertzian pressure of P_0 = 3 GPa. With this load the wear coefficient determined differs only slightly for the different revolution numbers by 1 and/or 2 million.

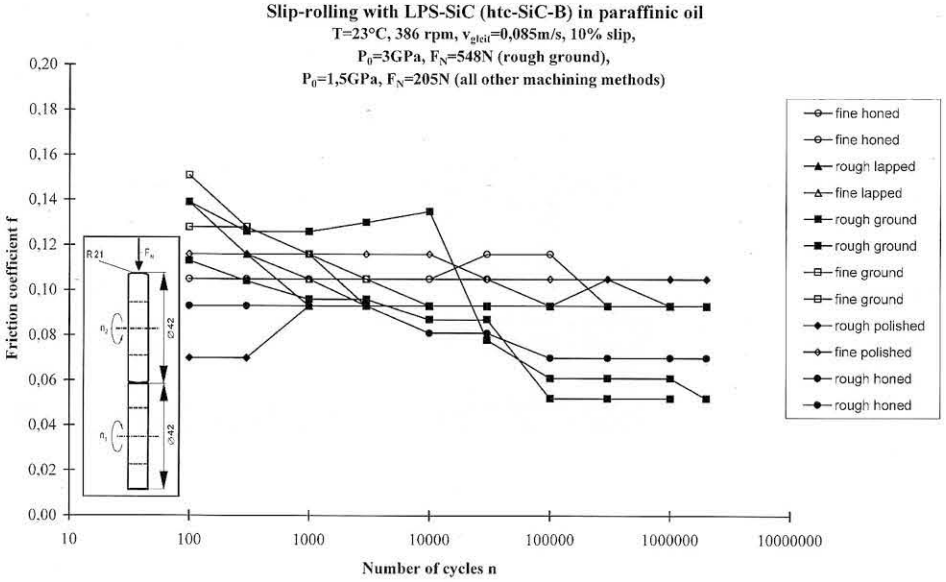

Fig. 81
Friction coefficient f as a function of the number of revolutions n for the material LPS-SiC under slip-rolling stress in paraffinic oil

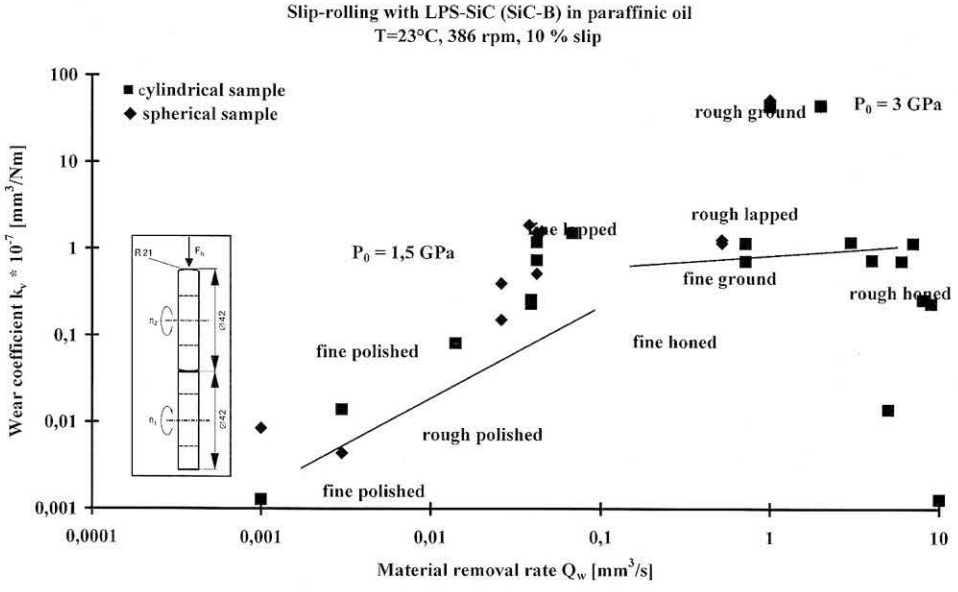

Fig. 82
Wear coefficient as a function of the rate of material removal during the surface finishing of the material LPS-SiC

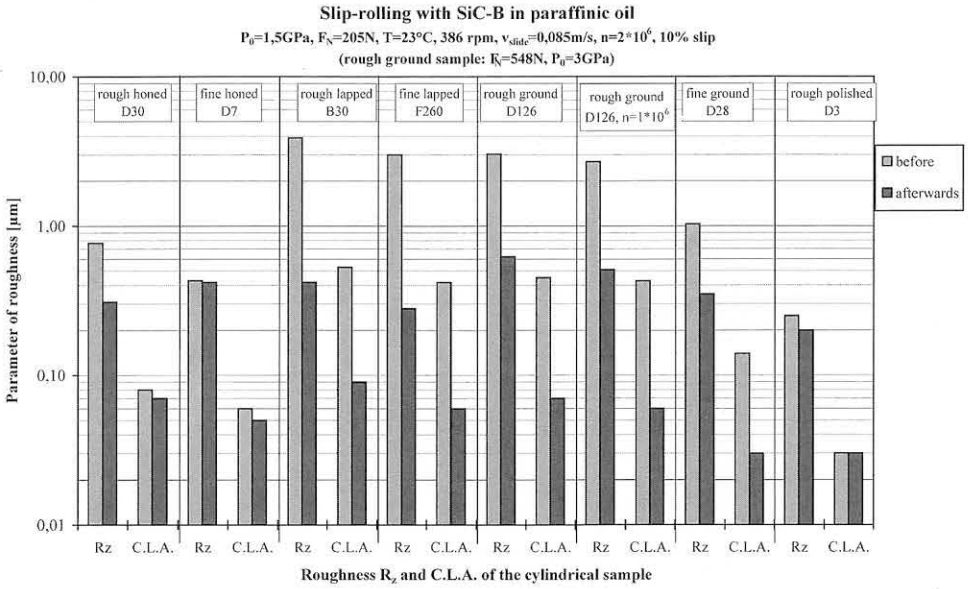

Fig. 83
Change of the averaged roughness R_z and mean peak-to-valley height C.L.A. a by the rolling load for the material LPS-SiC in paraffinic oil

In the comparison with the sintered SiC material (EKasic D) the roughly polished LPS-SiC test specimens exhibit a higher wear rates. The lapped test specimens achieve with the same initial Hertzian pressure of P_0 =1.5 GPa a comparable wear rate. The polished test specimens exhibit with a Hertzian pressure of P_0 = 1.5 GPa likewise a very low wear rate.

7.6.1.3 Surface roughnesses

If the averaged roughness R_z and the mean peak-to-valley height C.L.A. are regarded before and after the rolling load, then a slight difference of roughnesses is to be observed with the roughly and/or finely lapped function areas. Since roughnesses of the finely lapped and the roughly ground test specimens are almost alike after the finishing of the surfaces, also the effect of the varying initial Hertzian pressure can be observed at these test specimens. Despite the lower surface pressure in the case of the finely lapped rolling members, a stronger reduction of roughnesses is to be observed than with the roughly ground. The roughly polished function areas exhibit hardly any change of the averaged roughness R_z and the mean peak-to-valley height C.L.A. through the tribological load. The lower the initial surface roughnesses, the less these change under the tribological stress, which already with the finely honed sample surfaces becomes visible.

Also for this material roughness characteristic values can be indicated, for which still only a slight change is achieved by the intake behaviour. For an averaged roughness is the value $R_z \leq 0.2$ µm and for the mean peak-to-valley height C.L.A. ≤ 0.02 µm.

7.6.1.4 Surface analytics

Compared with the sintered SSiC samples, the roughness decreases with the LPS-SiC samples for all modes of handling through the rolling load and/or remains constant for the very finely worked surfaces. The wear rate of the ground LPS-SiC samples with an initial Hertzian pressure of P_0 = 3 GPa lies by two orders of magnitude over that of

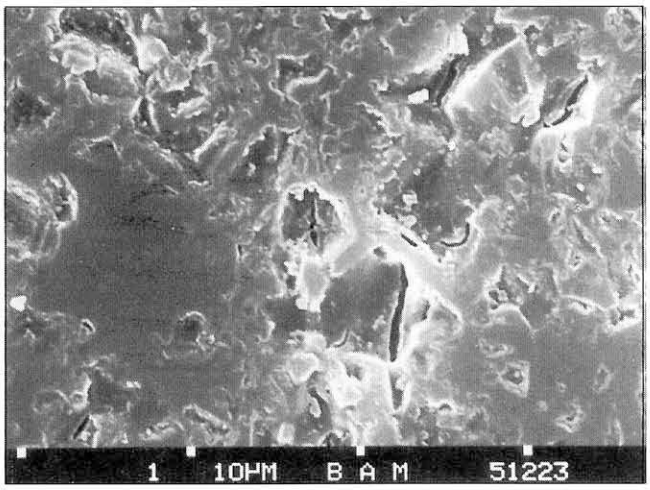

Fig. 84
*SEM picture of the wear track of the roughly polished, cylindrical sample after the slip-rolling wear (P_0 = 3 GPa, F_N = 548 N, n = 2 * 10^6 revolutions)*

the sintered SSiC samples. With the reduced Hertzian pressure of P_0 = 1.5 GPa, the wear rates for the materials SSiC and LPS-SiC are comparable with $k_v \approx 1\text{-}2*10^{-7}$ mm³/Nm.

In the SEM picture (Fig. 84) it is clearly recognized that the rolling load leads to the formation of cracks. Partially it comes to the smoothing of the surface as can be seen at the left in Fig. 84. The cracks lead in some areas of the tribo-track to the popping of the material, thus with a further continued rolling load it would lead to a possible material failure and pitting.

7.6.2 Summary of the tests with the material LPS-SiC

The material LPS-SiC is likewise as also the material SSiC suitable only with a modified initial Hertzian pressure of P_0 = 1.5 GPa for the slip-rolling wear. For this lower surface

pressure the finely finished (polished) function areas show a good wear behaviour; the wear rates are then at $k_v \approx 1*10^{-9}$ mm³/Nm.

For more roughly worked function areas no significant difference is recognizable in the wear rates, here then can be selected the more economical variation of the treating with the larger rate of material removal.

Under the slip-rolling load the finely honed surfaces show a good wear behaviour and an only slight decrease of surface roughnesses and concomitantly in the application also only a slight increase in clearance. This behaviour of the finely honed surfaces proves to be favourable if wear rate and economy are put into the ratio.

8 Comparison and discussion of the test results

The perceptions obtained on the slip-rolling wear behaviour of the different ceramic materials are to be put now with one another in relationship. Additionally tests with the well introduced and tested material 100Cr6 as rolling steel and were accomplished, in order to get a comparison possibility opposite a known material.

8.1 Comparison of the test results in paraffinic oil

Ceramics are less inclined contrary to the steel samples to adhesive wear and pitting. The improved wear resistance of the ceramic materials permits the use of interfacial media without EP-/AW-additives, like the paraffin oil used with the tests presented here.

The wear rate of engineering ceramics depends crucially on the finishing and associated achieved surface roughness. For all tested ceramic materials - with exception of SSiC with the initial Hertzian pressure of P_0 = 3GPa - the wear rate with small reduced peak heights R_{pk} is so low that the technical designer can decide whether a slight increase of the clearance through running-in with rough surfaces for the respective application is acceptable or whether finer finishing is to be done.

Engineering ceramics HIP-Si_3N_4, GPS-Si_3N_4-TiN and HIP-ZrO_2 are well suitable for the rolling abrasion in paraffinic oil (compare Fig. 85}. The material ZrO_2 shows the lowest wear rate compared with the other materials.

With all these materials a ,,best as possible „ treating can be done without, if a slight clearance increase is acceptable through the running-in process.

The materials based on SiC show a higher wear rate compared with the materials specified above. The material GPS-SiC-TiC shows a wear behaviour that is strongly dependent on the mode of finishing. A transition from a high-wear condition of the lapping to a low-wear condition in the case of polishing (small rates of material removal) and lapping (larger rates of material removal). Thus the material SiC-TiC is likewise quite suitable for the slip-rolling stress, whereby a finishing of the function area should be excluded by means of lapping.

Both SSiC and LPS-SiC are suitable under slip-rolling load only for a lower initial Hertzian pressure of P_0 = 1.5 GPa. The wear behaviour of the liquid phases of sintered material is comparable with that of the simply sintered SiC, although the LPS-SiC has a higher fracture toughness K_{IC} and flexural strength σ_{4Bb}. Both materials show with an

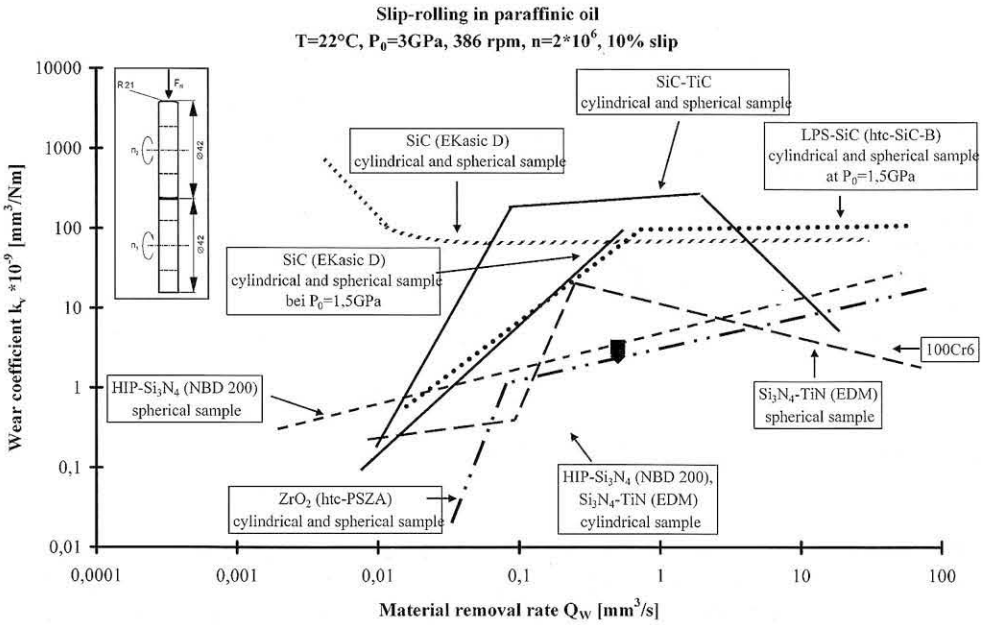

Fig. 85
Slip-rolling friction in unadditivated paraffinic oil with different ceramic materials

initial Hertzian pressure of P_0 = 1.5 GPa a decrease of the wear rate proportional to increasingly smaller rates of material removal, which means also a finer finishing. For polished function areas the wear rates are in the range of $k_v < 1 * 10^{-9}$ mm³/Nm, which is comparable with values for the materials HIP-Si_3N_4 or GPS-Si_3N_4-TiN.

For an initial Hertzian pressure of P_0 = 3 GPa, SSiC shows an increase of the wear rate for increasingly smaller rates of material removal, i.e. for finer final working. Polished surfaces show here the most unfavourable wear behaviour. The increase of the wear rate is accompanied by the increase of surface roughnesses from the tribological stress (compare Chapter 7.3.1.3).

The tests in unadditivated paraffinic oil show that most of the ceramic materials can be used favourably opposite 100Cr6 under slip-rolling load. Only the SiC of materials exhibit a higher wear rate. Materials such as HIP-ZrO_2, HIP-Si_3N_4 or GPS-Si_3N_4-TiN are superior to the slip-rolling steel in wear behaviour, particularly since here it is to be noted that for technical reasons the slip-rolling steel 100Cr6 could be loaded only with an initial Hertzian pressure of P_0 = 2 GPa.

With paraffinic oil as intermediate media the SiC materials and the Si_3N_4 materials inclusive of ZrO_2 in each case show similarities, so that these groups of materials were in each case regarded separately. Since surface roughnesses are a measure for the finishing process, the wear rat was analysed as a function of the reduced peak heights R_{pk}.

With the materials Si_3N_4, Si_3N_4-TiN and ZrO_2, which are quite suitable for the slip-rolling wear, a similar wear behaviour as a function of the reduced peak heights R_{pk} is to be recorded. The lower the surface roughness, the lower is also the wear rate. In Fig. 86 the course of the wear rates proves as diagonally running band with a

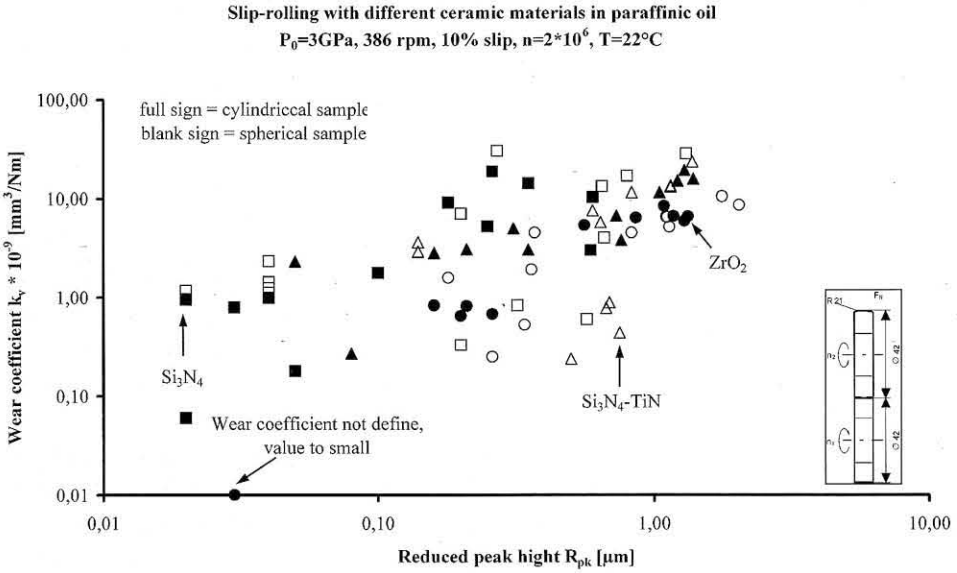

Fig. 86
Slip-rolling friction with the ceramic materials Si_3N_4, Si_3N_4-TIN and ZrO_2

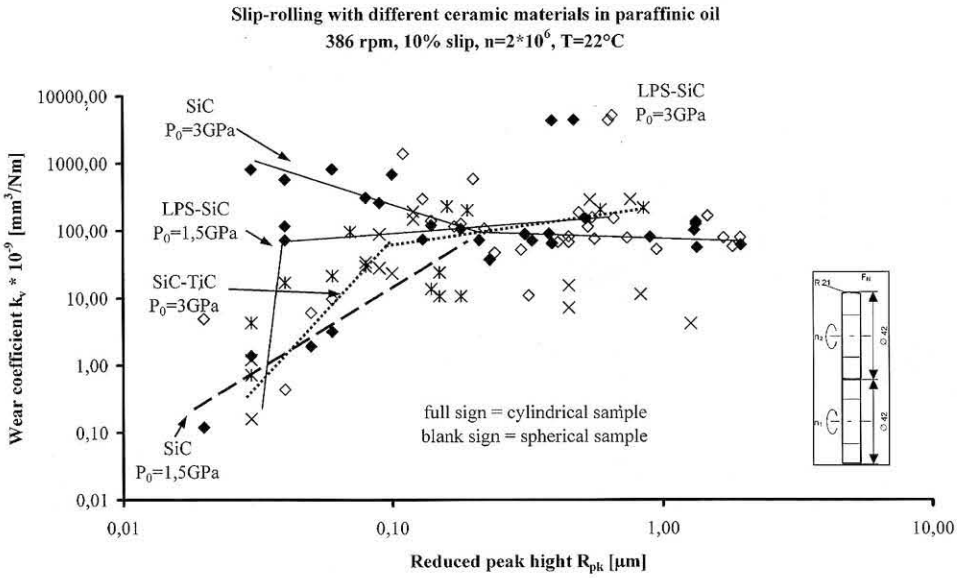

Fig. 87
Slip-rolling wear in unadditivated paraffinic oil with SSiC, LPS-SiC and SiC-TiC

spread in which the values for all materials lie. However, it is to be noted that for the material ZrO_2, for very finely finished (polished) surfaces, no wear coefficients could be determined (see also fig. 76).

The SiC materials do not show such a uniform picture of the wear coefficients as a function of the reduced peak height of R_{pk}.

The materials SSiC and LPS-SiC show a reduction of the wear coefficient for peak heights $R_{pk} < 0.1$ µm with an initial Hertzian pressure of $P_0 = 1.5$ GPa. With $P_0 = 3$ GPa SSiC shows an increase of the wear coefficient for increasingly smaller peak heights, on the other hand SiC-TiC shows like the other materials at $P_0 = 1.5$ GPa a reduction of the wear factor. In Fig. 87 it is recognizable that independent of the initial Hertzian pressure, the materials that are based on SiC exhibit similar wear coefficient within the range of $k_v = 1 * 10^{-7}$ mm³/Nm for $R_{pk} > 0.1$ µm.

For the tests in paraffinic oil it can be summarized that it will be not always necessary to apply the finest method of handling. Usually favourable wear rates can be achieved also with manufacturing processes such as precision grinding. Since such a finishing process exhibits a higher rate of material removal, it is economically more favourable than polishing, if a low clearance increase of the component for application is acceptable.

In earlier tests a dependence of the wear on fracture toughness K_{IC} could be determined [42, 44]. Since for all materials the precision grinding finishing process turned out as favourable, for this process the dependence on fracture toughness K_{IC} mentioned was exemplarily verified. The fracture toughness K_{IC} for the individual materials is to be inferred from table 2. In order to be able to make a statement, only results of the tests were used in paraffinic oil with an initial Hertzian pressure of $P_0 = 3$ GPa.

In Fig. 88 a dependence of the wear rates on fracture toughness can be seen. The wear coefficient k_v, decreases in reverse proportionally to fracture toughness K_{IC}.

8.2 Comparison of the test results in water

The frictional behaviour of the ceramic materials under water lubrication is different than with lubrication with paraffinic oil [45]. The friction coefficient with water lubrication is usually higher.

With the material HIP-Si_3N_4 a smoothing of the function area located in contact takes place; thus results a decrease of the coefficient of friction with increasing number of revolutions up to approx. n = 50,000 revolutions a stationary state is achieved and the coefficient of friction only slightly changes. This is also evident from Fig. 89.

The material SiC exhibits an almost constant coefficient of friction, which lies within the range between f= 0.18 and f = 0.14 (see Fig. 89). The resultant cracks with SiC are to be attributed to the brittleness of the material with the selected pressure.

Water is unsuitable for the lubrication of ZrO_2. With increasing revolution number the friction coefficient rises uninterrupted, so that only low revolution numbers of 10,000 and/or 30,000 could be achieved (compare Fig. 89). This is explainable by the increasing pitting, which is to be explained again by the frequent occurring of shear stresses with rising friction coefficient. Likewise the hydrothermal resistance of ZrO_2 is insufficient.

Si_3N_4-TiN likewise cannot be used under water lubrication. The TiN phase dissolves in water under the formation of titanium hydroxide. Thus it comes partly already after few revolutions to outbreaks and the failure of the material by break. The more roughly the function areas were worked, the sooner a material failure can be expected.

For the material SiC-TiC there appears an increase of the coefficient of friction to approx. 10,000 revolutions; subsequently, the friction coefficient remains approximately constant. The value for the friction coefficient remains always below f = 0.2.

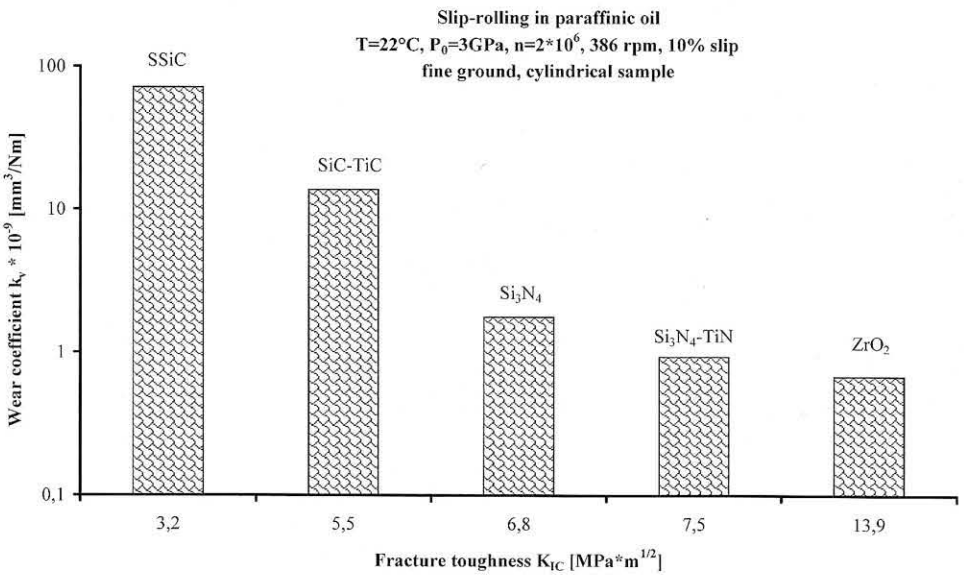

Fig. 88
Slip-rolling friction in paraffinic oil with different ceramic materials; wear coefficient for the finely polished cylindrical samples

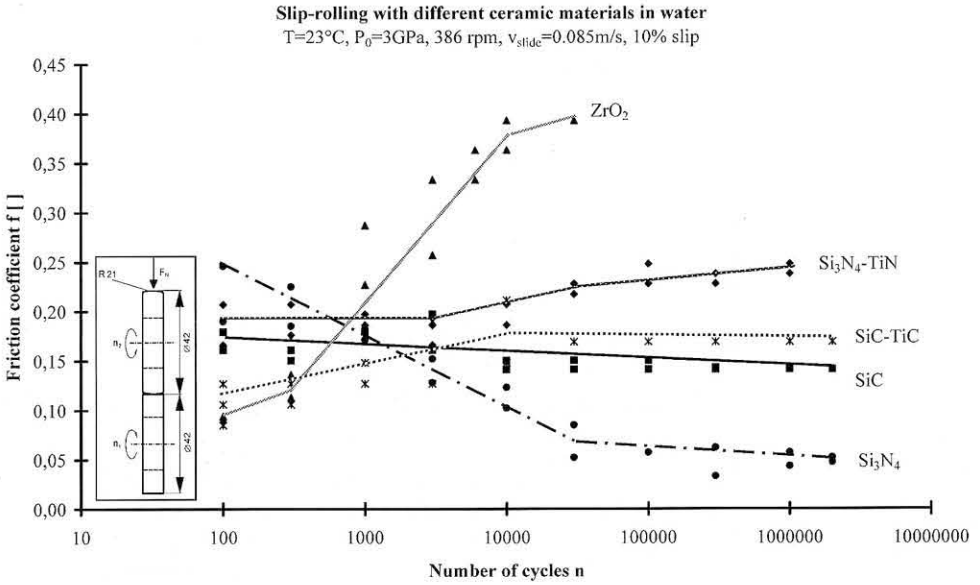

Fig. 89
Selected and typical evolution of the coefficients of friction for different ceramics under water lubrication

As only material HIP-Si_3N_4 is applicable in water and it comes neither to pitting nor to failure by breaking. However it is also to be noted here that under the lubrication with demineralized water, the wear rate is by two orders of magnitude over that with paraffinic oil lubrication [45].

With the material Si_3N_4-TiN, the wear rates could not be determined, since the failure through fracture of the sample results. After the rolling load the outbreaks can be easily recognized with the naked eye.

Also with the material SiC, a strong pitting effect after two million contortions is to be determined under water lubrication with an initial Hertzian pressure of 3 GPa, so that for the spherical test specimen no wear rate can be indicated. The cylindrical test specimen exhibits a wear coefficient within the range of $30*10^{-7}$ mm³/Nm and is comparable with that of SiC in paraffinic oil [46].

Due to the high coefficients of friction (see above) with the material ZrO_2, the tribological tests with contortions of 10,000 and/or 30,000 had to be broken off. Completely contrary to very good wear behaviour in paraffinic oil [16], the wear rate for all test specimens was at $2 * 10^{-5}$ mm³/Nm and thus higher by up to five orders of magnitudes. The starting pitting made impossible a continuation of the tribological stress. With ZrO_2 a dependence on the finishing of the function areas was to be recognized to that extent that the earlier the test had to be terminated, the rougher the surface roughness and thus the selected finishing behaviour. The spherical test specimens exhibited pitting that was too strong, so that a stylus profilometric evaluation was not possible.

The wear coefficient that could be evaluated are summarized in Fig. 90. It is quite evident that the materials with which pitting results (SiC and ZrO_2), exhibit a high wear rate under the rolling stress. With SSiC the wear rate could be determined only planimetrically on the cylindrical test specimens.

The material HIP-Si_3N_4 shows in water with the wear coefficient a dependence on the specimen geometry and

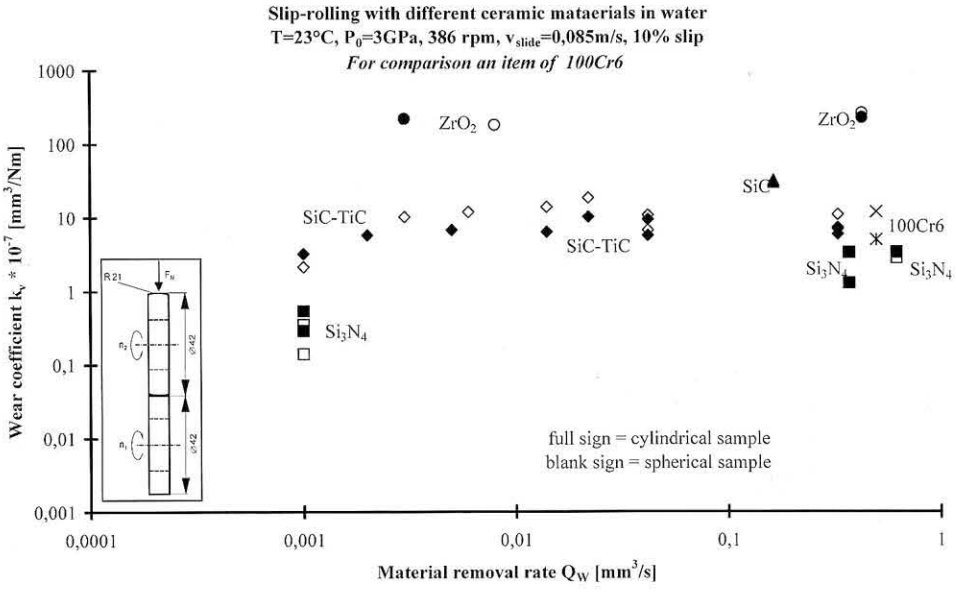

Fig. 90
Slip-rolling stress of different ceramic test specimens. Distinction in materials and geometry of the test specimens

the finishing of the function area. The finely worked surfaces show after two million revolutions a more reduced wear rate by approximately one order of magnitude than the roughly finished test specimens. Within the rough finishing no significant differences in wear behaviour resulted. The dependence of the finishing of the function area could already be accounted for with tests in paraffinic oil [32]. However the differences with respect to different sample geometry in wear behaviour during slip-rolling stress in water are not as pronounced as in paraffinic oil.

The material SiC-TiC shows similarly as HIP-Si_3N_4 a good wear behaviour under slip-rolling stress in water. The wear rates are higher by approx. a power of ten than with HIP-Si_3N_4, however a revolution number of $n \geq 1 * 10^{-6}$ revolutions with an initial Hertzian pressure of $P_0 = 3$ GPa can be achieved. In the wear track of SiC-TiC likewise after higher revolution numbers conical cracks appear which do not lead however for the time being to pitting, since through the slip-rolling stress an wear-reducing TiO_xC_y phase is formed.

If a strong formation of conical cracks and pitting has begun, the dependence of the wear rate on the specimen configuration is likewise annihilated, as can be seen with ZrO_2 in Fig. 90.

Compared with the ceramic materials also the roller and ball bearing steel 100Cr6 in water was tested at 2 GPa. The finely or roughly polished test specimen exhibited a wear coefficient for the cylindrical sample of $4.94 * 10^{-7}$ [mm^3/Nm] and of $11.70 * 10^{-7}$ [mm^3/Nm] for the spherical test specimen. Thus the wear coefficient of the roller and ball bearing steel with a similar finishing as that of HIP-Si_3N_4 is in the same order of magnitude, whereby the wear rates of HIP-Si_3N_4 at 3 GPa are somewhat lower. The somewhat lower wear rates of HIP-Si_3N_4 speak for a good interchangeability of ceramic in a similar application, which was accomplished so far with roller and ball bearing steels.

The roughnesses achieved during the finishing of the function areas are closely joined with the rate of material removal during the finishing; the rougher the function area, the larger also usually is the rate of material removal. Those surface roughness of the function area affects the wear behaviour of the component, which could already be accounted for with paraffinic oil as intermediate media [32].

In the case of HIP-Si_3N_4 an effect of the created surface roughness on the wear rates results. Larger reduced peak heights also cause a higher wear rate and correlate with manufacturing processes, which produce a rougher surface roughness, like grinding and honing. The polished surfaces with lower reduced peak heights show also a lower wear rate.

In water HIP-Si_3N_4 with the material a finer finishing of the function area for the slip-rolling stress is also of advantage (compare Fig. 91).

With HIP-Si_3N_4 a smoothing of the function area under the tribological load in water results. The more roughly the function area was finished, the greater the smoothing. Here the running-in can be used as additional „processing" of the component surface, if an increase of the clearance is acceptable. With the finely worked function areas (roughly polished) the reduction of surface roughnesses is only slight.

It can be clearly recognized in Fig. 91 that there is no influence of surface roughness on the wear rate with ZrO_2 and SiC, since there is pitting.

Although with the material SiC-TiC, pitting did not form after a million revolutions, this material also shows a constancy of the wear coefficient in relation to the reduced peak height of R_{pk}, as this can also be observed with the materials SiC and ZrO_2. This can have the cause that with the material SiC-TiC under the slip-rolling load a process roughness is formed which is independent of the finishing and which affects wear behaviour.

Thus the material HIP-Si_3N_4, processed with a fine finishing process (as, for example, polishing), is the only one of the tested engineering ceramics that can be used also under

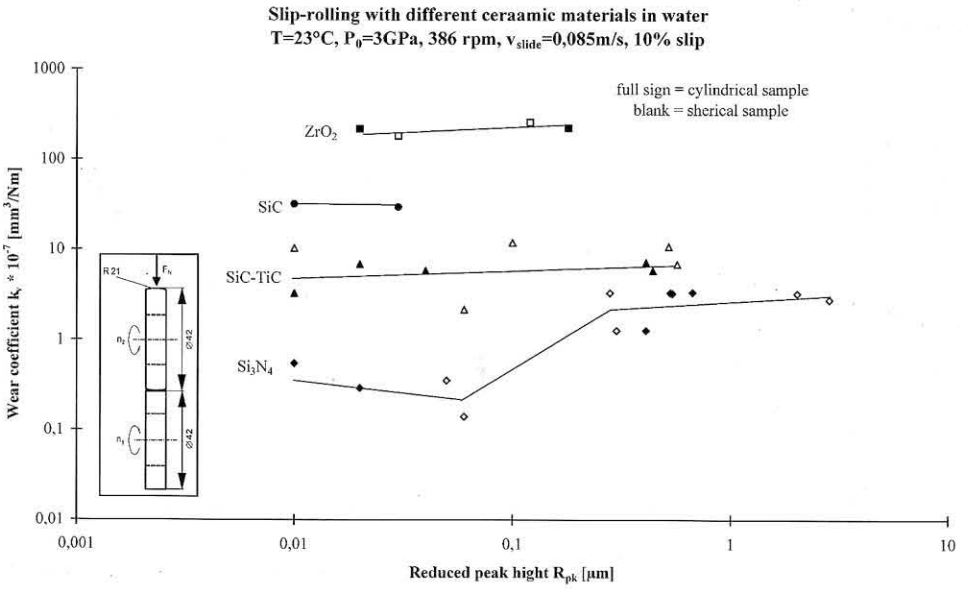

Fig. 91
Wear coefficient as a function of the reduced peak height before the test for the tested ceramics under slip-rolling stress in water

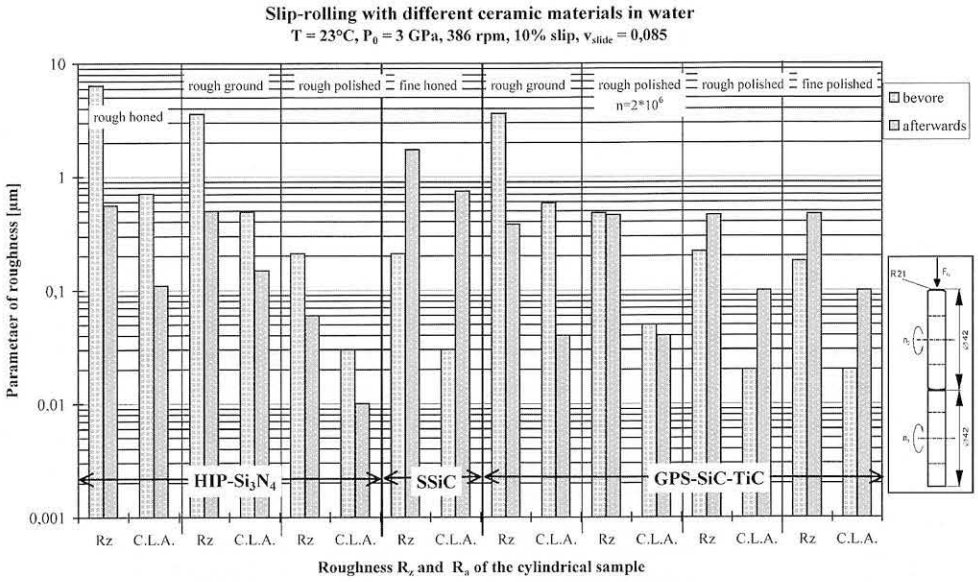

Fig. 92
Roughness characteristic values before and after the tribological stress in water for the different ceramic materials

rolling friction during water lubrication, without resulting in a failure of the component.

If the averaged roughness R_z and the mean peak-to-valley height C.L.A. before and after the slip-rolling stress for the respective cylindrical test specimen are regarded, then the difference for the material without pitting (HIP-Si_3N_4) and the material with pitting (SiC) shows up clearly.

In Fig. 92 the material SiC, with which it comes to pitting and conical cracks under the tribological stress in water, shows an increase of surface roughness by one order of magnitude.

For the material SiC-TiC a uniform behaviour of surface roughnesses through the intake does not appear. The more roughly finished function areas exhibit a smoothing of the surface after the running-in; in comparison the finely finished surfaces exhibit an increase of roughnesses. This is comparable with the material SSiC: the more finely it was finished, the more wear-resistant it appeared under the slip-rolling load; The TiC phase develops an wear-reducing layer, which, however, is not so stable that a material suitable for the slip-rolling wear has resulted.

Of the tested materials, HIP-Si_3N_4, GPS-Si_3N_4-TiN, GPS-SiC-TiC, HIP-ZrO_2 and SSiC only HIP-Si_3N_4 can be used favourably for the slip-rolling stress under water lubrication opposite 100Cr6 with an initial pressure of 3GPa.

With Si_3N_4-TiN the TiN phase in water over titanium hydroxide dissolves, it leads to cracks, outbreaks and thus to the material failure. The materials SiC and ZrO_2 show conical cracks and pitting during the slip-rolling stress in water, so that using them under water lubrication reduces the component reliability. SiC-TiC is more resistant to wear than the pure SSiC; however, it shows cracking likewise (compare Fig. 68), which would lead with a longer persisting slip-rolling load to a material failure.

Only Si_3N_4 shows a stable tribological behaviour without adhesive wear morphologies. The wear coefficient is by two orders of magnitude over that with paraffinic oil lubrication; however, no material failure occurs from breaking or pitting. The tribologically stressed surfaces of HIP-Si_3N_4 experience a smoothing under water lubrication through the running-in with the rolling load.

9 Appendix

Sample no. cylindrical sample spherical sample	Proces-sing	Material removal rate [mm³/s]	cylin-drical sample R_Z [µm] R_a [µm]	cylin-drical sample R_{vk} [µm] R_{pk} [µm]	spherical sample R_Z [µm] R_a [µm]	spherical sample R_{vk} [µm] R_{pk} [µm]	f at begin-ning	f at n_{total}	k_v at n_{total} [mm³/Nm] planimetr., cylindrical sample	k_v at n_{totals} [mm³/Nm] planimetr., spherical sample	k_v at n_{total} [mm³/Nm] planimetric, total	cylin-drical sample R_z [µm] R_a [µm] in track
ZO 002 ZO 021	rough honed D 30	0,373	3,87 0,47	1,30 0,26	5,43 0,74	2,19 0,27	0,054	0,064	$18,70 * 10^{-9}$	$30,20 * 10^{-9}$	$48,90 * 10^{-9}$	1,58 0,47
ZO 065 ZO 035	rough honed D 30	0,373	3,26 0,40	0,95 0,35	6,09 0,82	1,99 0,65	0,128	0,066	$14,20 * 10^{-9}$	$13,20 * 10^{-9}$	$27,40 * 10^{-9}$	
ZO 008 ZO 070	fine honed D 7	0,018	0,36 0,05	0,08 0,04	0,42 0,05	0,11 0,04	0,052	0,043	$0,98 * 10^{-9}$	$2,33 * 10^{-9}$	$3,31 * 10^{-9}$	
ZO 007 ZO 075	fine honed D 7	0,018	0,37 0,05	0,09 0,04	0,48 0,05	0,17 0,04	0,024	0,024	$0,99 * 10^{-9}$	$1,24 * 10^{-9}$	$2,23 * 10^{-9}$	
ZO 024 ZO 028	rough ground D 64	0,623	2,03 0,27	0,40 0,25	9,41 1,41	2,14 1,31	0,116	0,109	$5,20 * 10^{-9}$	$28,50 * 10^{-9}$	$33,70 * 10^{-9}$	0,61 0,11
ZO 051 ZO 022	rough ground D 64	0,623	1,67 0,22	0,35 0,18	7,68 1,20	1,69 0,80	0,147	0,121	$9,12 * 10^{-9}$	$16,87 * 10^{-9}$	$25,99 * 10^{-9}$	
ZO 096 ZO 079	fine ground D 15	0,005	0,44 0,06	0,09 0,05	0,48 0,08	0,11 0,04	0,085	0,081	$0,18 * 10^{-9}$	$1,43 * 10^{-9}$	$1,61 * 10^{-9}$	
ZO 053 ZO 095	fine ground D 15	0,005	0,96 0,14	0,20 0,10	2,37 0,40	0,49 0,32	0,083	0,081	$1,76 * 10^{-9}$	$0,83 * 10^{-9}$	$2,59 * 10^{-9}$	0,29 0,04
ZO 010 ZO 057	rough lapped F 240	0,036 0,037	4,54 0,71	0,94 0,73	5,66 0,87	1,24 0,89	0,100	0,085	$13,13 * 10^{-9}$	$4,46 * 10^{-9}$	$17,59 * 10^{-9}$	0,94 0,14
ZO 029 ZO 048	rough lapped PWB 30	0,032	4,52 0,70	0,93 0,59	5,11 0,78	1,26 0,66	0,097	0,085	$3,00 * 10^{-9}$	$4,00 * 10^{-9}$	$9,00 * 10^{-9}$	
ZO 032 ZO 018	rough lapped PWB 30	0,032	4,26 0,63	0,91 0,60	4,21 0,61	0,89 0,57	0,095	0,085	$10,30 * 10^{-9}$	$0,60 * 10^{-9}$	$10,90 * 10^{-9}$	0,96 0,19
ZO 050 ZO 054	fine lapped PWB 7	0,004	0,37 0,05	0,12 0,03	2,03 0,28	0,51 0,20	0,090	0,083	$0,79 * 10^{-9}$	$7,00 * 10^{-9}$	$7,79 * 10^{-9}$	0,34 0,05
ZO 061 ZO 057	fine lapped PWB 7	0,004	0,41 0,06	0,14 0,02	1,59 0,22	0,32 0,20	0,090	0,081	$0,95 * 10^{-9}$	$0,33 * 10^{-9}$	$1,28 * 10^{-9}$	
ZO 007 ZO 075	rough polished D 3	0,0007	0,18 0,03	0,04 0,02	0,40 0,05	0,15 0,02	0,090	0,081	$0,06 * 10^{-9}$	$1,17* 10^{-9}$	$1,23* 10^{-9}$	0,18 0,02
ZO 065 ZO 021	rough polished D 3	0,0007	0,23 0,03	0,05 0,02	0,48 0,06	0,18 0,04	0,083	0,081	not assignable	not assignable	not assignable	

Slip-rolling with HIP-Si_3N_4 (NBD 200) in paraffinic oil
F_N = 1005 N, P_0 = 3000 N/mm², v_{slide} = 0,085 m/s, n = 386 rpm, slip = 10 %,
$n_{total} = 2 * 10^6$, s_{slide} = 26.390 m, r.h. = 30 - 39 %

Sample no. cylindrical sample spherical sample	Processing	Material removal rate [mm³/s]	cylindrical sample R_Z [µm] R_a [µm]	cylindrical sample R_{vk} [µm] R_{pk} [µm]	spherical sample R_Z [µm] R_a [µm]	spherical sample R_{vk} [µm] R_{pk} [µm]	f at beginning	f at n_{total}	k_v at n_{total} [mm³/Nm] planimetr., cylindrical sample	k_v at n_{totals} [mm³/Nm] planimetr., spherical sample	k_v at n_{total} [mm³/Nm] planimetric, total	cylindrical sample R_z [µm] R_a [µm] in track
ZO 023 ZO 019	rough honed D 30	0,373	6,40 0,71	2,81 0,54	5,49 0,72	2,30 0,28	0,246	0,047	$3,27 * 10^{-7}$	$3,31 * 10^{-7}$	$6,58 * 10^{-7}$	0,56 0,11
ZO 005 ZO 043	rough honed D 30	0,373	3,62 0,40	0,97 0,41	4,48 0,58	1,52 0,30	0,235	0,052	$1,26 * 10^{-7}$	$1,26 * 10^{-7}$	$2,52 * 10^{-7}$	
ZO 071 ZO 037	rough ground D 64	0,623	3,59 0,49	1,02 0,67	12,33 2,21	3,94 2,03	0,194	0,057	$3,34 * 10^{-7}$	$3,26 * 10^{-7}$	$6,60 * 10^{-7}$	0,50 0,15
ZO 047 ZO 038	rough ground D 64	0,623	3,06 0,55	0,61 0,53	12,20 2,18	2,48 2,85	0,190	0,052	$3,33 * 10^{-7}$	$2,78 * 10^{-7}$	$6,11 * 10^{-7}$	
ZO 015 ZO 016	rough polished D 3	0,0007	0,21 0,03	0,04 0,02	0,44 0,06	0,13 0,06	0,071	0,021	$0,29 * 10^{-7}$	$0,14 * 10^{-7}$	$0,43 * 10^{-7}$	0,06 0,01
ZO 068 ZO 070	rough polished D 3	0,0007	0,15 0,02	0,04 0,01	0,39 0,05	0,11 0,05	0,095	0,005	$0,54 * 10^{-7}$	$0,35 * 10^{-7}$	$0,89 * 10^{-7}$	0,06 0,01

Slip-rolling with HIP-Si_3N_4 (NBD 200) in water:

F_N = 1005 N, P_0 = 3000 N/mm², v_{slide} = 0,085 m/s, n = 386 rpm, slip = 10 %, $n_{total} = 2 * 10^6$, s_{slide} = 26.390 m, r.h. = 30 - 39 %

Sample no. cylindrical sample spherical sample	Proces-sing	Material removal rate [mm³/s]	cylin-drical sample R_Z [µm] R_a [µm]	cylin-drical sample R_{vk} [µm] R_{pk} [µm]	spherical sample R_Z [µm] R_a [µm]	spherical sample R_{vk} [µm] R_{pk} [µm]	f at begin-ning	f at n_{total}	k_v at n_{total} [mm³/Nm] planimetr., cylindrical sample	k_v at n_{totals} [mm³/Nm] planimetr., spherical sample	k_v at n_{total} [mm³/Nm] planimetric, total	cylin-drical sample R_Z [µm] R_a [µm] in track
021 AE 020 AE	rough honed D 46	0,438	3,09 0,37	1,05 0,19	3,26 0,42	0,83 0,47	0,112	0,083	$11,25 * 10^{-9}$	$11,53 * 10^{-9}$	$22,78 * 10^{-9}$	0,59 0,15
022 AE 019 AE	rough honed D 46	0,438	3,94 0,44	1,22 0,20	3,61 0,38	1,15 0,22	0,112	0,091	$15,03 * 10^{-9}$	$13,07 * 10^{-9}$	$28,10 * 10^{-9}$	0,52 0,13
014 AE 004 AE	fine honed D 7	0,011	0,30 0,03	0,07 0,03	0,78 0,08	0,20 0,04	0,091	0,095	not assignable	not assignable	not assignable	0,14 0,02
012 AE 003 AE	fine honed D 7	0,011	0,34 0,04	0,08 0,03	0,62 0,06	0,14 0,04	0,091	0,095	$0,27 * 10^{-9}$	$3,62 * 10^{-9}$	$3,88 * 10^{-9}$	0,15 0,02
AE 021 AE 019	rough ground D 126	0,85	3,13 0,42	0,76 0,28	3,62 0,55	0,67 0,71	0,095	0,087	$3,78 * 10^{-9}$	$0,78 * 10^{-9}$	$4,57 * 10^{-9}$	0,58 0,13
AE 022 AE 020	rough ground D 126	0,85	2,97 0,40	0,73 0,24	3,10 0,50	0,64 0,54	0,095	0,087	$6,69 * 10^{-9}$	$5,76 * 10^{-9}$	$12,45 * 10^{-9}$	
033 AE 006 AE	fine ground D 15	0,025	1,76 0,25	0,35 0,24	3,24 0,58	0,60 0,50	0,093	0,085	$3,03 * 10^{-9}$	$7,58 * 10^{-9}$	$10,61 * 10^{-9}$	
010 AE 018 AE	fine ground D 15	0,025	1,74 0,27	0,31 0,20	2,93 0,52	0,69 0,41	0,093	0,085	$5,00 * 10^{-9}$	$0,89 * 10^{-9}$	$5,89 * 10^{-9}$	0,42 0,07
024 AE(2)[1] 031 AE(2)	fine ground[2] D 15	0,010 0,008	0,83 0,11	0,14 0,10	1,19 0,17	0,27 0,16	0,093	0,087	$0,93 * 10^{-9}$	not assignable	not assignable	
032 AE (2) 009 AE	rough lapped F 240	0,072 0,059	5,97 0,93	1,09 0,88	7,43 1,19	1,58 1,05	0,099	0,081	$25,56 * 10^{-9}$	$31,49 * 10^{-9}$	$57,05 * 10^{-9}$	0,58 0,10
007 AE 009 AE *F_N=1005N*	rough lapped PWB 30	0,020	6,23 0,93	1,29 0,96	5,41 0,87	1,38 0,79	0,104	0,085	$19,23 * 10^{-9}$	$23,64 * 10^{-9}$	$42,87 * 10^{-9}$	0,71 0,09
029 AE 027 AE	rough lapped PWB 30	0,046 0,047	5,71 0,88	1,39 0,58	5,40 0,81	1,15 0,83	0,095	0,089	$15,83 * 10^{-9}$	$13,46 * 10^{-9}$	$29,29 * 10^{-9}$	0,36 0,07
008 AE 006 AE *F_N=1005N*	fine lapped PWB 7	0,010	1,17 0,15	0,21 0,17	1,62 0,48	0,75 0,23	0,104	0,085	$3,06 * 10^{-9}$	$0,44 * 10^{-9}$	$3,50 * 10^{-9}$	0,31 0,04
032 AEX[1] 015 AEX	fine lapped PWB 7	0,004 0,002	0,84 0,09	0,16 0,13	1,36 0,17	0,50 0,25	0,091	0,093	$2,82 * 10^{-9}$	$0,24 * 10^{-9}$	$3,06 * 10^{-9}$	
023 AE 030 AE	rough polished D 3	0,029 0,034	0,17 0,02	0,03 0,02	0,39 0,05	0,10 0,03	0,091	0,081	not assignable	not assignable	not assignable	0,13 0,02
023 AE(2) 030 AE(2)	rough polished D 3	0,002 0,006	0,24 0,03	0,05 0,03	0,45 0,21	0,14 0,07	0,089	0,087	$2,31 * 10^{-9}$	$0,58 * 10^{-9}$	$2,90 * 10^{-9}$	
024 AE 031 AE	fine polished D 1	0,019 0,058	0,19 0,02	0,03 0,02	0,32 0,04	0,09 0,03	0,095	0,091	$0,08 * 10^{-9}$	not assignable	not assignable	0,15 0,02

Slip-rolling with Si_3N_4-TiN (EDM) in paraffinic oil;

F_N = 1150 N, P_0 = 3000 N/mm², v_{slide} = 0,085 m/s, n = 386 rpm, slip = 10 %,
$n_{total} = 2 * 10^6$, s_{slide} = 26.390 m, r.h. = 30 - 39 %

Sample no. cylindrical sample spherical sample	Process-sing	Material removal rate [mm³/s]	cylin-drical sample R_Z [µm] R_a [µm]	cylin-drical sample R_{vk} [µm] R_{pk} [µm]	spherical sample R_Z [µm] R_a [µm]	spherical sample R_{vk} [µm] R_{pk} [µm]	f at begin ning	f at n_{total}	k_v at n_{total} [mm³/Nm] planimetr., cylindrical sample	k_v at n_{totals} [mm³/Nm] planimetr., spherical sample	k_v at n_{total} [mm³/Nm] planimetric, total	cylin-drical sample R_z [µm] R_a [µm] in track
016 AE 017 AE	rough honed D 46	0,435	3,67 0,50	0,84 0,47	2,38 0,31	0,65 0,20	0,207					Pump damage d break-ing-off
011 AE 005 AE F_N=480N	fine honed D 7	0,011	0,29 0,03	0,06 0,03	0,63 0,06	0,15 0,04	0,149	0,099	$13{,}51 * 10^{-7}$	$63{,}86 * 10^{-7}$	$77{,}37 * 10^{-7}$	
028 AE 025 AE	rough lapped PWB 30	0,040 0,052	5,68 0,83	1,20 0,79	5,67 0,79	1,13 0,80	0,207	n≈ $1*10^6$, 0,238	not assignable, fatigue	not assignable, fatigue		not assig-nable, fatigue
008 AE 026 AE	fine lapped PWB 7	0,008 0,009	0,88 0,28	0,20 0,15	1,00 0,12	0,33 0,12	0,166	n≈ $1*10^6$, 0,248	not assignable, fatigue	not assignable, fatigue		not assig-nable, fatigue

Slip-rolling with Si_3N_4-TiN (EDM) in water;

F_N = 1150 N, P_0 = 3000 N/mm², v_{slide} = 0,085 m/s, n = 386 rpm, slip = 10 %, $n_{total} = 2 * 10^6$, s_{slide} = 26.390 m, r.h. = 30 - 39 %

Slip-rolling in paraffinic oil with SiC (EKasic D)

F_N = 665 N, P_0 = 3000 N/mm², v_{slide} = 0,085 m/s, n = 386 rpm, slip = 10 %, n_{total} = 2 * 10^6, s_{slide} = 26.390 m, r.h. = 30 - 39 %

Sample no. cylindrical sample spherical sample	Processing	Material removal rate [mm³/s]	cylindrical sample R_z [µm] R_a [µm]	cylindrical sample R_{vk} [µm] R_{pk} [µm]	spherical sample R_z [µm] R_a [µm]	spherical sample R_{vk} [µm] R_{pk} [µm]	f at beginning	f at n_{total}	k_v at n_{total} [mm³/Nm] planimetr., cylindrical sample	k_v at n_{totals} [mm³/Nm] planimetr., spherical sample	k_v at n_{total} [mm³/Nm] planimetric, total	cylindrical sample R_z [µm] R_a [µm] in track
AR 097 AR 092	rough honed D 30	0,48	4,44 0,55	1,31 0,34	3,30 0,40	0,74 0,31	0,122	0,082	102,76 * 10^{-9}	79,17 * 10^{-9}	181,93 * 10^{-9}	0,62 0,10
AR 095 AR 094	rough honed D 30	0,48	1,14 0,09	0,21 0,07	1,58 0,14	0,41 0,08	0,140	0,086	72,95 * 10^{-9}	68,00 * 10^{-9}	140,96 * 10^{-9}	
AR 095 AR 094	fine honed D 7	0,164	0,41 0,06	0,09 0,05	1,03 0,10	0,32 0,08	0,093	0,072	260,00 * 10^{-9}	11,00 * 10^{-9}	271,00 * 10^{-9}	0,83 0,20
AR 096 AR 091	fine honed D 7	0,164	0,33 0,04	0,08 0,02	0,95 0,10	0,19 0,06	0,093	0,072	312,00 * 10^{-9}	53,00 * 10^{-9}	365,00 * 10^{-9}	0,46 0,07
bm 015 bm 029	rough ground D 126	0,74	5,80 0,91	1,33 0,52	6,58 1,06	1,47 0,93	0,125	0,090	138,47 * 10^{-9}	169,24 * 10^{-9}	307,71 * 10^{-9}	0,84 0,16
bm 020 bm 026	rough ground D 126	0,74	6,27 0,87	1,33 0,57	8,18 1,47	1,68 1,26	0,140	0,090	128,08 * 10^{-9}	79,92 * 10^{-9}	208,00 * 10^{-9}	
bm 012 bm 014	fine ground D 15	0,03	1,70 0,19	0,31 0,19	2,10 0,25	0,45 0,22	0,115	0,079	89,36 * 10^{-9}	82,64 * 10^{-9}	172,00 * 10^{-9}	0,59 0,10
bm 021 bm 024	fine ground D 15	0,03	1,84 0,17	0,33 0,18	2,26 0,31	0,53 0,26	0,115	0,079	71,31 * 10^{-9}	114,75 * 10^{-9}	186,06 * 10^{-9}	
bm 03 AR 026	rough lapped PWB 30	0,061 0,031	6,59 0,89	1,34 0,88	7,43 1,06	1,94 0,62	0,233	0,179	57,43 * 10^{-9}	81,07 * 10^{-9}	138,50 * 10^{-9}	0,29 0,08
bm 010 bm 016	rough lapped PWB 30	0,019 0,028	7,20 0,98	1,95 0,76	5,70 0,68	1,82 0,30	0,129	0,093	62,21 * 10^{-9}	59,10 * 10^{-9}	121,31 * 10^{-9}	
bm 01 bm 02	fine lapped PWB 7	0,003	1,73 0,16	0,39 0,10	1,70 0,18	0,45 0,12	0,100	0,079	64,79 * 10^{-9}	67,81 * 10^{-9}	133,00 * 10^{-9}	0,64 0,12
bm 011 bm 025	fine lapped PWB 7	0,002	2,74 0,29	0,90 0,11	2,17 0,19	0,56 0,07	0,122	0,082	81,20 * 10^{-9}	76,33 * 10^{-9}	157,53 * 10^{-9}	
bm 07 bm 09	rough polished D 3	0,002	0,38 0,03	0,10 0,02	0,49 0,05	0,14 0,03	0,086	0,072	688,95 * 10^{-9}	1409,74 * 10^{-9}	2098,69 * 10^{-9}	0,39 0,11
AR 095 AR 019	rough polished D 3	0,002	0,35 0,05	0,06 0,04	0,85 0,08	0,20 0,04	0,179	0,143	824,65 * 10^{-9}	587,29 * 10^{-9}	1411,9 * 10^{-9}	0,43 0,06
bm 05 AR 087	fine polished D 1	0,003 0,001	0,15 0,02	0,04 0,01	0,42 0,03	0,13 0,01	0,197	0,172	576,80 * 10^{-9}	299,15 * 10^{-9}	875,95 * 10^{-9}	n.a., Pitting
bm 04 AR 074	fine polished D 1	0,001 0,002	0,12 0,01	0,03 0,01	0,52 0,10	0,11 0,09	0,197	0,161	818,93 * 10^{-9}	1403,50 * 10^{-9}	2232,43 * 10^{-9}	n.a., Pitting
bm 011§ AR 094§	rough lapped PWB 30/ rough polished D 3	0,02 0,002	6,39 0,87	1,33 0,88	 0,48 0,04	 0,14 0,02	0,143	0,072	476,44 * 10^{-9}	590,67 * 10^{-9}	1067,11 * 10^{-9}	0,61 0,10

n.a.: not assignable
§ mashined a second time

Slip-rolling in paraffinic oil with SiC (EKasic D)

F_N = 250 N, P_0 = 1500 N/mm², v_{slide} = 0,085 m/s, n = 386 rpm, slip = 10 %, n_{total} = 2 * 10^6, s_{slide} = 26.390 m, r.h. = 30 - 39 %

Sample no. cylindrical sample spherical sample	Processing	Material removal rate [mm³/s]	cylindrical sample R_z [µm] R_a [µm]	cylindrical sample R_{vk} [µm] R_{pk} [µm]	spherical sample R_z [µm] R_a [µm]	spherical sample R_{vk} [µm] R_{pk} [µm]	f at beginning	f at n_{total}	k_v at n_{total} [mm³/Nm] planimetr., cylindrical sample	k_v at n_{totals} [mm³/Nm] planimetr., spherical sample	k_v at n_{total} [mm³/Nm] planimetric, total	cylindrical sample R_z [µm] R_a [µm] in track
bm 018 bm 019	fine ground D 15	0,03	1,29 0,14	0,22 0,18	2,31 0,34	0,52 0,22	0,133	0,095	105,96 * 10^{-9}	108,18 * 10^{-9}	214,14 * 10^{-9}	0,33 0,09
bm 017 bm 027	fine ground D 15	0,03	1,53 0,16	0,25 0,23	2,13 0,28	0,45 0,24	0,133	0,105	37,02 * 10^{-9}	46,91 * 10^{-9}	83,93 * 10^{-9}	0,44 0,07
bm 06 AR 083	fine polished D 1	0,002 0,007	0,26 0,03	0,07 0,02	0,52 0,05	0,17 0,02	0,105	0,105	not assignable	not assignable	not assignable	
bm 06 AR 083*	fine polished D 1	0,002 0,007	0,26 0,03	0,07 0,02	0,52 0,05	0,17 0,02	0,095	0,086	0,12 * 10^{-9}	4,90 * 10^{-9}	5,02 * 10^{-9}	

* n_{total} = 20*10^6

Sample no. cylindrical sample spherical sample	Processing	Material removal rate [mm³/s]	cylindrical sample R_z [µm] R_a [µm]	cylindrical sample R_{vk} [µm] R_{pk} [µm]	spherical sample R_z [µm] R_a [µm]	spherical sample R_{vk} [µm] R_{pk} [µm]	f at beginning	f at n_{total}	k_v at n_{total} [mm³/Nm] planimetr., cylindrical sample	k_v at n_{totals} [mm³/Nm] planimetr., spherical sample	k_v at n_{total} [mm³/Nm] planimetric, total	cylindrical sample R_z [µm] R_a [µm] in track
AR 097 AR 092	fine honed D 7	0,164	0,31 0,04	0,07 0,03	0,91 0,09	0,18 0,06	0,161	0,143	29,61 * 10^{-7}	not assignable	not assignable	
AR 098 AR 093	fine honed D 7	0,164	0,21 0,03	0,05 0,01	0,88 0,09	0,19 0,08	0,179	0,143	31,81 * 10^{-7}	not assignable	not assignable	1,74 0,75

Slip-rolling in water with SiC (EKasic D);

*F_N = 665 N, P_0 = 3 GPa, v_{slide} = 0,085 m/s, n = 386 rpm, slip = 10 %, n_{total} = 2 * 10^6, s_{slide} = 26.390 m, r.h. = 30 - 39 %*

Slip-rolling in paraffinic oil with SiC-TiC

F_N = 563 N, P_0 = 3000 N/mm^2, v_{slide} = 0,085 m/s, n = 386 rpm, slip = 10 %, n_{total} = 2 * 10^6, s_{slide} = 26.390 m, r.h. = 30 - 39 %

Sample no. cylindrical sample spherical sample	Processing	Material removal rate [mm^3/s]	cylindrical sample R_z [µm] R_a [µm]	cylindrical sample R_{vk} [µm] R_{pk} [µm]	spherical sample R_z [µm] R_a [µm]	spherical sample R_{vk} [µm] R_{pk} [µm]	f at beginning	f at n_{total}	k_v at n_{total} [mm^3/Nm] planimetr., cylindrical sample	k_v at n_{totals} [mm^3/Nm] planimetr., spherical sample	k_v at n_{total} [mm^3/Nm] planimetric, total	cylindrical sample R_z [µm] R_a [µm] in track
024 AD§ 018 AD§	rough honed D 15	0,003 0,002	0,34 0,04	0,07 0,04	1,15 0,15	0,24 0,08	0,093	0,085	17,07 * 10^{-9}	34,07 * 10^{-9}	51,13 * 10^{-9}	0,36 0,07
026 AD§ 020 AD§	rough honed D 15	0,006 0,002	0,65 0,07	0,12 0,06	1,17 0,16	0,26 0,10	0,101	0,093	21,56 * 10^{-9}	23,52 * 10^{-9}	45,08 * 10^{-9}	0,34 0,07
027 AD§ 025 AD§	fine honed D 7	0,007 0,003	0,82 0,09	0,15 0,08	1,17 0,13	0,28 0,09	0,101	0,089	29,89 * 10^{-9}	28,01 * 10^{-9}	57,90 * 10^{-9}	0,29 0,08
028 AD§ 029 AD§	fine honed D 7	0,010 0,0,003	0,66 0,22	0,12 0,07	1,25 0,14	0,29 0,09	0,106	0,085	96,43 * 10^{-9}	89,01 * 10^{-9}	185,43 * 10^{-9}	0,24 0,03
027 AD§ 018 AD§	rough ground D 126	0,33	4,04 0,64	0,64 0,57	4,56 0,86	0,85 0,64	0,152	0,085	50,83 * 10^{-9}	59,28 * 10^{-9}	110,11 * 10^{-9}	0,49 0,05
024 AD§ 025 AD§	rough ground D 126	0,33	4,08 0,64	0,88 0,73	4,52 0,84	0,80 0,82	0,110	0,085	79,86 * 10^{-9}	68,15 * 10^{-9}	148,00 * 10^{-9}	0,51 0,05
026 AD 020 AD*	rough ground D 30	0,32	1,19 0,19	0,32 0,18	3,23 0,76	0,74 0,45	0,097	0,085	10,81 * 10^{-9}	7,31 * 10^{-9}	18,12 * 10^{-9}	0,69 0,10
024 AD 018 AD	grob geschliffen D 30	0,32	1,14 0,16	0,25 0,15	3,66 0,83	0,82 0,45	0,097	0,085	10,80 * 10^{-9}	15,50 * 10^{-9}	26,30 * 10^{-9}	0,61 0,07
028 AD 025 AD	fine ground D 15	0,33	0,93 0,12	0,24 0,15	4,30 1,03	0,74 0,83	0,093	0,085	24,29 * 10^{-9}	11,52 * 10^{-9}	35,82 * 10^{-9}	0,55 0,06
027 AD 029 AD	fine ground D 15	0,33	1,04 0,15	0,24 0,14	4,84 1,01	0,68 1,27	0,093	0,089	13,79 * 10^{-9}	4,24 * 10^{-9}	18,03 * 10^{-9}	
016 AD 015 AD	rough lapped PWB 30	0,044 0,042	4,27 0,65	0,94 0,59	5,07 0,73	1,25 0,54	0,144	0,089	207,46 * 10^{-9}	291,75 * 10^{-9}	499,21 * 10^{-9}	0,24 0,08
016 AD§ 017 AD§	rough lapped PWB 30	0,061 0,078	6,94 1,02	1,41 0,85	6,41 0,93	1,27 0,76	0,118	0,085	220,51 * 10^{-9}	293,49 * 10^{-9}	514,00 * 10^{-9}	0,90 0,12
019 AD 017 AD	fine lapped PWB 7	0,005 0,004	1,35 0,18	0,35 0,19	1,68 0,22	0,44 0,12	0,110	0,085	201,28 * 10^{-9}	192,29 * 10^{-9}	393,57 * 10^{-9}	0,23 0,09
019 AD§ 015 AD§	fine lapped PWB 7	0,004	1,53 0,19	0,30 0,16	1,75 0,21	0,45 0,12	0,127	0,076	231,08 * 10^{-9}	149,10 * 10^{-9}	380,18 * 10^{-9}	0,69 0,14
022 AD 014 AD	rough polished D 3	0,003	0,23 0,03	0,04 0,03	0,75 0,07	0,19 0,03	0,093	0,093	0,72 * 10^{-9}	1,22 * 10^{-9}	1,94 * 10^{-9}	0,15 0,02
023 AD 012 AD	fine polished D 1	0,001 0,003	0,25 0,03	0,04 0,03	0,46 0,04	0,13 0,03	0,097	0,097	4,29 * 10^{-9}	0,16 * 10^{-9}	4,44 * 10^{-9}	0,16 0,02

* *n = 3,5.10^6*

§ *mashined a second time*

Slip-rolling in water with SiC-TiC

F_N = 563 N, P_0 = 3 GPa, v_{slide} = 0,085 m/s, n = 386 rpm, slip = 10 %, n_{total} = 1 * 10^6, s_{slide} = 13.195 m, r.h. = 30 - 39 %

Sample no. cylindrical sample spherical sample	Proces-sing	Material removal rate [mm^3/s]	cylin-drical sample R_Z [µm] R_a [µm]	cylin-drical sample R_{vk} [µm] R_{pk} [µm]	spherical sample R_Z [µm] R_a [µm]	spherical sample R_{vk} [µm] R_{pk} [µm]	f at begin-ning	f at n_{total}	k_v at n_{total} [mm^3/Nm] planimetr., cylindrical sample	k_v at n_{totals} [mm^3/Nm] planimetr., spherical sample	k_v at n_{total} [mm^3/Nm] planimetric, total	cylin-drical sample R_z [µm] R_a [µm] in track
028 AD§ 020 AD§	rough ground D 126	0,33	3,64 0,59	0,63 0,41	4,27 0,78	0,96 0,57	0,127	0,169	7,16 * 10^{-7}	6,90 * 10^{-7}	14,06 * 10^{-7}	0,38 0,04
026 AD 029 AD	rough ground D 126	0,33	3,49 0,55	0,94 0,44	4,419 0,70	0,91 0,52	0,127	0,169	5,83 * 10^{-7}	10,80 * 10^{-7}	16,63 * 10^{-7}	0,63 0,14
026 AD§ 018 AD§	fine ground D 28	0,042	0,98 0,17	0,18 0,10	2,53 0,43	0,39 0,38	0,118	0,190	5,70 * 10^{-7}	6,69 * 10^{-7}	12,39 * 10^{-7}	0,22 0,03
024 AD§ 020 AD§	fine ground D 28	0,042	1,07 0,15	0,22 0,10	2,99 0,56	0,43 0,54	0,110	0,203	9,42 * 10^{-7}	10,76 * 10^{-7}	20,18 * 10^{-7}	0,44 0,09
019 AD§ 017 AD§	rough lapped B 30	0,014 0,031	5,06 0,78	1,01 0,62	5,48 0,82	1,49 0,65	0,118	0,186	10,20 * 10^{-7}	18,37 * 10^{-7}	28,58 * 10^{-7}	0,36 0,10
023 AD§ 015 AD§	fine lapped B 7	0,011 0,018	1,33 0,16	0,37 0,09	1,20 0,13	0,28 0,10	0,118	0,195	6,33 * 10^{-7}	13,84 * 10^{-7}	20,17 * 10^{-7}	0,36 0,10
019 AD 015 AD*	rough polished D 3	0,005 0,006	0,22 0,02	0,05 0,02	1,03 0,13	0,41 0,10	0,106	0,169	6,82 * 10^{-7}	12,00 * 10^{-7}	18,82 * 10^{-7}	0,46 0,10
023 AD§ 012 AD§	rough polished D 3	0,002 0,001	0,48 0,05	0,12 0,04	0,89 0,12	0,27 0,06	0,085	0,169	5,77 * 10^{-7}	2,15 * 10^{-7}	7,93 * 10^{-7}	0,46 0,04
016 AD 017 AD	fine polished D 1	0,001 0,003	0,18 0,02	0,05 0,01	0,44 0,04	0,13 0,01	0,106	0,169	3,24 * 10^{-7}	10,30 * 10^{-7}	13,54 * 10^{-7}	0,47 0,10

§ *mashined a second time*

* *n = 2 . 10^6*

Sample no. cylindrical sample spherical sample	Processing	Material removal rate [mm³/s]	cylindrical sample R_z [µm] R_a [µm]	cylindrical sample R_{vk} [µm] R_{pk} [µm]	spherical sample R_z [µm] R_a [µm]	spherical sample R_{vk} [µm] R_{pk} [µm]	f at beginning	f at n_{total}	k_v at n_{total} [mm³/Nm] planimetr., cylindrical sample	k_v at n_{totals} [mm³/Nm] planimetr., spherical sample	k_v at n_{total} [mm³/Nm] planimetric, total	cylindrical sample R_z [µm] R_a [µm] in track
082 AA 072 AA	rough honed D 30	0,43	4,74 0,53	1,29 0,30	3,29 0,44	0,83 0,30	0,100	0,068	$5,95 * 10^{-9}$	$4,51 * 10^{-9}$	$10,46 * 10^{-9}$	1,17 0,27
090 AA 069 AA	rough honed D 30	0,43	4,57 0,51	1,33 0,27	2,98 0,43	1,12 0,18	0,097	0,079	$6,63 * 10^{-9}$	$6,50 * 10^{-9}$	$13,13 * 10^{-9}$	
046 AA 035 AA	fine honed D 7	0,011	0,93 0,10	0,16 0,10	0,98 0,10	0,18 0,07	0,082	0,076	$0,83 * 10^{-9}$	$1,57 * 10^{-9}$	$2,40 * 10^{-9}$	0,40 0,06
092 AA 080 AA	fine honed D 7	0,011	1,04 0,11	0,20 0,11	1,23 0,13	0,26 0,14	0,083	0,076	$0,65 * 10^{-9}$	$0,25 * 10^{-9}$	$0,90 * 10^{-9}$	
044 AA 030 AA	rough ground D 126	0,89	6,07 0,94	1,18 0, 38	8,63 1,48	2,04 0,94	0,094	0,079	$6,64 * 10^{-9}$	$8,66 * 10^{-9}$	$15,30 * 10^{-9}$	1,06 0,32
045 AA 029 AA	rough ground D 126	0,89	5,38 0,81	1,09 0,66	8,10 1,28	1,77 1,21	0,094	0,079	$8,42 * 10^{-9}$	$10,53 * 10^{-9}$	$18,95 * 10^{-9}$	1,25 0,29
050AA 039 AA	fine ground D 15	0,025	1,30 0,19	0,26 0,19	2,44 0,46	0,34 0,35	0,082	0,076	$0,68 * 10^{-9}$	$0,53 * 10^{-9}$	$1,21 * 10^{-9}$	0,38 0,19
049 AA 031 AA	fine ground D 15	0,025	1,10 0,14	0,21 0,13	2,23 0,41	0,37 0,39	0,082	0,076	$0,82 * 10^{-9}$	$4,53 * 10^{-9}$	$5,35 * 10^{-9}$	
042 AA 071 AA	rough lapped F 240	0,029	4,74 0,68	1,43 0,37	2,66 0,35	0,89 0,28	0,095	0,076	$3,99 * 10^{-9}$	$6,38 * 10^{-9}$	$10,38 * 10^{-9}$	0,72 0,12
074 AA 079 AA	rough lapped PWB 30	0,026 0,022	3,55 0,48	0,56 0,82	4,84 0,68	1,14 0,62	0,094	0,079	$5,38 * 10^{-9}$	$5,16 * 10^{-9}$	$10,54 * 10^{-9}$	0,52 0,08
088 AA 037 AA	rough lapped PWB 30	0,013 0,010	4,61 0,71	0,86 0,70	4,02 0,60	1,11 0,21	0,095	0,076	$6,42 * 10^{-9}$	$6,55 * 10^{-9}$	$12,97 * 10^{-9}$	0,85 0,11
093 AA 077 AA	fine lapped PWB 7	0,006 0,011	0,28 0,04	0,07 0,03	1,31 0,15	0,31 0,17	0,082	0,077	n.a.	n.a.	n.a.	0,24 0,03
084 AA 036 AA	fine lapped PWB 7	0,001 0,006	0,89 0,08	0,25 0,04	1,08 0,13	0,36 0,04	0,080	0,076	n.a.	$1,90 * 10^{-9}$	n.a.	0,36 0,04
087 AA 038 AA	rough polished D 3	0,006 0,004	0,13 0,02	0,03 0,02	0,20 0,02	0,04 0,02	0,063	0,065	n.a. (still after $n=10^7$)	n.a. (still after $n=10^7$)	n.a. (still after $n=10^7$)	0,13 0,02

n.a.: not assignable

Slip-rolling in paraffinic oil with ZrO_2 (htc-PSZA);

F_N = 1575 N, P_0 = 3000 N/mm², v_{slide} = 0,085 m/s, n = 386 rpm, slip = 10 %,
$n_{total} = 2 * 10^6$, s_{slide} = 26.390 m, r.h. = 30 - 39 %

Sample no. cylindrical sample spherical sample	Processing	Material removal rate [mm³/s]	cylindrical sample R_z [µm] R_a [µm]	cylindrical sample R_{vk} [µm] R_{pk} [µm]	spherical sample R_z [µm] R_a [µm]	spherical sample R_{vk} [µm] R_{pk} [µm]	f at beginning	f at n_{total}	k_v at n_{total} [mm³/Nm] planimetr., cylindrical sample	k_v at n_{totals} [mm³/Nm] planimetr., spherical sample	k_v at n_{total} [mm³/Nm] planimetric, total	cylindrical sample R_z [µm] R_a [µm] in track
089 AA 067 AA §	rough honed D 30	0,43	2,69 0,37	0,75 0,18	1,28 0,19	0,39 0,12	0,091	0,393	$2,24 * 10^{-5}$	$2,58 * 10^{-5}$	$4,83 * 10^{-5}$	n.a.; pitting
047AA 078 AA $	rough polished D 3	0,003 0,008	0,17 0,02	0,03 0,02	0,33 0,03	0,08 0,03	0,094	0,393	$2,19 * 10^{-5}$	$1,81 * 10^{-5}$	$4,00 * 10^{-5}$	n.a.; pitting

n.a.: not assignable

Slip-rolling in water with ZrO_2 (htc-PSZA);
F_N = 1575 N, P_0 = 3000 N/mm², v_{slide} = 0,085 m/s, n = 386 rpm, slip = 10 %, r.h. = 30 - 39 %

§ n_{total} = 10.000, s_{slide} = 131,95 m, it was not possible to continue the test, because the friction coefficient was to high and pitting starts

$ n_{total} = 30.000, s_{slide} = 395,85 m it was not possible to continue the test, because the friction coefficient was to high and pitting starts.

Slip-rolling in paraffinic oil with LPS#-SiC (SiC-B)

F_N = 205 N, P_0 = 1,5 GPa, v_{slide} = 0,085 m/s, n = 386 rpm, slip = 10 %, n_{total} = 2 * 10^6, s_{slide} = 26.390 m, r.h. = 30 - 39 %

#: Liquid Phase Sintered

Sample no. cylindrical sample spherical sample	Processing	Material removal rate [mm^3/s]	cylindrical sample R_z [µm] R_a [µm]	cylindrical sample R_{vk} [µm] R_{pk} [µm]	spherical sample R_z [µm] R_a [µm]	spherical sample R_{vk} [µm] R_{pk} [µm]	f at beginning	f at n_{total}	k_V at n_{total} [mm^3/Nm] planimetr., cylindrical sample	k_V at n_{totals} [mm^3/Nm] planimetr., spherical sample	k_V at n_{total} [mm^3/Nm] planimetric, total	cylindrical sample R_z [µm] R_a [µm] in track
02 BU§ 07 BU§	rough honed D 30	0,72 0,52	0,77 0,08	0,15 0,04	1,92 0,23	0,46 0,17	0,093	0,093	72,26 * 10^{-9}	116,73 * 10^{-9}	188,99 * 10^{-9}	0,31 0,07
03 BU§ 09 BU§	rough honed D 30	0,72 0,52	0,72 0,08	0,15 0,04	1,75 0,20	0,37 0,18	0,093	0,070	115,88 * 10^{-9}	127,67 * 10^{-9}	243,55 * 10^{-9}	0,34 0,08
03 BU§ 07 BU§	fine honed D 7	0,039 0,026	0,43 0,06	0,09 0,06	0,46 0,05	0,10 0,06	0,105	0,093	3,17 * 10^{-9}	9,69 * 10^{-9}	12,85 * 10^{-9}	0,42 0,05
02 BU§ 09 BU§	fine honed D 7	0,039 0,026	0,35 0,04	0,08 0,05	0,42 0,05	0,10 0,05	0,105	0,093	1,83 * 10^{-9}	6,07 * 10^{-9}	7,90 * 10^{-9}	
01 BU 09 BU*	rough ground D 126	0,33	3,03 0,45	0,51 0,39	4,74 0,91	0,93 0,65	0,135	0,052	4381,40 * 10^{-9}	5252,40 * 10^{-9}	9633,90 * 10^{-9}	0,62 0,07
03 BU 07 BU 1)*	rough ground D 126	0,33	2,71 0,43	0,57 0,47	4,06 0,77	0,86 0,63	0,113	0,052	4490,20 * 10^{-9}	4415,40 * 10^{-9}	8905,60 * 10^{-9}	0,51 0,06
02 BU§ 09 BU§	fine ground D 28	0,042	1,03 0,14	0,21 0,14	3,28 0,55	0,42 0,66	0,151	0,093	120,19 * 10^{-9}	154,30 * 10^{-9}	274,49 * 10^{-9}	0,35 0,03
03 BU§ 07 BU§	fine ground D 28	0,042	0,98 0,12	0,21 0,13	2,41 0,44	0,40 0,30	0,128	0,093	74,28 * 10^{-9}	52,20 * 10^{-9}	126,48 * 10^{-9}	0,32 0,12
04 BU 11 BU	rough lapped PWB 30	0,068 0,038	3,89 0,53	0,77 0,52	4,29 0,60	0,88 0,49	0,139	0,093	151,77 * 10^{-9}	188,14 * 10^{-9}	339,91 * 10^{-9}	0,42 0,09
05 BU 12 BU	fine lapped F 360	0,014 0,045	3,00 0,42	0,64 0,38	3,97 0,57	0,77 0,55	0,139	0,093	91,15 * 10^{-9}	159,71 * 10^{-9}	250,85 * 10^{-9}	0,28 0,06
04 BU§ 10 BU	rough polished D 3	0,003	0,25 0,03	0,06 0,03	1,00 0,07	0,23 0,04	0,070	0,105	1,39 * 10^{-9}	0,44 * 10^{-9}	1,83 * 10^{-9}	0,20 0,03
05 BU§ 11 BU§	fine polished D 1	n.b.	0,12 0,01	0,03 0,01	0,86 0,08	0,19 0,04	0,116	0,093	n.a.	7,15 * 10^{-9}	n.a.	0,14 0,01

n.a.: not assignable

§ mashined a second time

*1) n=1*10^6 *cycles*

** F_N = 548 N, P_0 = 3 GPa*

10 Literature

[1] W.G. Hosang
Results and Design Techniques from the Application of Ceramic Ball Bearings to the MERADCOM 10 kW Turbine,
AIAA-87-1844, 23rd Joint Propulsion Conference 1987, San Diego, USA

[2] J.F. Chudecki
Ceramic bearings - Application and performance advantages in industrial applications,
SAE-TP-891904, (1989)

[3] F.J. Ebert
Keramik in Wälzlagern für die Luft- und Raumfahrt,
in: „Hochleistungskeramik in FAG Wälzlagern", FAG Kugelfischer Georg Schäfer KGaA, Schweinfurt, Germany, Publ.-Nr. WL 40 204 DA

[4] W. Hörning
Neue FAG Spindellager - Hybridlager mit Stahlringen und Keramikkugeln,
in: „Hochleistungskeramik in FAG Wälzlagern", FAG Kugelfischer Georg Schäfer KGaA, Schweinfurt, Germany, Publ.-Nr. WL 40 204 DA

[5] D. Steinmann
Siliziumnitrid-Keramik für Kugeln und Kugellager,
cfi/ Ber. DKG 67 [12] (1990), 584

[6] H. Knoch
Keramische Gleitlager aus gesintertem Siliciumcarbid
Kap. 7 in: „Tribologisches Verhalten keramischer Werkstoffe - Grundlagen und Anwendungen",
Ed.: W.J. Bartz, Esslingen: expert-Verlag, (1993)

[7] B. Löffelbein, M. Woydt, K.-H. Habig
Medienschmierung ingenieurkeramischer Gleitpaarungen
Tribologie + Schmierungstechnik, 39. Jahrgang, Nr. 1, 1992, 3-9

[8] M. Woydt, U. Effner
Machining and slip-rolling of ceramics
AGARD-CP-589, Conference Proceedings, 6-7 May 1996, Sesimbra, Prortugal, p. 7-1 - 7-6

[9] T. Rabe, BAM-V.41, eigene Herstellung der Bundesanstalt für Materialforschung und -prüfung (BAM), D-12200 Berlin

[10] Technical Data Sheet
Engineered ceramics - general characteristics,
Elektroschmelzwerk Kempten GmbH (ESK), 87405 Kempten, Germany

[11] Technical Data Sheet
Silicon Carbide Properties, SiC-B
htc-hightech ceram, Dr. Steinmann + Partner, 53945 Blankenheim, Germany

[12] I. Dörfel, U. Effner, S. Glaubitz, W. Österle, E. Rudolph
Charakterisierung hochfester ZrO2-Werkstoffe
Tagungsband „Werkstoffwoche '96", Stuttgart, 28.-31. Mai 1996, DGM Informationsgesellschaft-Verlag, Oberursel, (1996), Band 6, S. 691-702, ISBN 3-88355-234-8

[13] T. Rabe, R. Wäsche
Gasdrucksintern von SiC/TiC-Keramiken,
Tagungsband der Jahrestagung 1993 der Deutschen Keramischen Gesellschaft, Weimar, 06.-08.10.1993, S. 266-268

[14] A. Skopp, M. Woydt
Ceramic-ceramic composite materials with improved friction and wear properties
Tribol. Intern. 25 [1], (1992), p. 61-70

[15] M. Woydt, J. Schwenzien
Dry and water-lubricated slip-rolling of Si3N4- and SiC-bassed ceramics
Tribol. Intern. 26 [3], (1993), p. 165-173

[16] U. Effner und M. Woydt
Zirkondioxid: Ein neuer Wälzlagerwerkstoff?
Keramische Zeitschrift 48 (12), 1996, S. 389-393

[17] U. Effner und M. Woydt
Zirkondioxid: Ein neuer Werkstoff für Wälzkontakte? (Zirconia: A new rolling bearing material?)
Tribologie & Schmierungstechnik, 44. Jahrgang, 1997, Heft 3, S. 124-127

[18] T. Nishioka, K. Matsunuma, T. Yamamoto, A. Yamakawa, M. Miyake,
Development of high strength Si3N4 materials for automobile parts,
Sumitomo Electric Technical Review, June 1993, No. 36, p. 77-83

[19] K.D. Mörgenthaler,
Keramikteile im Motorenbau, Anforderungen und Eigenschaften,
in: Keramik in Wissenschaft und Praxis, Mechanische Eigenschaften keramischer Konstruktionswerkstoffe, Hrg.: G. Grathwohl, Oberursel: DGM Informationsgesellschaft mbH Verlag, (1993) p. 17-28

[20] C. Gilbert, R. Daushardt, R. Ritchie,
Behaviour of cyclic fatigue cracks in monolithic Si3N4,
J. Am. Ceram. Soc. 78 [9] (1995), p. 2291-3000

[21] R. Stevens,
Zirconia and zirconia ceramics,
Second edition, 1986, July, Magnesium Elektron Ltd.

[22] L.S. Sigl, H.J. Kleebe
Flüssigphasengesintertes Siliciumcarbid
Tagungsband „Werkstoffwoche '98", München, 12.-15. Oktober 1998, DGM Informationsgesellschaft-Verlag, Frankfurt/M., (1998), Hrg.: J. Heinrich, G. Ziegler, W. Hermel, H. Riedel, Band VII, Symposium 9, ISBN 3-88355-274-7, im Druck

[23] V. Carle, U. Schäfer, U. Täffner, F. Predel, R. Telle, G. Petzow
Keramographie von Hochleistungskeramiken - Werkstoffbeschreibung, Präparation, Ätztechniken, und Gefügebeschreibung,
Pract. Metallographie 28 (1991), S. 420-434

[24] N.N.
Abnützungsmaschine für Metalle
Zeitschrift des VDI, 66 [15], 1922, 377-378

[25] K.-H. Habig, M. Gienau, B. Löffelbein
Nitrierschichten
FVV-Vorhaben Nr. 554 unter dem Förderzeichen BMWi/ AiF Nr. 9045 – Abschlußbericht 1996

[26] P. Studt, G. Bartelt
Verschleiß und Reibung keramischer Werkstoffe bei Mischreibung: Einfluß von Schmieröladditiven,
Tribologie + Schmierungstechnik, 39, Nr. 5 (1992), S. 282-287

[27] Angaben der Firma E. Merck, 64271 Darmstadt, Deutschland

[28] V.S. Yushchenko, E.D. Shchukin
Rehbinder Effect
Encycl. Mater. Sci. Enging. 6 (1986), p. 4162-4166

[29] G. Heinicke, K. Beyer
Der Rehbindereffekt - Wesen und Anwendung,
Wissenschaft und Forschung 27, Nr. 12 (1977), S. 522-526

[30] K. Adachi, K. Hokkirigawa,
Wear of materials,
ASME (1991), p. 333 - 338

[31] H. Czichos, K.-H. Habig
Tribologie Handbuch - Reibung und Verschleiß
Braunschweig: Vieweg Verlag, 1992

[32] U. Effner, M. Woydt, E. Westkämper, L. Höhne, J. Gäbler,
Economical machining and tribological rolling wear of ceramics,
Proceedings, International Tribology Conference, 29.10.-02.11.1995, Yokohama, Japan, Vol. 1, S. 503-508

[33] E. Westkämper, G. Kappmeyer, H.-W. Hoffmeister
Einfluß der Fertigungsverfahren Langhubhonen und Schleifen auf die Oberflächenausbildung und die tribologischen Eigenschaften keramischer Bauteile,
Tagungsband „Werkstoffwoche '96", Stuttgart, 28.-31. Mai 1996, DGM Informationsgesellschaft-Verlag, Oberursel, (1996), Hrg.: A. de Paoli, Band 5, S. 303-308, ISBN 3-88355-233-X

[34] J. Gäbler, H.-W. Hoffmeister, U.-P. Weigmann
Läppen und Polieren von Ingenieurkeramik,
Tagungsband „Werkstoffwoche '96", Stuttgart, 28.-31. Mai 1996, DGM Informationsgesellschaft-Verlag, Oberursel, (1996), Hrg.: A. de Paoli, Band 5, S. 135-140, ISBN 3-88355-233-X

[35] M. Haubold, B. Rotter, T. Brücher
Nachweis von bearbeitungsbedingten mechanischen Oberflächenspannungen mittels Akustomikroskopie,
Proc. annual. conf. of the DGZfP (Vol. 37), Garmisch-Partenkirchen, Deutschland, 17.-19.5.1993, S. 608-615

[36] S. Bosek
Akustische Mikroskopie,
Phys. Bl. 49, Nr. 6 (1993), S. 497-502

[37] DIN 50320,
Verschleiß; Begriffe, Systemanalyse von Verschleißvorgängen, Gliederung des Verschleißgebietes,
DIN-Taschenbuch 246, Tribologie, Berlin, Beuth-Verlag (1990), S. 203-210

[38] K.-H. Zum Gahr
Furchungsverschleiß; Reibung und Verschleiß; Mechanismus - Prüfungstechnik - Werkstoffverhalten,
Deutsche Gesellschaft für Metallkunde e.V., Oberursel, Ed.: K.-H. zum Gahr, (1980)

[39] H.K. Tönshoff, J. Peddinghaus, H.-G. Wobker,
Tribologische Verhältnisse zwischen Schleifscheibe und Werkstück,
in: „Tribologie 2000",
Ed.: W.J. Bartz, Technische Akademie Esslingen, 2, (1992), 18.11-1

[40] DIN 4768
Ermittlung der Rauheitsmeßgrößen Ra, Rz, Rmax mit elektrischen Tastschnittgeräten, Grundlagen,
August 1974, Normenausschuß Länge und Gestalt (NLG) im DIN Deutsches Institut für Normung e.V., Burggrafenstr. 6, 10787 Berlin, Deutschland

[41] DIN 4776
Kenngrößen R_k, R_{pk}, R_{vk}, M_{r1}, M_{r2} zur Beschreibung des Materialanteils im Rauheitsprofil, Meßbedingungen und Auswerteverfahren, Anwendungshinweise und Beispiele,
Mai 1990, Normenausschuß Länge und Gestalt (NLG) im DIN Deutsches Institut für Normung e.V., Burggrafenstr. 6, 10787 Berlin, Deutschland

[42] M.N. Gardos, R.G. Hardisty,
Fracture Toughness- and Hardness-Dependent Polishing Wear of Silicon Nitride Ceramics
Tribol. Trans. 36 [4], (1993), p. 652-660

[43] B. Löffelbein, M. Woydt, K.-H. Habig
Reibungs- und Verschleißuntersuchungen an Gleitpaarungen aus ingenieurkeramischen Werkstoffen in wäßrigen Lösungen,
BAM-Forschungsbericht 186, Bundesanstalt für Materialforschung und -prüfung,
D-12200 Berlin, (1992)

[44] A.G. Evans, T.R. Wilshaw,
Quasi-Static Solid Particle Damage in Brittle Solids - I. Observation, Analysis and Implications,
Acta Metall. 24, (1976), 939

[45] U. Effner, M. Woydt
Bearbeitung und Wälzreibung von Ingenieur-Keramiken in Wasser und Öl
VDI Berichte No. 1207, (1995), 223-233

[46] U. Effner, J. Gäbler, M. Hartelt, D. Klaffke, Th. Naeve, G. Spur, U.-P. Weigmann, E. Westkämper, M. Woydt
Einfluß der Bearbeitung auf das Verhalten von SiC (EKasic D) unter Gleit-, Schwingungs- und Wälzreibung
Tagungsband der DGM Tagung „Reibung und Verschleiß", Bad Nauheim, 21./22. März 1996